MODELING AND PERFORMANCE OF A PNEUMATIC/HYDRAULIC HYBRID ACTUATOR WITH TUNABLE MECHANICAL IMPEDANCE

by

Mark Alan Kleidon

B.S., University of California, Santa Barbara

SUBMITTED TO THE DEPARTMENT OF MECHANICAL ENGINEERING IN PARTIAL FULFILLMENT OF THE REQUIREMENTS FOR THE DEGREE OF

MASTER OF SCIENCE

at the

MASSACHUSETTS INSTITUTE OF TECHNOLOGY

September 1983 ie Feb 84

Signature of Author _____
Department of Mechanical Engineering
September 12, 1983

Certified by _____
Neville Hogan
Thesis Supervisor

Accepted by _____
Warren M. Rohsenow
Chairman, Department Committee

Modeling and Performance of a Pneumatic/Hydraulic Hybrid Actuator
With Tunable Mechanical Impedance

by

Mark Alan Kleidon

Submitted to the Department of Mechanical Engineering on September 12, 1983 in partial fulfillment of the requirements for the degree of Master of Science.

Abstract

Industrial application of computer controlled manipulators has been limited primarily to tasks involving minimal or no mechanical interaction between the manipulator and its environment. A recent area of research in motion control directed at coping with mechanical interaction has been termed *Impedance Control.* Typically, the actuators employed in impedance control schemes have fixed static and dynamic characteristics, mechanical impedance at the endpoint being varied and controlled with feedback. This work investigates the potential of a Pneumatic/Hydraulic hybrid actuator to control mechanical impedance via a combination of *control of natural machine behavior* and feedback. The implementation of a controller to tune impedance at the endpoint is presented which provides stiffness performance ranging from 2000 lb_f/ft to a nearly backdrivable actuator.

As an aid to understanding the physics of the device two mathematical models are developed: one a fifth order non-linear model for computer simulation and the other a simpler model applicable to the methods of linear control theory. An evaluation of both open and closed-loop performance makes evident the actuator's good and bad features. Finally, design recommendations for futher work to improve the the realizable impedance range and ensure closed-loop stability are discussed.

Thesis Supervisor: Neville Hogan
Title: Associate Professor

Acknowledgments

I would like to take this opportunity to thank my advisor, Professor Neville Hogan. His friendship, guidance, and constant enthusiasm have helped make this project personally rewarding. I've appreciated the opportunity to have worked in the Robotics Lab of the Laboratory for Manufacturing and Productivity where the experimental portions of this thesis were performed. I'm grateful to Kamal Youcef-Toumi for his advice and tolerance of me constantly bogarting electronic instruments. I'd also like to thank Professor H.M. Paynter for inventing the bond graph, as it has become an indespensible tool in this dynamic systems modeler's bag of tricks. Gary, Jim, Scott, Steve, Dirk, and Steve I thank for making up a relaxed office environment and dispelling my illusion that all MIT students are nerds. In particular, I thank my parents, to whom I dedicate this thesis, for 24 years of continuous support, love, and guidance; their old fashioned values of hard work, unselfishness, and personal integrity will remain with me forever.

To Josephine and Kenneth

Table of Contents

List of Figures

List of Tables

Nomenclature

A_o	Electro-pneumatic servovalve orifice area
A_d	Damper valve orifice area
a_d	Dimensionless damper valve orifice area
A_h	Hydraulic piston area
A_p	Pneumatic piston area
A_s	Electro-pneumatic servovalve spool end area
a_s	Dimensionless electro-pneumatic servovalve orifice area
b	Viscous damping coefficient
b^*	Reference viscous damping coefficient
b_h	Linearized hydraulic damping coefficient
b_L	Environment friction coefficient
c	Speed of sound in air
C_{air}	Air compliance
C_d	Electro-pneumatic servovalve discharge coefficient
C_{do}	Damper valve discharge coefficient
C_P	Linearized servovalve load pressure flow sensitivity
c_p	Dimensionless linearized servovalve load pressure flow sensitivity
C_z	Linearized servovalve flow gain
c_z	Dimensionless linearized servovalve flow gain
δ_h	Dimensionless hydraulic damping coefficient
δ_b	Dimensionless viscous damping coefficient
$\Delta \mathbf{e}$	Incremental effort vector
f	Dimensionless force

NOMENCLATURE (cont.)

F_{coul}	Coulomb friction force
F_{ext}	External force
F_{td}	Force at the actuator/environment interface
h	Specific enthalpy
h_{Atm}	Specific enthalpy of the atmosphere
h_{S_L}, h_{S_R}	Input enthaplies to left and right air chambers
I	Electo-pneumatic servo-current
i_s	Dimensionless electro-pneumatic servo-current
I^*	Reference electro-pneumatic servo-current
k	Ratio of specific heats
$\mathbf{K}$	Stiffness matrix
K^*	Reference air stiffness
K_a	Servoamplifier gain
K_F	Force feedback gain
k_f	Dimensionless force feedback gain
K_{fb}	Electro-pneumatic servovalve feedback spring stiffness
K_s	Electro-pneumatic servovalve spool position/current gain
K_T	Electro-pneumatic servovalve torque motor constant
K_θ	Electro-pneumatic servovalve jet-pipe preamplifier gain
K_v	Velocity feedback gain
k_v	Dimensionless velocity feedback gain
K_x	Position feedback gain
k_x	Dimensionless position feedback gain
l_a	Dimensionless air leakage coefficient

NOMENCLATURE (cont.)

m	Actuator mass
$\frac{dm}{dt}$	Mass flow rate of air
M_L	Environment mass
n	Polytropic exponent
P	Air pressure
P_{Atm}	Atmospheric pressure
P_L, P_R	Left and right air chamber pressures
P_{S_L}, P_{S_R}	Input pressures to left and right air chambers
p_L, p_R	Dimensionless left and right air pressures
P^*	Reference air pressure
P_{pl}	Pneumatic load pressure
p_{pl}	Dimensionless Pneumatic load pressure
P_{hl}	Hydraulic load pressure
p_{hl}	Dimensionles hydraulic load pressure
Q	Volumetric flow rate of air
q	Dimensionless volumetric flowrate of air
Δq	Incremental displacement vector
Q_{rated}	Rated volumetric flow rate of oil
Q_{Load}	Pneumatic load flow (volumetric flow rate)
$\frac{dQ}{dt}$	Rate of heat flow
r	Electro-pneumatic servovalve feedback spring length
R	Gas constant for air
R_{al}	Air leakage coefficient
r_b	Damping coefficient ratio: Total damping/Viscous damping

NOMENCLATURE (cont.)

r_m	Mass ratio: Total mass/Actuator mass
r_ρ	Air density ratio: Air density/Reference air density
ρ	Air density
ρ^*	Reference air density
ρ_{av}	Average air density
ρ_{oil}	Oil density
s	Specific entropy
S	Total entropy
s_v	Dimensionless ram velocity
s_x	Dimensionless ram position
$\frac{dS}{dt}, \frac{dS_{env}}{dt}$	Rate of entropy flow
t	Time
T	Temperature and Electro-pneumatic servovalve time constant
T^*	Reference temperature
τ	Dimensionless time
τ_m	Electro-pneumatic servovalve motor torque
θ_a	Electro-pneumatic servovalve torque motor armature position
u	Specific internal energy
U	Total internal energy
v	Ram velocity
v^*	Reference ram velocity
V	Air velocity and Air chamber volume
V_L, V_R	Left and right air chamber volumes
V^*	Reference air chamber volume

NOMENCLATURE (cont.)

v_{ss}	Steady state ram velocity
ν_L, ν_R	Dimensionless left and right air chamber volume
$\frac{dV}{dt}$	Time rate of change of air cylinder chamber volume
w	Electro-pneumatic servovalve port width
ω_n^*	Reference natural frequency
x	Ram position
x^*	Reference ram position
$\mathbf{X}$	State vector
$\Delta\mathbf{X}$	Incremental state vector
z	Electro-pneumatic servovalve spool position
z^*	Reference electro-pneumatic servovalve spool position
ζ^*	Reference damping ratio

Chapter 1
Introduction

1.1 Opening Statement

A great deal of recent work in motion control reseach has been directed toward the development of more sophisticated feedback control techniques in order to improve performance and adaptability of robotic manipulators. One such approach termed *impedance control* [14] has involved control of a manipulator's mechanical impedance at the endpoint via linear and non-linear feedback.

Past work has answered many questions as to why impedance control is desirable and has demonstrated its feasibility with the appropriate closed-loop control; but the control of the natural impedance of actuators (e.g. open-loop stiffness and damping) has, to date, received little attention. Typically, the choice of actuators for a particular impedance control scheme is based on bandwidth, speed of response, and maximum force output considerations; attempts to change the open-loop behavior of actuators almost always involve closing feedback loops around a system.

This work considers the *design of actuators for impedance control* in the hope that by improving adaptability (i.e. the range of realizalble mechanical impedance) of actuators via the forward path, the overall performance capabilities of manipulators can be improved. The great advantage of changing impedance without feedback is that open-loop actuators rarely exhibit instability, which in a closed-loop system with powerful actuators can be costly and dangerous.

1.2 Background

The state-of-practice in robotics can be divided into two general approaches to control of manipulators: position or path control, and force or compliant motion control. Path control is applicable to tasks in which the manipulator's environment is such that mechanical interaction is negligible. Transporting an object in free space along a specified trajectory is an example. Most industrial manipulators fall into this catagory. Automated welding, one of the more successful applications of robotics to date, requires precise control of endpoint position; but the manipulator never actually touches its workpiece, hence there is no mechanical interaction force.

The second approach, more recent and more sophisticated, is force or compliant motion control. A manipulator required to follow kinematic constraints imposed by objects in its workspace is an example. One scheme is to monitor the interference forces that will inevitably occur and use that information to alter the position of the manipulator to reduce these forces. This type of control enabled solution of the problem of placing a peg in a close-fitting chamfered slot [22]. *Passive* (i.e. non-active sensory feedback) compliant motion control has been applied successfully in the form of the remote centered compliance [11], which can be considered a mechanical analog of force feedback, allowing lateral and rotational realignment of the manipulator endpoint in response to lateral forces and moments.

Both of these approaches have been successful for application to a class of manipulatory tasks in which the manipulator does no work on its environment (*workless interaction*). Path control relies on detailed knowledge of the environment so that objects with which the manipulator might develop non-negligible interaction forces can be avoided, hence the work done is zero. Compliant motion control relies on a kinematic constraint to determine the path of the manipulator. Since the manipulator does not displace objects in its environment, but either traces them or moves out of their way, this is also an example of a workless

interaction.

A broader class of manipulatory tasks involves *non-zero work interactions* with the environment. Tasks falling into this catagory (e.g. drilling, bolting, grinding, etc.) have seen little application in industrial robotics. Neither force nor position control alone are adaquate for this kind of interaction. Position contolled devices are, in general, composed of very stiff actuators, tending to develop large unpredictable interaction forces with objects lying between them and their commanded positions.

Force controlled devices go where the environment rather than the controller dictates. Sophisticated combinations of force control in one direction and position control in another can produce *smart* manipulators able to put pegs in holes, but such interactions are still workless—in one direction the force is zero, in the other the displacement is zero.

The limited success of force and position control for tasks requiring work to be done on the environment points to a fundamental restriction imposed on energetic interaction between physical systems: *it is not possible for one of two interacting systems to prescribe both the effort (e.g. force) and the flow (e.g. velocity) at the point of interaction* [24].

An ideal position contoller can impose a precise displacement on an object, but it can't, at the same time, control the interaction force. Correspondingly, an ideal force controller can exert a desired force but cannot control position in the same direction. If the work done on the environment is to be controlled, controlling only the force or only the position is not enough. One potentially successful strategy is to control one of the two variables at the interaction port while also controlling the relation between the them.

In the approach termed impedance control it is assumed that the manipulator environment is, in general, an admittance (e.g. a mass), hence the manipulator should be an impedance [16]. The basic idea is to control the nominal manipulator position while also controlling the relation between the deviation from the commanded position and the resulting

interaction force. Different tasks will require different manipulator impedances seen by the environment, hence a manipulator with tunable impedance is essential.

1.3 Past Work in Impedance Control

Changing the impedance of a device for different tasks is hardly a new concept. Automobile transmissions have been providing a variable impedance interface between engines and inertial loading for decades. In a manipulator however, changing a transmission ratio is usually not a practical way to tune mechanical impedance. A successful application of impedance control for avoidance of obstacles in a manipulator's workspace employed a semi-backdrivable dc torque motor, with stiffness and damping controlled by variable position and velocity feedback [3].

Another demonstration of the feasibility of impedance control was performed on a two-joint serial link manipulator using dc *pancake* motors with non-linear control of endpoint impedance [9]. This work developed a controller with a computational load comparing favorably with other manipulator control techniques.

There is evidence that mammalian motion is controlled partially by tuning of the impedance about joints via co-contraction of opposing muscles [13]. This notion is the basis of an elbow prosthesis simulator with tunable mechanical impedance developed for research in prosthetics [1].

1.4 Objective of this Thesis

It is proposed that a possible approach to impedance control is to first establish the widest possible range of stiffness and damping inherent in an actuator by altering the physical properties of the device, then attempt more precise control of impedance via artificial

means (i.e. electronic feedback).

The actuator chosen for this project is a hybrid of active pneumatic and semi-active hydraulic components, based on the assumption that stiffness can be changed with variable pressure in the pneumatic part of the system, while damping is controlled by variable flow area in a closed hydraulic cicuit. Hardware is assembled to determine the range of impedance achievable through natural means. A compliant, minimally damped actuator results from lowering air pressure and widening hydraulic flow area, while a stiffer, highly damped actuator results from high pressure and narrow flow area.

Also considered is a special controller design implemented on experimental hardware to tune stiffness and damping seen at the actuator endpoint. This controller employs force feedback to make the pneumatic part of the system (basically a flow source with a variable orifice) look more like an effort source to its environment. Then outer position and velocity control loops are used to control stiffness and damping.

Pneumatic systems are typically difficult to control because of the compressibility of air. Energy enters the system from what can be idealized as an unlimited source (the receiver of an air compressor) through a controlled gate (a servovalve) and is first stored in the compressed air before being transformed into mechanical energy (e.g. force and translation). A dc motor is similar in that electrial energy enters the system through a controlled voltage source and is stored in the inductance of a coil before being transformed (through a gyrator) into rotation of the motor and load inertia. The time constant associated with the motor inductance, however, is typically much faster than that of an air chamber, hence its contribution to parasitic energy storage does not complicate control to the degree characteristic of compressibility in a pneumatic system.

Successful closed-loop control of the pneumatic power input to the system requires a thorough dynamic model of the hybrid actuator. A good model also aids in the design and

selection of actuator components and provides a quantitative understanding of the factors affecting performance—especially the inherent impedance of the device. A substantial portion of this work is directed at developing and testing dynamic models for these purposes.

1.5 Summary of the Following Chapters

The next chapter briefly discusses the experimental hardware used in the project. Chapter 3 presents the development of a non-linear model suitable for digital simulation of the hybrid actuator which is quite robust for application in a variety of conditions. In Chapter 4 the model is reduced to a simple linear model useful in the design of controllers and applicable to the powerful methods of linear control theory. Chapter 5 discusses the natural impedance range of the actuator and presents the design and performance of the impedance controller implemented. In the final chapter recommendations for further work in this area are given, including design recommendations for a working prototype.

Chapter 2
Experimental Hardware

2.1 Power Transducers

Because the purpose of the experimental hardware used in this project was for verification of dynamic models and demonstration of variable and tunable impedance, choice of hardware was limited to commercially available components. This presented some problems with non-ideal behavior, such as excessive friction and leakage, that could most likely be minimized with proper design, especially in the passive hydraulic portion of the system.

Shown in the photograph of Figure 2-1, the assembled hardware is made up of linear pneumatic and hydraulic actuators.

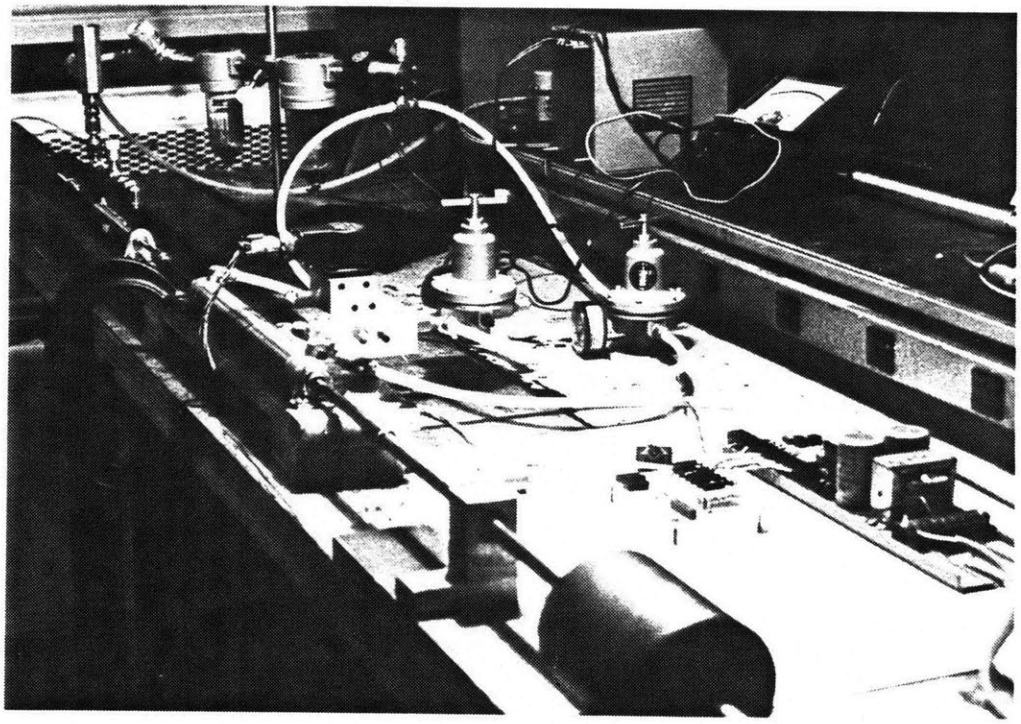

Figure 2-1: Experimental hardware.

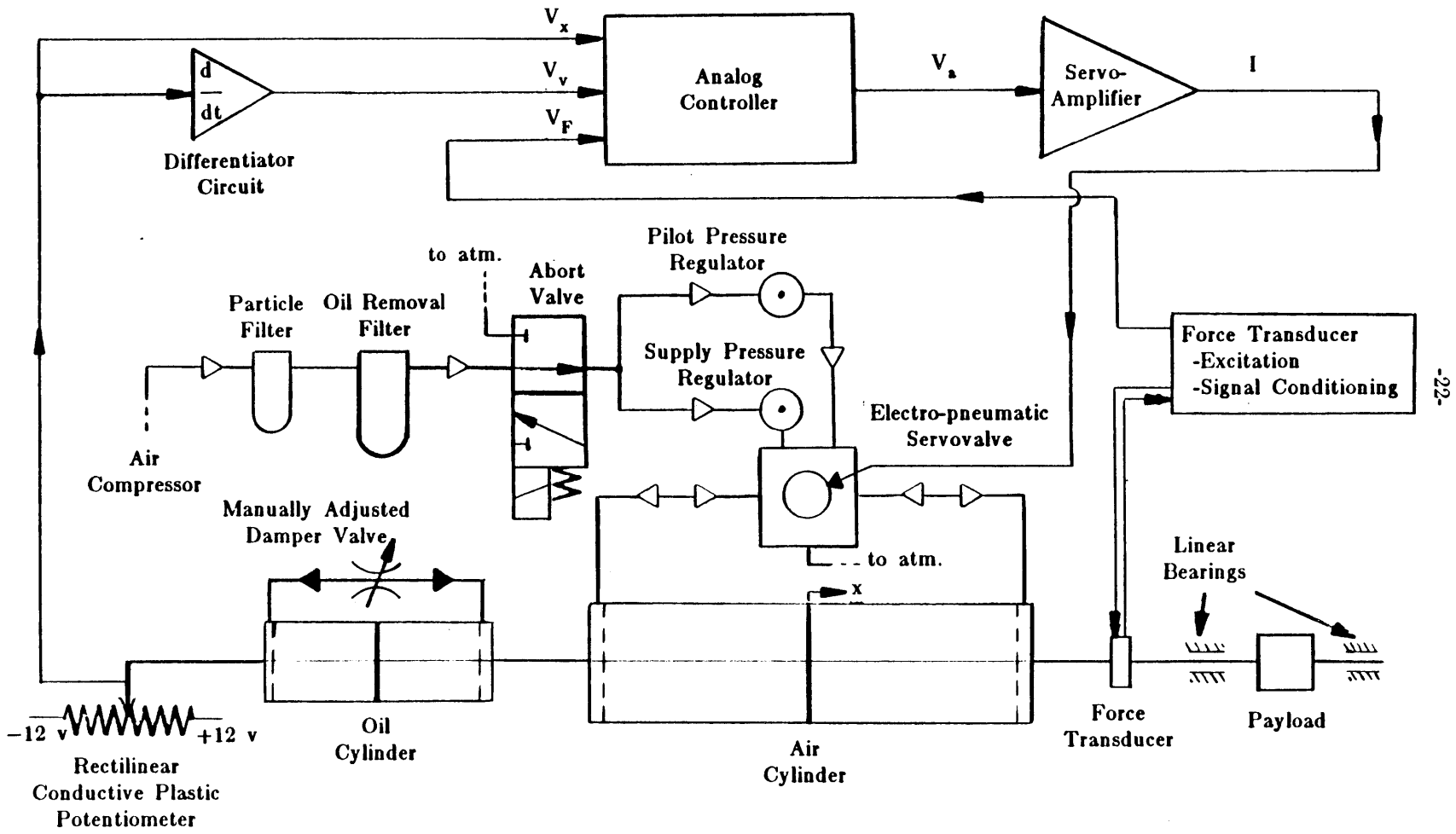

Figure 2-2: Schematic of experimental hardware.

For simplicity motion was restricted to one-degree-of-freedom; linear actuators were chosen and arranged in tandem as shown. The arrangement was such that the hydraulics could be easily removed in order to test the pneumatic system alone.

2.2 Electro-pneumatic Servovalve

The most interesting part of the experimental hardware is the *electro-pneumatic servovalve*, giving proportional control of air flow to and from the pneumatic cylinder. Briefly, the servovalve is of the *jet-pipe* design with a first-stage torque motor and jet-pipe preamplifier and a second-stage four-way sliding spool with mechanical force feedback to control it.

The valve, manufactured by Atchley Controls, Inc., is shown in Figure 2-3.

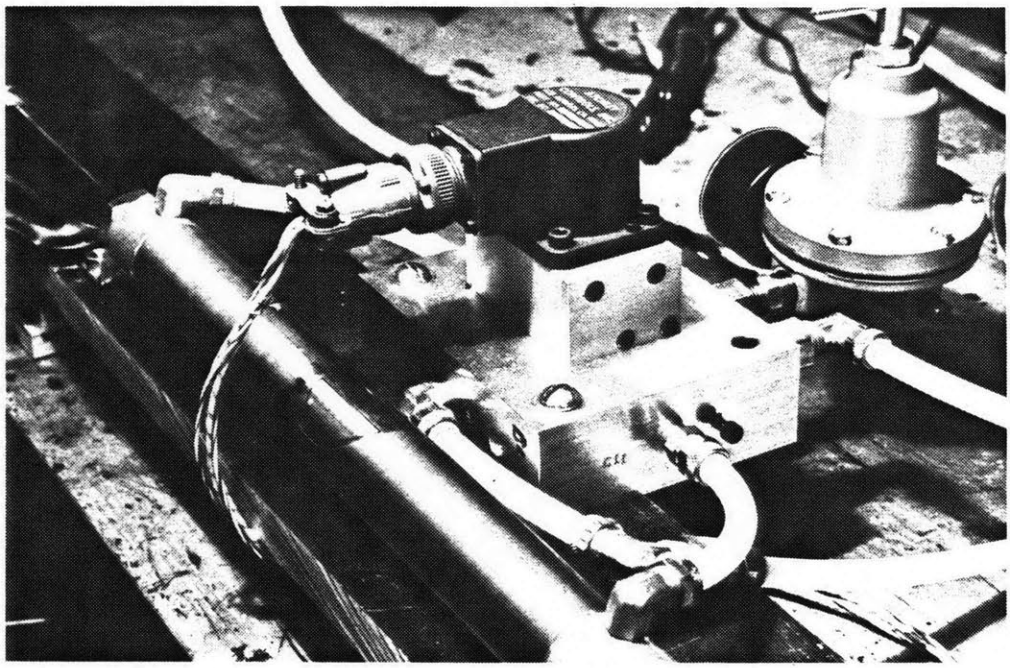

Figure 2-3: Electro-pneumatic servovalve.

Its operation is quite similar to that of more common nozzle-flapper servovalves (the spool moves to a position at which motor torque is balanced by a feedback spring torque

dependent on spool displacement). The jet-pipe design, however, offers a distinct advantage: fluid passages in the jet-pipe are nearly an order of magnetude larger than those found in the nozzle-flapper valve [4]. The jet-pipe valve is much less sensitive to fluid contamination and will pass particles as large as 100 microns without failure.[1] Even so, proper air line preparation is necessary (i.e. particle and oil removal filters in the supply line). The servovalve is controlled by a Moog model 121-103 current drive servo-controller.

2.3 Tuning of Impedance

Air pressure and the hydraulic flow are are adjusted manually. In a later design each can be controlled by a remote input, but for the purposes of this preliminary design study the added complication is unnecssary.

In the closed hydraulic circuit no provisions are made to supply oil lost through external leakage. The experimental hardware is not required to operate for any extended period of time and the circuit is simple enough that lost fluid can be added quickly and trapped air easily purged. In Chapter 6 the design of an oil circuit containing an accumulator to make up lost fluid as well as pressurize the circuit is discussed.

The controller built for tuning of impedance was composed entirely of analog components (i.e. operational amplifiers) mainly because the objectives of this stage of the project did not warrant the complications of digital control.

---

[1] Failure in the nozzle-flapper valve due to clogging in the very small fluid passages in the first stage can be caused by contaminants as small as 30 microns.

2.4 Force Measurement

Not shown in Figure 2-1, but shown in the schematic of Figure 2-2, is the force transducer used to implement the impedance controller discussed in Chapter 5. It was a Lebow model 3132 general purpose load cell with a 500 lb_f capacity, maximum deflection of 0.005 inches, repeatability of ± 0.05 % of the rated output, and linearity of ± 0.10 % of the rated output. As part of the impedance controller it lay between the output of the actuator and the environment simulated by a mass free to move in one direction; hence, it measures the force at the actuator/environment interaction port.

2.5 Data Acquisition

Position and velocity were measured using a rectilinear conductive plastic potentiometer and an analog differentiator. The combination of the low noise output of the potentiometer and a low pass filter on the differentiator produced an adaquate velocity signal.

Data was recorded on a 14 channel FM tape recorder (Racal STORE 14D Instrumentation Recorder) before being digitized on a PDP 11/34 computer. The tape speed used (7.5 in/sec) gives the recorder a bandwidth of approximately 0 to 2.5 Khz, an interchannel time displacement error[2] of ± 3 μs, and a signal to noise ratio of 48 dB.

---

[2]The observed error between adjacent tracks on the same head after record/replay measured according to I.R.I.G. 118-73

Chapter 3
Non-linear Analysis of the Hybrid Actuator

3.1 Modeling Strategy

One of the major objectives of this thesis is to develop mathematical models for use in design of the hybrid actuator. These models help quantify static and dynamic effects observed in the physical system, suggesting techniques by which the natural and controlled behavior can be altered, while providing a method of testing these techniques before the expensive and time consuming task of designing and constructing a prototype is undertaken.

The modeling approach begins by describing, rather qualitatively, all of the major dynamic effects present in the real actuator. Because the actuator is made up of many different types of dynamic elements (mechanical, electrical, pneumatic, and hydraulic), a lumped parameter rather than a distributed parameter approach is taken. The basic assumption is that energy storage and dissipation effects are confined to discrete regions of the system rather than distributed over the system volume.

Section 3.2 of this chapter is devoted entirely to the development of a conceptual model that includes a treatment of thermodynamics in the pneumatic portion of the system, and oil compressibility and inertia in the hydraulic portion—a useful exercise toward gaining an intuitive feel for the degree of complexity required for meaningful computer simulations.

In Section 3.3, as applications require more workable models, simplifications are made; some effects are approximated by functional relations and others are neglected. In this way at each stage of simplification the modeler knows of the effects present in the real system which less complete models will be unable to describe, rather than being forced to retreat back to the basic physics of the situation after observing phenomena which a hastily developed

approximate model does not explain.

In the following chapter a linear model is developed which, though inadaquate for simulation of the time response of the actuator, is quite powerful when applied to the methods of linear control theory.

3.2 Conceptual Actuator Model

The first step in formulating a description of the actuator is system reticulation, the process of placing idealized boundaries between the system and its environment and identifying subsystems and the structure through which they exchange power. As shown in Figure 3-1, the basic components of the system are the electro-pneumatic servovalve, the hydrualic damper valve, the air and oil cylinder chambers and their respective power transforming pistons, and the moving mass of the actuator.

These components exchange power with the environment through five external ports. The pneumatic ports, consisting of a compressed air source and standard air sink, are the most obvious. Less obvious, and possibly of questionable significance are the two thermal ports included for completeness. The remaining port is the point at which the endpoint of the actuator comes into contact with the part of the environment to be manipulated. It is here that control of the mechanical impedance of the actuator seen by the environment is desired.

At this point it is helpful to introduce Paynter's bond graphs into the analysis, as they are an attractive method of representing the flow of power and information between dynamic elements in a complex system. Those unfamiliar with the concept and use of bond graphs are refered to a new book by Rosenberg and Karnopp [25] which is an excellent introduction to systems modeling via bond graphs for application in a variety of physical domains.

Bond graphs provide a convenient notation for depicting causality in a physical system.

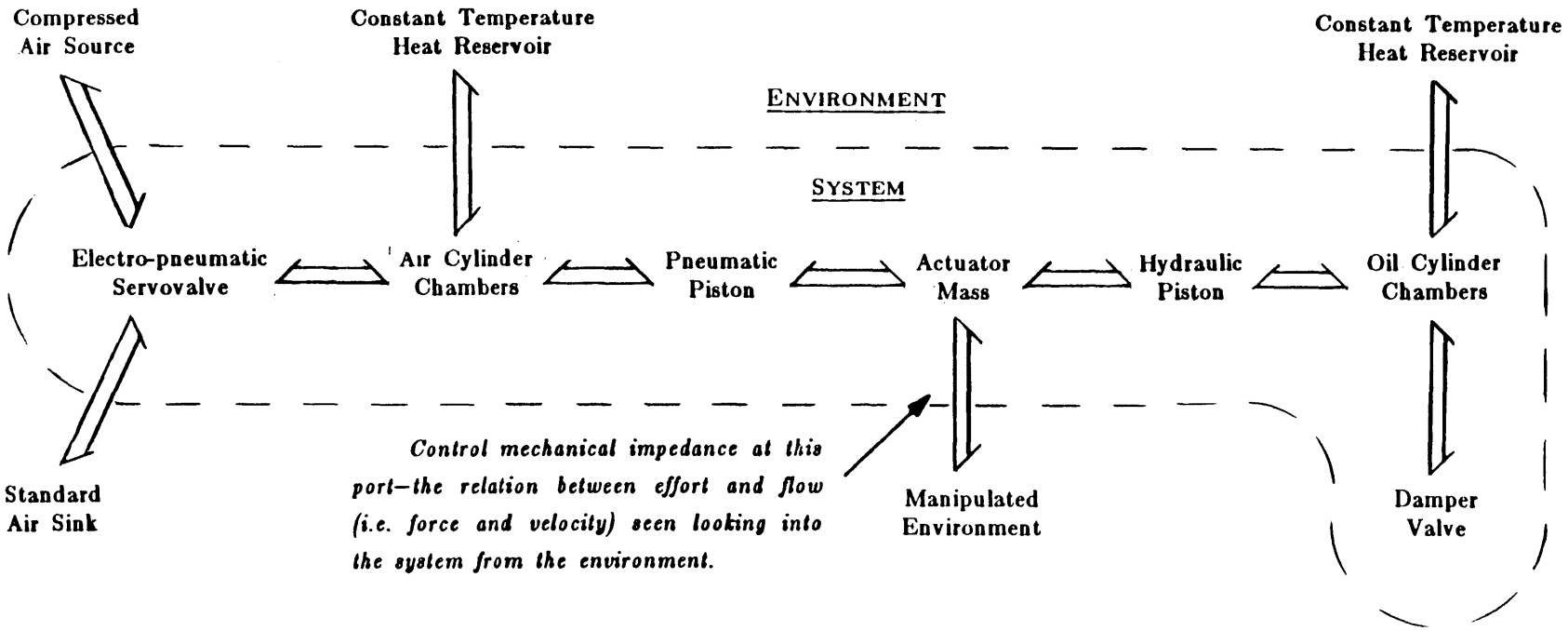

Figure 3-1: System reticulation.

The interaction between two elements of a system across a power bond is such that either element can prescribe only one of the power duals (an effort or a flow) on that bond, the second being determined by the other element. In a bond graph this fundamental restriction is depicted by the causal stroke on the power bond and provides a check on the logical consistency of the model.

To complete the reticulation process more specific statements about the elements making up the subsystems defined in Figure 3-1 are made. These elements are then assembled into a conceptual bond graph model which is used as a starting point toward more specific modeling. The objective is not to develop an elaborate mathematical formulation, but rather to provide a conceptual basis identifying—in terms of energy ports and power flow—all of the major dynamic effects present in the real system.

3.2.1 External Energy Ports

Consider now in more detail the types of ports through which the system and environment exchange energy.

3.2.1.1 Pneumatic Ports

At the pneumatic ports the instantaneous power flow is the sum of two effects: flow work and the convection of internal energy. (It is assumed that the flow rates are sufficiently low to neglect kinetic energy.) The flow work (or hydrostatic power) is the product of static pressure, P, and volumetric flow rate, Q. The internal energy flow is the product of the specific internal energy, u, and the mass flow rate, dm/dt.

A bond graph model of the pneumatic environment appears in Figure 3-2a. Since mass and volume flow rates are related by the fluid density, the use of a density modulated transformer is helpful since the two power flow terms mentioned above lie in different effort/flow domains [17].

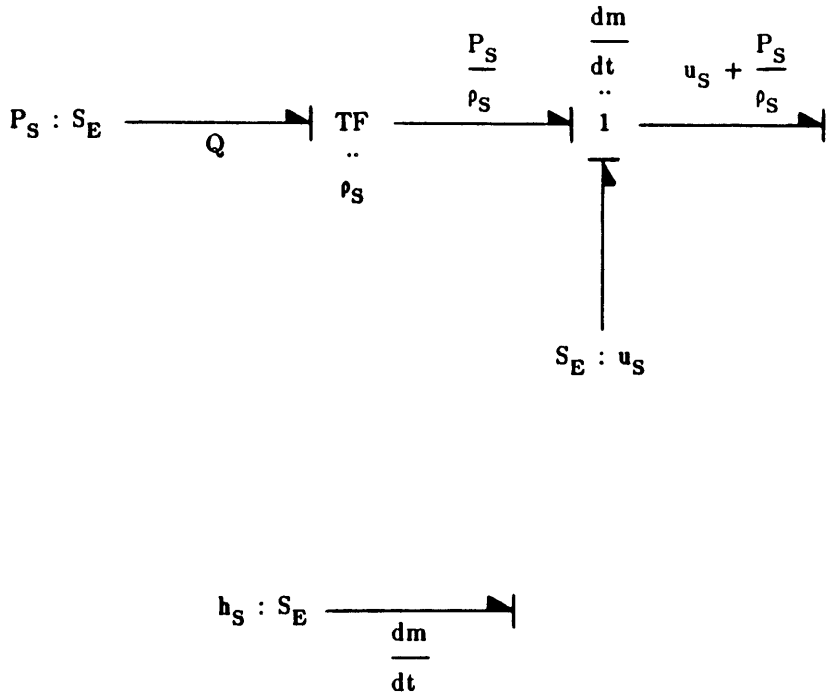

Figure 3-2: Pneumatic source bond graphs.

An effort source representing the constant supply pressure lies on one side of the transformer in the P-Q domain, while another effort source representing the constant supply specific internal energy lies on the other in the u-dm/dt domain.[3] The net effect results in the pneumatic ports appearing to the system as constant specific enthapy sources in the h-dm/dt domain (Figure 3-2b), where specific enthalpy is defined by

$$h = u + \frac{P}{\rho} . \tag{3.1}$$

In practice, the pneumatic ports are neither ideal pressure nor ideal enthalpy sources. The pressure regulator, located immediately upstream of the servovalve, tends to lose output pressure at high flowrates. Since long supply lines may be required to separate the regulator from the actuator in order to minimize weight in a later design, transport delay may also be

---

[3] A similar bond graph may be drawn for the atmospheric port.

a problem.

3.2.1.2 Thermal Ports

At the thermal ports energy flow between the system and the environment is in the form of heat transfer, the instantaneous power, dQ/dt, given by the product of the thermodynamic temperature, T, and the rate of entropy flow, dS/dt, or

$$\frac{dQ}{dt} = T\frac{dS}{dt}. \tag{3.2}$$

At this point only an acceptable model of the environment is desired. A discussion of the nature of the heat transfer, which will lie somewhere between the extremes of the adiabatic case (no heat transfer) and the isothermal case (sufficient heat transfer to maintain constant temperature), is taken up in a latter section.

The environment bounding the fluid chamber is idealized as a constant temperature heat reservoir large enough to provide or accept any amount of heat without changing temperature. In bond graph terms this corresponds to an effort source of constant temperature capable of handling any required entropy flow.

3.2.1.3 Manipulation Port

Modeling of the manipulation port is not as straightforward as the previous two cases since a robotic manipulator is likely to encounter many different types of environments. Tasks may range from transporting a rigid mass in space to interacting with compliant objects or stiff mechanisms with complex kinematic constraints (such as other manipulators). It has been argued that the most general model of a manipulator environment is an admittance (e.g. a mass) based on reasoning that it is always possible to impose an arbitrary force on the environment but not always possible to impose an arbitrary velocity [16].

For this one degree-of-freedom analysis the interaction occurs across a single bond with the instantaneous power given by the product of the interaction force and the velocity of the

manipulator endpoint. Since one of the objectives of impedance control is to minimize the detail with which the environment need be known ahead of time to complete a given task, it does not make sense to attempt to model the environment in detail; yet calling it only an admittance, from a modeling point of view, is not sufficient to fully characterize the dynamic interaction at the manipulation port.

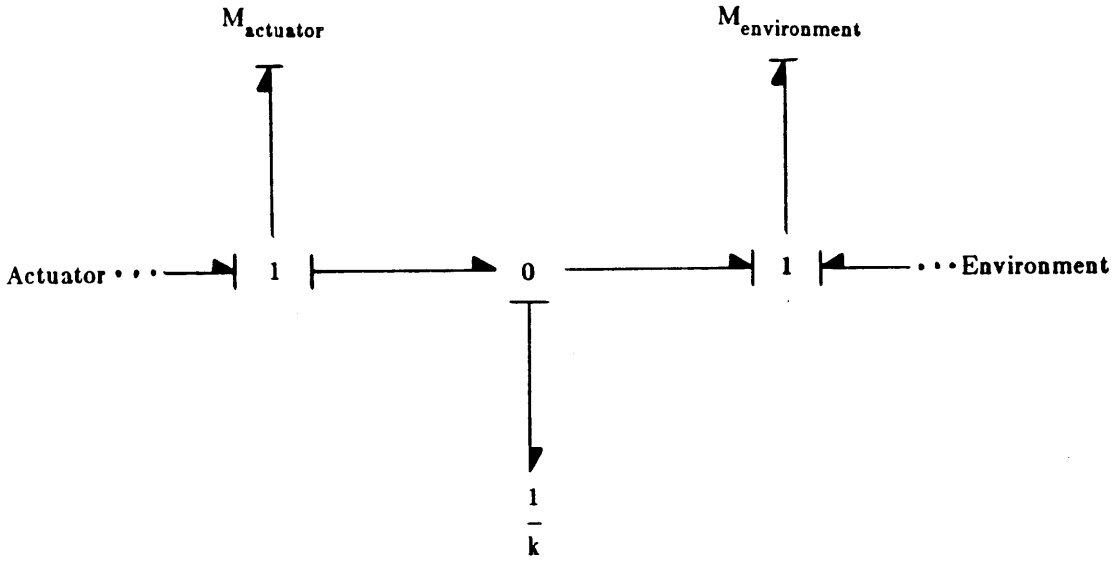

Figure 3-3: Compliant interface between actuator and environment inertias.

At the very least the manipulator environment (also refered to as the workpiece) will have mass. If the mass is a sizeble fraction of the manipulator mass and the two are rigidly coupled, then the open-loop manipulator dynamics and closed-loop stability bounds will vary depending on the mass of the workpiece. Note the loss of generality in assuming a rigid coupling. In general, there is always a compliant interface between the two masses (see Figure 3-3), be it a property of the workpiece, a force transducer, or only the elasticity of the manipulator structure.

In the latter two examples the compliance can be made very small with proper design and may be neglected. The former case requires detailed knowledge of the environment and

is not addressed in this analysis. Hence, the minimum model of the manipulation environment is a mass. For completeness (and because it does not increase the order of the model) a linear friction element is also included in the manipulation environment.

3.2.2 Actuator Subsystems

Now consider the subsystems defined in Figure 3-1 contained within the system boundry.

3.2.2.1 Hydraulic Subsystem

In the hydraulic subsystem energy storage occurs in the form of the kinetic energy of the fluid particles lumped in a one-port inertance element and the elastic energy of the fluid lumped in a one-port capacitance element. It is assumed that a thermodynamic analysis is unnecessary since fluid density variations due to compressibility are small. Thermal effects should show up as static parameter variations such as density and viscosity changing with temperature, rather than significant dynamic effects.

The majority of energy dissipation in the hydraulic subsystem occurs in the damper valve; however, other losses take place due to fluid friction in the cylinder and connecting conduit, as well as leakage past the ram. Each of these effects is lumped in its own one-port resistance element with the the damper valve resistance statically modulated by orifice area.

The elements mentioned above are assembled in the hydraulic subsystem bond graphs of Figure 3-4. (The reader should take the time to be convinced that the two structures of Figure 3-4 are indeed equivalent.) If the oil compliance elements are assumed nodic, then the bond graph can be reduced to the structure shown in Figure 3-5.[4] Technically the compliance elements are not really nodic since oil compressibility is dependent upon volume,

---

[4]Nodicity implies the constitutive relation is independent of a change in the origin of its displacement variables.

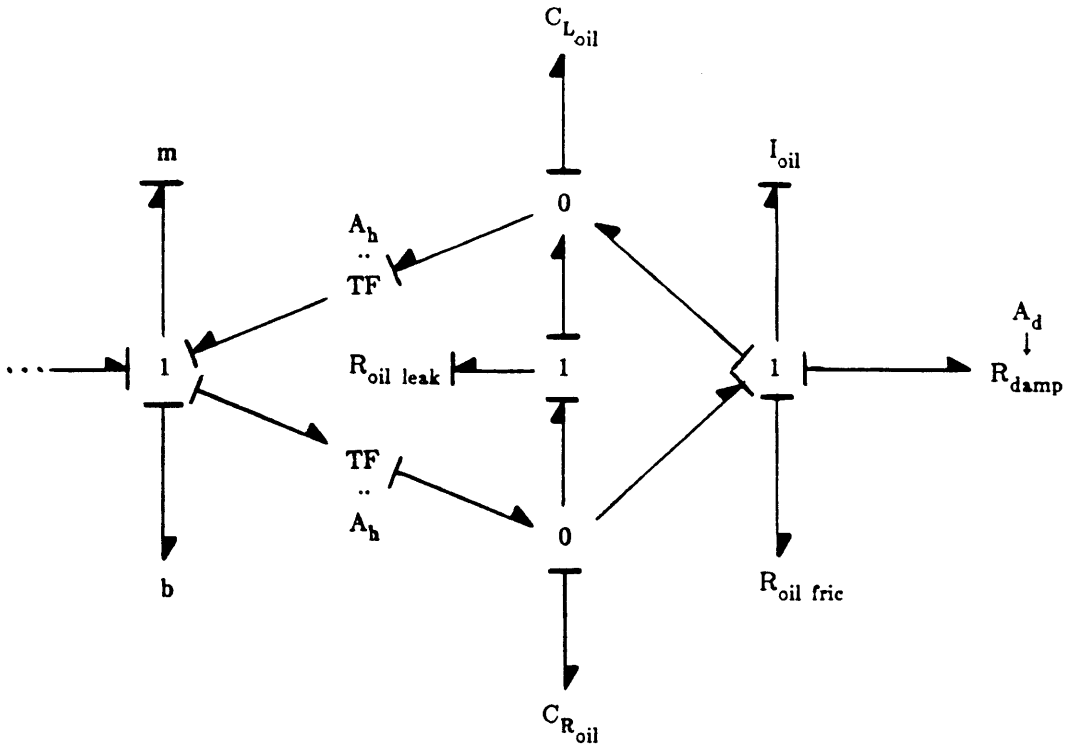

This structure is in every way equivalent to:

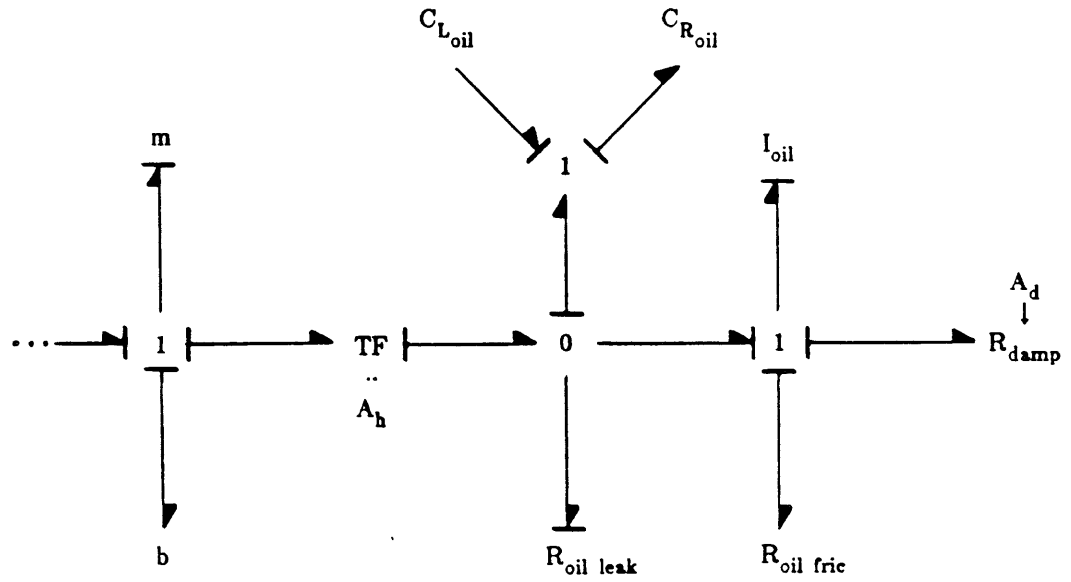

Figure 3-4: Hydraulic subsystem bond graphs.

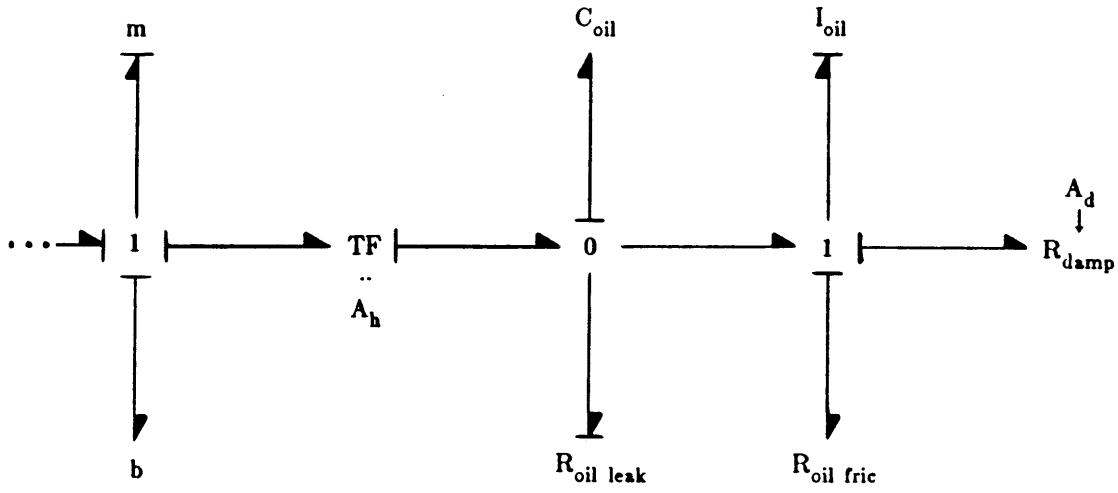

Figure 3-5: Reduced hydraulic subsystem bond graph.

but this fact is overlooked in favor of a less complex model.

3.2.2.2 Pneumatic Subsystem

Orifice Flow

Before attempting to describe behavior inside the air cylinder, consider the problem of modeling compressed air flow through the electro-pneumatic servovalve. The nature of the device is such that flow may originate from either the constant enthalpy source, flowing into a variable downstream condition (the air cylinder), or from the air cylinder (a variable upstream condition), flowing into the constant enthalpy sink. The size of each orifice as well as which side of the air cylinder is connected to supply and which to atmosphere depends on the spool position, z.

In order to develop a consistent bond graph model of the servo-orifices the following assumptions are made:

1. Flow of energy through the servo-orifices occurs in the h-m domain.
2. The flow is steady.

3. The upstream condition, be it supply, exhaust, or a cylinder chamber, is a stagnation condition.

4. Flow is one dimensional.

The first assumption follows from the devlopment of the pneumatic source model. The second assumption is equivalent to assuming the process involves no energy storage, implying that any change in the input variables will appear instantaneously at the output variables. The third assumption greatly simplifies the analysis and is not unreasonable since under most conditions the air passing through the orifices will have a much greater velocity than the air in either the cylinder or the supply and exhaust lines.

Applying the steady-flow energy equation to a stationary control volume surrounding the fluid from the stagnation condition to the orifice, gives

$$\frac{V^2}{2} = h_o - h \ . \tag{3.3}$$

Using continuity for steady flow, the mass flow rate is then written as

$$\frac{dm}{dt} = C_d \rho_o A_o \sqrt{2(h_o - h)} \ , \tag{3.4}$$

where the discharge coefficient, C_d, is included to account for non-ideal behavior (such as two- and three-dimensional effects). The orifice area is given by

$$A_o = wz \ , \tag{3.5}$$

where w is the constant port width.

Since the servo-orifices do not store energy and are not power conservative (i.e. $[dm/dt]\, h_o \neq [dm/dt]\, h$) they are modeled as resistance elements modulated by the servovalve spool position and the air density at the orifice. Equation (3.4) is a relation between a flow and an effort difference, hence the resistance is a one-port element attached to a 1-junction.

Obtaining a consistent expression for the air density at the orifice is complicated both by the switching of the direction of flow and by the possibility of flow choking. When flow is

subsonic and recovery negigible the density at the orifice is the same as the downstream condition. When flow is choked the situation becomes increasingly complex and is probably beyond the scope of a lumped parameter analysis. Clearly, further simplification is required; however, consider the causality assignment for the one-port resistance implied by the choking phenonmenon.

Flow choking implies that a state of maximum flow per unit area has been reached given the upstream condition and that no further changes in the downstream condition will increase mass flow (see reference [27]). This suggests that it is not always possible to impose an arbitrary flow through the orifice. Rather, the mass flow is determined by the orifice given the conditions up- and downstream. Therefore, the only consistent causal assignment for the resistance is admittance causality with an enthalpy difference defined to the element by the rest of the system and the mass flow defined by the resistance.

Electro-pneumatic Servovlave

Up to this point very little has been said about how the electro-pneumatic servovalve is to be modeled. Figure 3-6 shows a rough schematic of the valve taken from reference [4] wherein its design and operation are described in detail.

A bond graph model of the servovalve shown in Figure 3-7 contains four independent energy storage elements: air compliance and torque motor armature inertia in the first stage, and spool inertia and feedback spring compliance in the second stage. For purposes of this analysis a model so complex is unwarranted. A much simpler description is obtained with the following assumptions:

1. The volume of air in the first stage is small enough to neglect air compliance.
2. The inertias of the armature and spool are small.
3. Fricton is negligible.
4. The servoamplifier is an ideal current source, hence the inductance and resistance

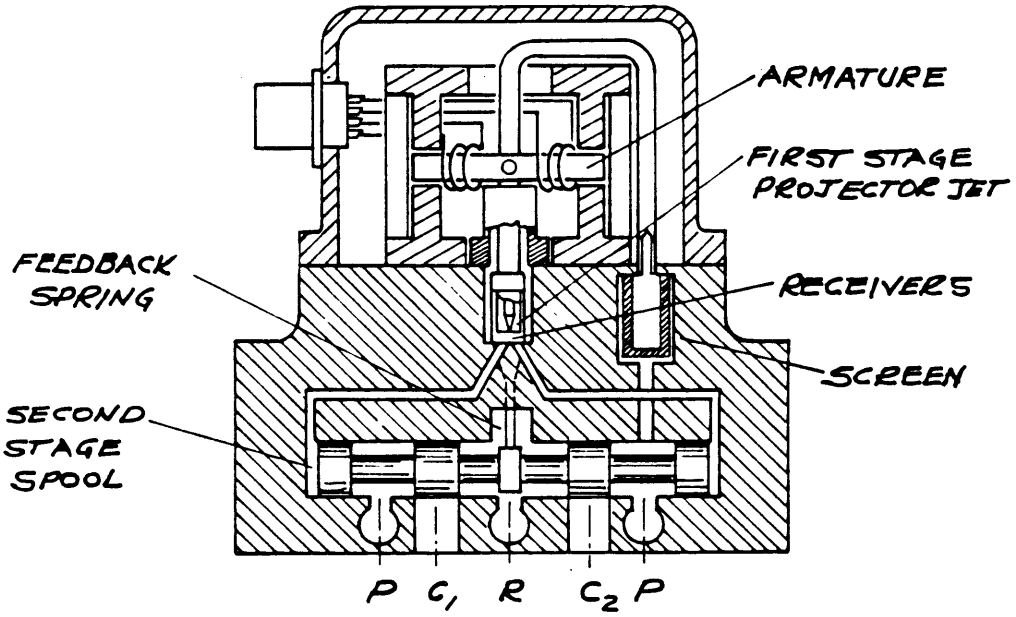

Figure 3-6: Electro-pneumatic servovalve schematic.

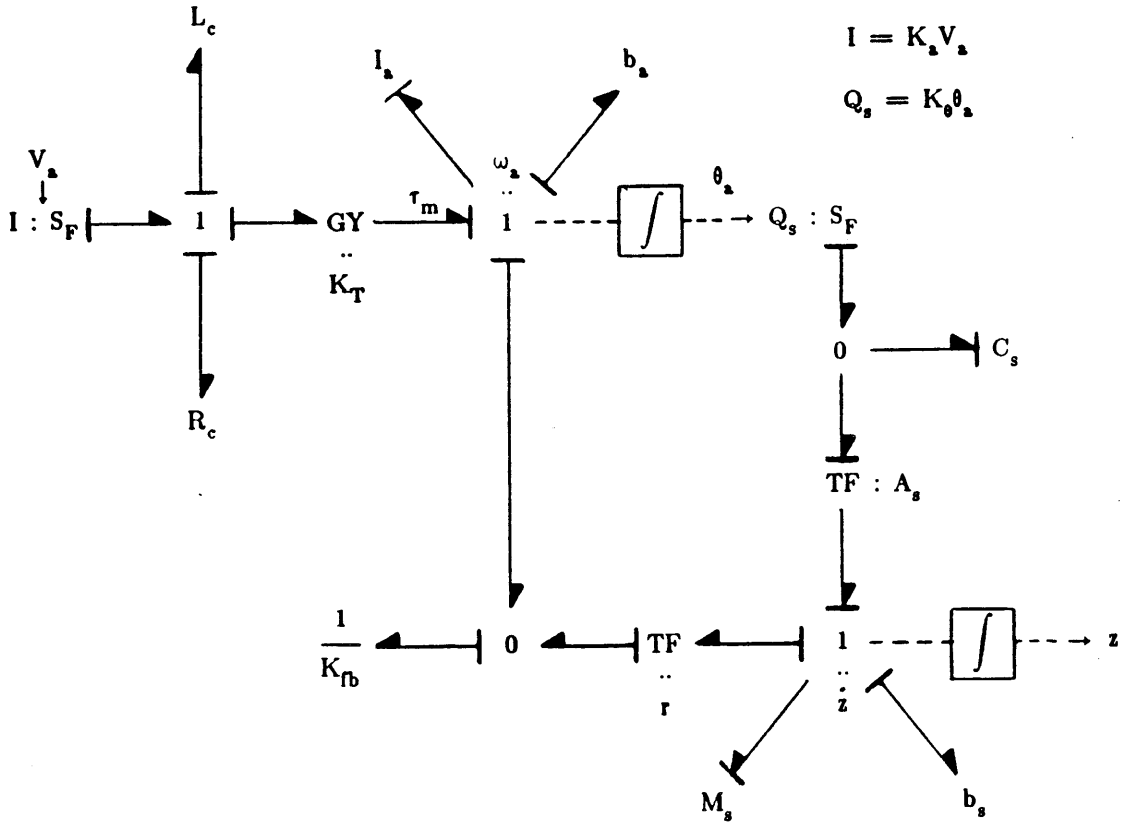

Figure 3-7: Electro-pneumatic servovalve bond graph.

of the coil are not important.

With the assumptions above the bond graph takes the form of Figure 3-8. Note the many changes in causality assignments.

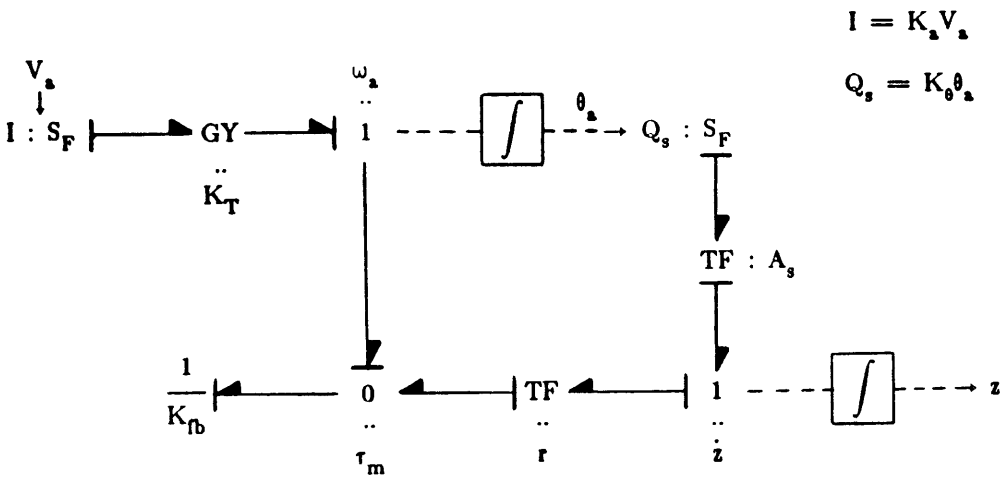

Figure 3-8: Reduced electro-pneumatic servovalve bond graphs.

There are no independent energy storage elements; however, equations written from this bond graph do contain dynamic terms due to the presence of integrators. The equations follow. For the torque motor:

$$\tau_m = K_T I \,, \tag{3.6}$$

the jet-pipe preamplifier:

$$A_s z = K_\theta \theta_a \,, \tag{3.7}$$

and the feedback spring:

$$\theta_a = \frac{\tau_m}{K_{fb}} - \frac{z}{r} \,. \tag{3.8}$$

Combining results gives

$$T \frac{d}{dt} z = -z + K_s I \,, \tag{3.9}$$

where

$$T = \frac{rA_s}{K_\theta}$$

and

$$K_s = \frac{K_T r A_s}{K_{fb}}.$$

In electro-hydraulic servovalves the time constant, T, is usually assumed small enough to neglect spool dynamics (mainly because the supply pressure driving the jet-pipe preamplifier is quite large, resulting in a large K_θ value). In the pneumatic case supply pressure is much lower[5], hence spool dynamics may be important under some conditions and may effect stability when electronic feedback loops are closed around the system.

Air Cylinder Chambers

Modeling of the pneumatic cylinder chambers is somewhat more complex than in the hydraulic case. Since the compressibility of air is much greater than that of oil, fluid density changes are such that a treatment of the thermodynamics of the situation is necessary. As before, energy storage and dissipation are lumped into discrete model elements (in this case multi-port elements), assuming that wave propagation, turbulence, and other continuum phenomena can be neglected.

Modeling of energy storage is based upon two assumptions:

1. The stored energy is the total internal energy, U, of the fluid in the chamber.
2. Energy enters and leaves the chamber via three ports: a thermal port with power flow given by TdS/dt; a convective port with power flow given by hdm/dt; and a mechanical work port with power flow given by PdV/dt.

(Note that the first assumption implies kinetic energy of the fluid particles is neglected.)

---

[5]Most hydraulic valves are rated from 1500 to 3000 psi, while the pneumatic valve has a maximum supply of 200 psi.

By definition, the total internal energy depends on both the specific internal energy and the total mass of air in the chamber volume, or

$$U = mu.$$

Recall from thermodynamics that the specific internal energy can be expressed as a function of two independent variables or

$$u = u(s,v) ,$$

where s is specific entropy and v specific volume. Hence, the total internal energy can be written as

$$U = U(S,V,m) ,$$

where S (= ms) is the total entropy and V (= mv) the total volume. Since it is assumed that U is conserved and is also a function of three displacements (S,V,m), the storage of energy within an air chamber can be described by a three-port capacitance field.[6]

Figure 3-9 shows such a field incorporated into a bond graph model of a single air chamber. Energy flows between the servovalve and the field via the convective bond and between the field and the pneumatic piston via the work bond. Heat flows between the field and the environment through a power conservative two-port thermal resistor for which it is assumed that

$$T_{env} \frac{dS_{env}}{dt} = \frac{dQ}{dt} = T \frac{dS}{dt} \tag{3.10}$$

and

$$\frac{dS}{dt} - \frac{dS_{env}}{dt} \geq 0 . \tag{3.11}$$

In reference [19], using equations (3.10) and (3.11) and noting that the absolute temperatures T and T_{env} are always positive, it is reasoned that the only consistant causal form is as

---

[6]Indeed, the idea of modeling a compressible fluid via a capacitance field is not new. Karnopp [17] shows how the Gibb's equation for a simple compressible substance may be represented as a two-port C-field with a thermal port (TdS/dt) and a work port (PdV/dt). He also considers--in the isentropic case--the addition of a convective port (hdm/dt) for open systems.

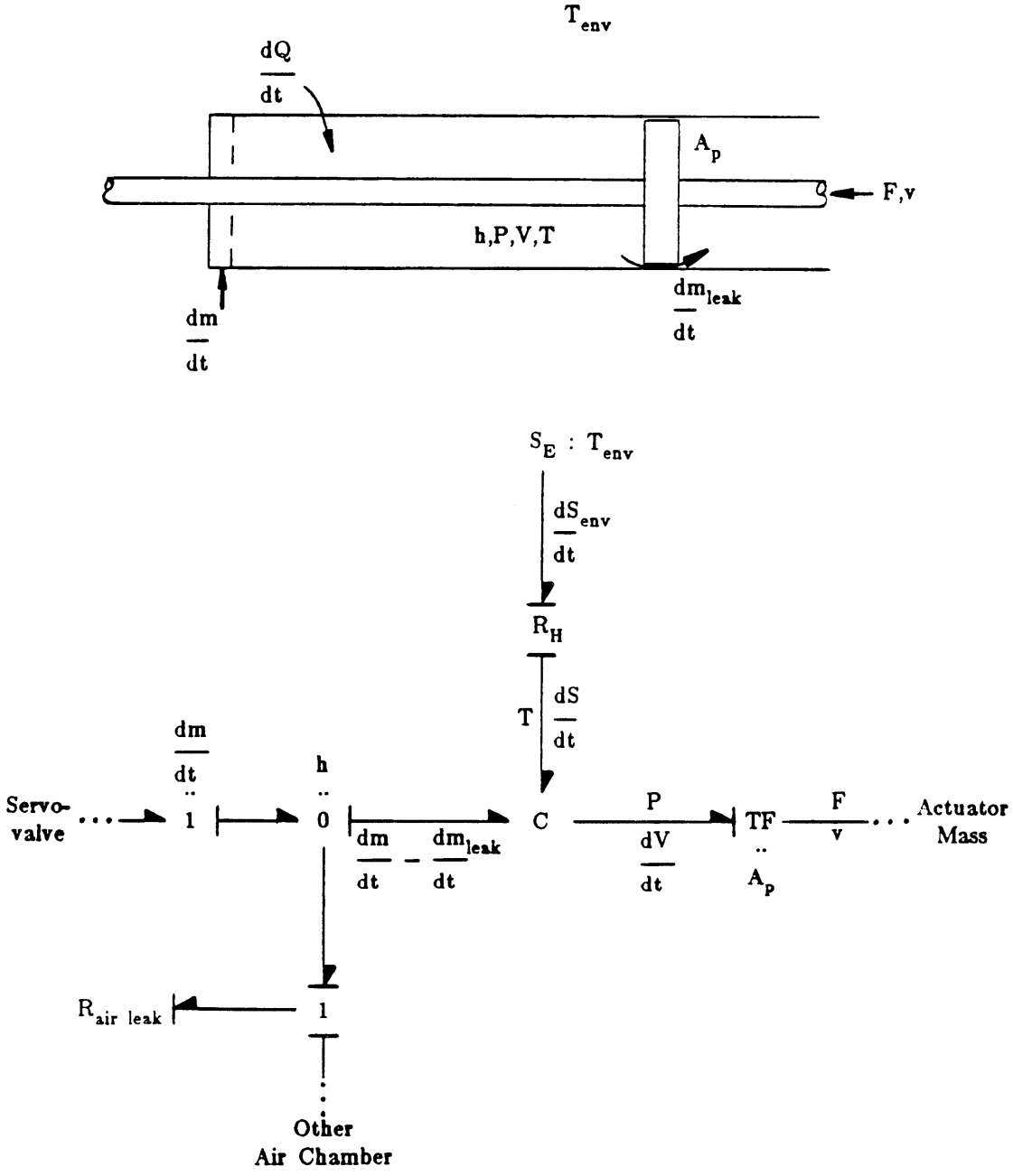

Figure 3-9: Air chamber and bond graph.

shown in Figure 3-9 with the entropy flows defined by the resistor.

Readers unfamiliar with the concept of multiport fields are refered to Chapter 7 of reference [19]. The basic assumption behind a C-field representation is that the stored energy can be expressed as a single-valued scalar function of a vector of displacements. As in the case of a one-port capacitance it is assumed that there exist static constitutive relations between the efforts and the displacement vector. In this case:

$$T = T(\mathbf{q}) ,$$

$$P = P(\mathbf{q}) ,$$

$$h = h(\mathbf{q}) ,$$

where the displacement vector is

$$\mathbf{q} = \begin{bmatrix} m \\ S \\ V \end{bmatrix} .$$

Energy dissipation in the air cylinder chamber is modeled assuming fluid friction is negligible and leakage past the ram (represented as a one-port R) is a mass flow dependent on the enthalpy difference between the two chambers.

3.2.3 Complete System Bond Graph

The assemblege of elements and subsystems defined in the previous sections is shown in Figure 3-10. All mechanical friction in both the hydraulic and pneumatic subsystems is lumped into a single one-port resistance whose velocity is defined by the lumped mass of the actuator.

In the following sections the conceptual bond graph of Figure 3-10 is used as a starting point in developing a non-linear set of dynamic equtions suitable for digital simulation and a linearized model useful in controller design.

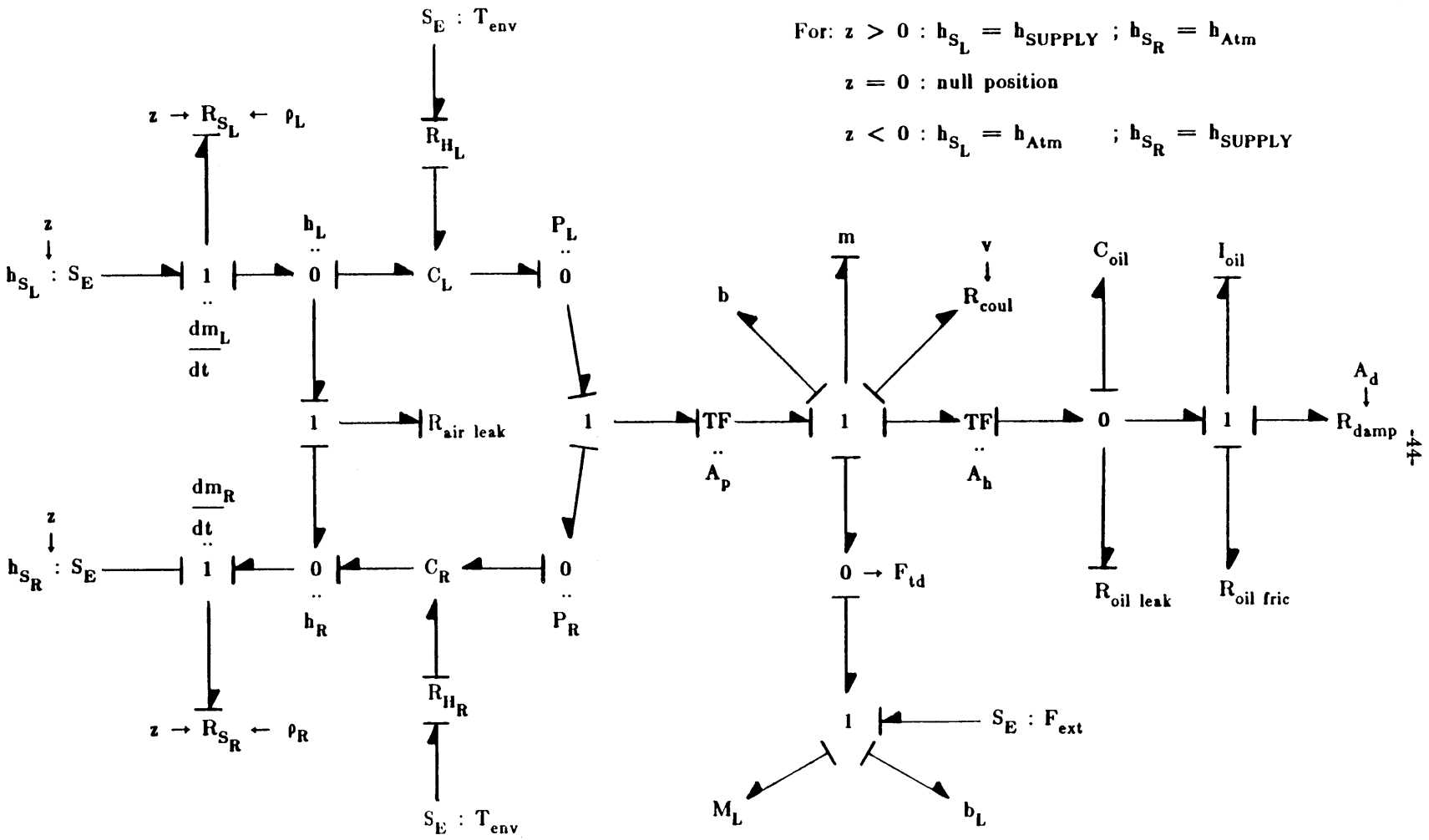

Figure 3-10: Complete system bond graph.

3.3 Simplified Actuator Model

Generating a detailed set of constitutive relations for the complete system bond graph of Figure 3-10 is a formidable task and perhaps of marginal benefit. Recall that the objectives of the non-linear model are to simulate the effects of parameter changes and to test controller designs. It may be possible to achieve these objectives with a simpler model. Indeed, Bass [5] found that results of simulations based on a bond graph model similar to Figure 3-10 do not differ significantly from those based on a model neglecting air thermodynamics, oil inertia, and oil compliance, implying that a simplified model may adaquately represent the real system.[7]

3.3.1 Pneumatic Subsystem in the P-Q Domain

Consider the consequences of modeling the pneumatic subsystem completely in the P-Q domain rather than using a thermodynamic analysis corresponding to Figure 3-10. Basically, this amounts to using an acoustic approximation in which compliance and resistance coefficients are calculated at a mean pressure, temperature, and density [25].

The most obvious consequence is the removal of the thermal ports and the thermal resistor describing heat transfer. This amounts to assuming an adiabatic process which is not a gross approximation provided the process happens fast enough that there isn't sufficient time for heat transfer to occur. It may, at first, appear contradictory to evaluate fluid parameters at a constant temperature and then call the the process adiabatic rather than isothermal. Please note that the use of an average air temperature is an engineering approximation and not an assumption of isothermal flow.

---

[7]The major differences in the complete bond graph of reference [5], aside from the fact that *ON/OFF* pneumatic valves are assumed rather than an electro-pneumatic servovalve, is the omission of the thermal ports and modeling of orifice flow of air in the P-Q domain.

Another consequence of working in the P-Q domain involves neglecting the convection of internal energy into and out of the air cylinder chambers. Technically, the energy stored within the air chambers is still in the form of internal energy of the fluid; however, in this case it is thought of as elastic energy in much the same way as one thinks of stored energy in a mechanical spring. Energy is now idealized as entering and leaving the air chambers at the convective ports in the form of flow work only, hence power flow on what was an hdm/dt bond becomes

$$h\frac{dm}{dt} = \frac{P}{\rho}\frac{dm}{dt} = PQ \ . \tag{3.12}$$

In the linear case (or for small changes of variables) the consequences are equivalent to neglecting all but one of the terms in the original stiffness matrix of the three-port C-field. For causality as shown in Figure 3-10 the constitutive relation for the field is of the form

$$\begin{bmatrix} \Delta h \\ \Delta T \\ \Delta P \end{bmatrix} = \begin{bmatrix} \frac{\partial h}{\partial m} & \frac{\partial T}{\partial m} & \frac{\partial P}{\partial m} \\ \frac{\partial h}{\partial S} & \frac{\partial T}{\partial S} & \frac{\partial P}{\partial S} \\ \frac{\partial h}{\partial V} & \frac{\partial T}{\partial V} & \frac{\partial P}{\partial V} \end{bmatrix} \begin{bmatrix} \Delta m \\ \Delta S \\ \Delta V \end{bmatrix}$$

or

$$\Delta \mathbf{e} = \mathbf{K}\Delta \mathbf{q} \tag{3.13}$$

where $\mathbf{K}$ is the stiffness matrix. Under this assumption all of the partial derivatives except $\partial P/\partial V$ must vanish and what remains of the constitutive law is

$$\Delta P = \partial P/\partial V \ \Delta V \ , \tag{3.14}$$

where $1/(\partial P/\partial V)$ is the air compliance.

For the acoustic approximation the air compliance expression takes the form

$$C_{air} = 1/(\partial P/\partial V) = \frac{V}{\rho_{av}c^2} \ , \tag{3.15}$$

where ρ_{av} is the average air density, and c is the speed of sound in air.[8] Using the perfect gas relations

$$P = \rho RT$$

and

$$c = \sqrt{kRT} ,$$

and approximating the temperatures in each expression as being equal, the acoustic air compliance expression can be rewritten as

$$C_{air} = \frac{V}{kP_{av}} , \tag{3.16}$$

which is identical to the result obtained by applying conservation of energy assuming an adiabatic process of a perfect gas. (See Chapter 16 of reference [7].)

Yet another consequence of modeling air flow in the P-Q domain arises in the constitutive relations for the pneumatic servo-orifices, which now take the form

$$Q = \frac{dm/dt}{\rho_{av}} = C_d w z \sqrt{\frac{2}{\rho_{av}} (P_S - P)} , \tag{3.17}$$

where the approximations

$$h_s - h = \frac{P_s}{\rho_s} - \frac{P}{\rho}$$

and

$$\rho_s = \rho_{av} = \rho$$

have been made.

---

[8] Recall: $c = \sqrt{\partial P/\partial \rho}$

3.3.2 Simplified Hydraulic Subsystem

In the hydraulic subsystem oil compliance and inertia are neglected, reducing the order of the model further by two states. The compressibility of oil becomes a noticable effect when large loads are applied rapidly or with the damper valve closed, conditions in which the pneumatic subsystem plays a minor role, suggesting that modeling of the hydraulics as an isolated system for such cases would make more sense.

3.3.3 Description of Friction

Mechanical friction is modeled as a superposition of a time-invariant sliding friction force and a force varying linearly with velocity. In addition, the hardware is observed to possess significant *stiction* or breakaway friction (force to be overcome to initiate motion), and this is also included in the model. The static friction is rather unpredictable and increases with time when the ram is allowed to rest in one position. It is for this reason that a dither signal is often superimposed on the servovalve input in similar servo-systems. (The IBM RS/1 Robot uses such a dither signal in its electro-hydraulic servovalves [26].)

3.3.4 Simplified Bond Graph and Equations for Simulation

A bond graph model based on the simplifications described above appears in Figure 3-11. The pneumatic subsystem is modeled completely in the P-Q domain, the compressed and atmospheric air sources becoming constant pressure ports. Leakage past the pneumatic piston remains since the viscosity of air is quite low, and is assumed a linear function of the pressure drop across the piston. In the hydraulic case leakage (as well as oil compliance and inertia) is neglected reducing the passive hydraulic subsystem to a non-linear resistance *statically* modulated by the damper valve area and acting through a transformer.

It is straightforward to write state equations directly from the bond graph of Figure

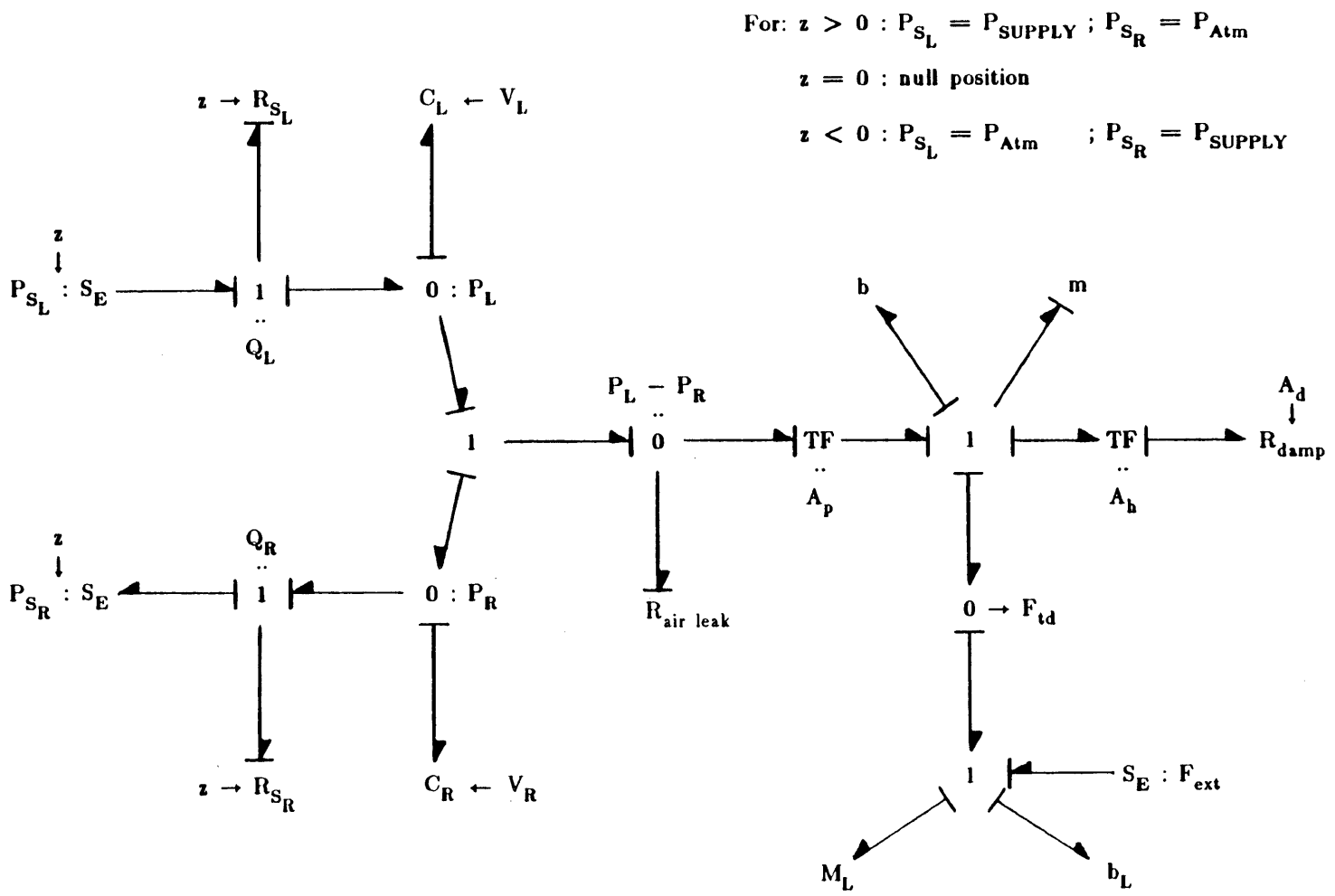

Figure 3-11: Simplified bond graph.

3-11 and the electro-pneumatic servovalve bond graph of Figure 3-8. Though the combined system contains only three independent energy storage elements, the resulting set of equations is fifth order due to the presence of two integrators in the system (one corresponding to the spool dynamics and the other the integration of velocity to obtain position).

The set of first order differential equations used for the non-linear simulation are given below. For the ram position:

$$\frac{d}{dt} x = v , \tag{3.18}$$

the ram velocity:

$$(m + M_L) \frac{d}{dt} v = A_p(P_L - P_R) - (b + b_L) v - A_h P_{hl} + F_{ext} + F_{coul} , \tag{3.19}$$

the left air chamber pressure:

$$\frac{V_L}{kP_{av}} \frac{d}{dt} P_L = Q_L - A_p v - R_{al} (P_L - P_R) , \tag{3.20}$$

the right air chamber pressure:

$$\frac{V_R}{kP_{av}} \frac{d}{dt} P_R = Q_R + A_p v + R_{al} (P_L - P_R) , \tag{3.21}$$

and the spool position:

$$T \frac{d}{dt} z = -z + K_s I . \tag{3.22}$$

Expressions for the auxiliary variables follow. For the left air chamber volume:

$$V_L = V^* + A_p x , \tag{3.23}$$

the right air chamber volume:

$$V_R = V^* - A_p x , \tag{3.24}$$

the hydraulic load pressure:

$$P_{hl} = \left[\frac{A_h}{C_{do} A_d} \right]^2 \frac{\rho_{oil}}{2} |v| v , \tag{3.25}$$

the left air chamber volume flow rate:

$$Q_L = C_d w\,|z|\,\sqrt{\frac{2}{\rho_{av}}\,|P_{S_L} - P_L|}\;\;\mathrm{sgn}(P_{S_L} - P_L)\;, \tag{3.26}$$

and the right air chamber volume flow rate:

$$Q_R = C_d w\,|z|\,\sqrt{\frac{2}{\rho_{av}}\,|P_{S_R} - P_R|}\;\;\mathrm{sgn}(P_{S_R} - P_R)\;. \tag{3.27}$$

In the next section this simplified (but still non-linear) model is simulated using Runge-Kutta fourth order integration and is shown to match the response of the experimental hardware with tolerable error for a variety of conditions.

3.3.5 Performance of the Non-linear Model

The objective of this section is to demonstrate that the non-linear model does indeed work and can be used to design the actuator. After writing the equations of the previous section in dimensionless form, the model is applied to three cases of increasing complexity:

1. The open-loop time response of force output for a step in servo-current with the servovalve initially in the null position and the ram immobilized.
2. The open-loop time response of ram velocity for a step input with the ram initially at rest.
3. The closed-loop time response of ram position for a step in the command position using linear position feedback.

3.3.5.1 Non-linear Model in Dimensionless Form

Before attempting to program the equations of Section 3.3.4 for digital simulation it is convenient to convert the model into dimensionless form. This simplifies the numerical integration in addition to arranging the system parameters into a form useful from a design viewpoint.

The dimensionless state, control, and auxiliary variables and their corresponding reference

parameters are defined in Tables 3-I and 3-II. The remaining dimensionless parameters are summarized in Table 3-III and the resulting dimensionless state and auxilliary equations appear in Appendix A.

3.3.5.2 Force Response With Ram Immobilized

With the experimental hardware and sensors avaliable a very simple test of the pneumatic portion of the model can be performed by immobilizing the cylinder ram and recording the time response of the force output. Since the effects of sliding friction, load inertia, and passive hydraulic damping are temporarily eliminated, the servovalve flow, air compliance, and leakage coefficients are determined independent of other parameters. In addition, the force time history becomes a good indication of the delay time required to fill and empty the cylinder chambers and how the response time changes as the chamber volumes change.

A schematic of the experimental set-up showing the three ram positions used appears in Figure 3-12a. Because of the nature of the servovalve, it is not possible for the pressures in each chamber to be initially at atmospheric pressure. These pressures equalize at a value dependent upon the valve's leakage at in the null position (approximately 80% of the supply pressure). Hence the time response of the output force depends as much on flow out of the exhaust chamber as flow from supply.

With the ram immobilized the dimensionless model (see Appendix A) becomes third order. For the left air chamber pressure:

$$\frac{\gamma_L}{kp_{av}} \frac{x^*}{v^*} \omega_n^* \frac{d}{d\tau} p_L = C_d a_s \sqrt{\frac{1}{r_\rho}(p_S - p_L)} - l_a(p_L - p_R) , \tag{3.28}$$

and the right air chamber pressure:

$$\frac{\gamma_R}{kp_{av}} \frac{x^*}{v^*} \omega_n^* \frac{d}{d\tau} p_R = -C_d a_s \sqrt{\frac{1}{r_\rho}(p_R - p_{Atm})} + l_a(p_L - p_R) , \tag{3.29}$$

and the spool position:

Table 3-I: Dimensionless State, Control, and Auxiliary Variables

STATE VARIABLES	
Ram Position	$s_x = \frac{x}{x^*}$
Ram Velocity	$s_v = \frac{v}{v^*}$
Left Air Chamber Pressure	$p_L = \frac{P_L}{P^*}$
Right Air Chamber Pressure	$p_R = \frac{P_R}{P^*}$
Pneumatic Servo-Orifice Area	$a_s = \frac{wz}{wz^*}$
AUXILIARY VARIABLES	
Left Air Chamber Volume	$\mathcal{V}_L = \frac{V_L}{V^*}$
Right Air Chamber Volume	$\mathcal{V}_R = \frac{V_R}{V^*}$
Left Air Chamber Volume Flow Rate	$q_L = \frac{Q_L}{A_p v^*}$
Right Air Chamber Volume Flow Rate	$q_R = \frac{Q_R}{A_p v^*}$
Hydraulic Load Pressure	$p_{hl} = \frac{P_{hl}}{P^*_{hl}}$
External Force	$f_{ext} = \frac{F_{ext}}{A_p P^*}$
Coulomb Friction	$f_{coul} = \frac{F_{coul}}{A_p P^*}$
DIMESIONLESS TIME	$\tau = \omega_n^* t$
DIMENSIONLESS CONTROL VARIABLE	
Pneumatic Servo-Current	$i_s = \frac{I}{I^*}$
DIMENSIONLESS CONTROL PARAMETER	
Damper Valve Orifice Area	$a_d = \frac{A_d}{A_d^*}$

Table 3-II: Reference Variables

Air Pressure	P^*	=	P_{SUPPLY}	= 125 psia	=	$1.8\text{x}10^4 \frac{lb_f}{ft^2}$
Air Temperature	T^*	=	T_{SUPPLY}	= 60 oF	=	520 oR
Air Density	ρ^*	=	$\frac{P^*}{RT^*}$	= $1.2\text{x}10^{-5} \frac{slugs}{in^3}$	=	$0.02 \frac{slugs}{ft^3}$
Air Chamber Volume	V^*	=	V_I	= $6.0\ in^3$	=	$3.5\text{x}10^{-3}\ ft^3$
Spool Position	z^*	=	z_{max}	= 0.020 in	=	0.0017 ft
Ram Position	x^*	=	$\frac{V^*}{A_p}$	= 5.6 in	=	0.47 ft
Ram Velocity	v^*	=	$\frac{wz^*}{A_p}\sqrt{2RT^*}$	= $113 \frac{in}{sec}$	=	$9.4 \frac{ft}{sec}$
Pneumatic Servo-Current	I^*	=	I_{rated}	= 10 ma		
Damper Orifice Area	A_d^*	=	$(A_d)_{max}$	= $0.028\ in^2$	=	$1.9\text{x}10^{-4}\ ft^2$
Hydraulic Load Pressure	P_{hl}^*	=	$\left[\frac{A_h v^*}{A_d^*}\right]^2 \frac{\rho_{oil}}{2}$	= 30.5 psid	=	$4.4\text{x}10^3 \frac{lb_f}{ft^2}$
Air Stiffness	K^*	=	$\frac{A_p^2 P^*}{V^*}$	= $24 \frac{lb_f}{in}$	=	$290 \frac{lb_f}{ft}$
Viscous Damping	b^*	=	$\frac{A_p P^*}{V^*}$	= $1.2 \frac{lb_f\text{-sec}}{in}$	=	$14 \frac{lb_f\text{-sec}}{ft}$
Natural Frequency	ω_n^*	=	$\sqrt{K^*/m}$	= $76 \frac{rad}{sec}$		
Damping Ratio	ζ^*	=	$\frac{b^*}{2\sqrt{K^* m}}$	= 1.9		

where w = Servovalve port width = 0.37 in = 0.031 ft

A_p = Pneumatic piston area = $1.1\ in^2$ = $7.5\text{x}10^{-3}\ ft^2$

A_h = Hydraulic piston area = $0.2\ in^2$ = $1.4\text{x}10^{-4}\ ft^2$

m = Actuator mass = 1.6 lb_m = 0.050 slugs

Table 3-III: Dimensionless Parameters

Actuator Viscous Damping Coefficient	$\delta_b = \frac{b}{b^*}$
Hydraulic Damping Coefficient	$\delta_h = \frac{A_h}{A_p} \frac{P_{hl}^*}{P^*}$
Air Leakage Coefficient	$l_a = \frac{R_{al}}{A_p^2} b^*$
Mass Ratio	$r_m = \frac{m + M_L}{m}$
Damping Coefficient Ratio	$r_b = \frac{b + b_L}{b}$
Average Air Density Ratio	$r_\rho = \frac{\rho_{av}}{\rho^*}$
Average Air Pressure Ratio	$p_{av} = \frac{P_{av}}{P^*}$
Linearized Flow Gain	$c_z = \frac{C_z z^*}{A_p v^*}$
Linearized Load Pressure Flow Sensitivity	$c_p = \frac{C_p}{2A_p^2} b^*$

$$T\,\omega_n^* \frac{d}{d\tau} a_s = -a_s + i_s \,, \tag{3.30}$$

where

$$f_{out} = p_L - p_R - f_{coul} \,. \tag{3.31}$$

Parameter values used in these simulations and those of the following two sections discussing the open-loop velocity and closed-loop position responses, respectively, are summarized in Table 3-IV.

The model and hardware responses appear in Figure 3-12b, c, and d showing the change in response time as the supply chamber volume increases and the exhaust chamber volume decreases. Clearly the venting of air from the exhaust chamber is the dominant effect. As the exhaust chamber volume decreases the force output reaches steady state in less time. This effect is due mostly to the high initial pressure in each chamber. The supply chamber need only raise its pressure by about 20% of the supply pressure, while the exhaust chamber must lower its pressure from 80% of supply to atmospheric pressure (about 10% of supply for P^* equal to 125 psia).

For this simple case the model and hardware results show good agreement. Note that the dimensionless steady state force output is not equal to unity as might first be expected. This is a consequence of normalizing the model with respect to absolute pressure rather than pressure above atmospheric. Barring non-ideal effects the maximum possible dimensionless force output would be

$$f_{max} = \frac{(P^* - P_{Atm})A_p}{P^* A_p} = 0.88 \,.$$

But because of leakage and the coulomb friction force in the cylinder seals, the actuators dimensionless force output is approximately 0.82, or 93% of its maximum possible value.

Table 3-IV: Dimensionless Parameter Values Used for Simulations

Actuator Viscous Damping Coefficient	δ_b	=	0.40
Hydraulic Damping Coefficient	δ_h	=	0.76
Air Leakage Coefficient	l_a	=	0.050
Mass Ratio	r_m	=	0.37
Damping Coefficient Ratio	r_b	=	1.0
Average Air Density Ratio	r_ρ	=	0.81
Average Air Pressure Ratio	p_{av}	=	0.64
Ratio of Specific Heats	k	=	1.4
Pneumatic Servovalve Time Constant	$T\ \omega_n^*$	=	0.6
Pneumatic Servovalve Discharge Coefficient	C_d	=	0.65
Hydraulic Damper Valve Discharge Coefficient	C_{do}	=	0.16
Atmospheric Pressure Ratio	p_a	=	0.12
External Force	f_{ext}	=	0.0

Coulomb Friction

–No Hydraulic Damping	f_{stat}	=	0.044	f_{slip}	=	0.016
–Hydraulic Damping	f_{stat}	=	0.052	f_{slip}	=	0.030

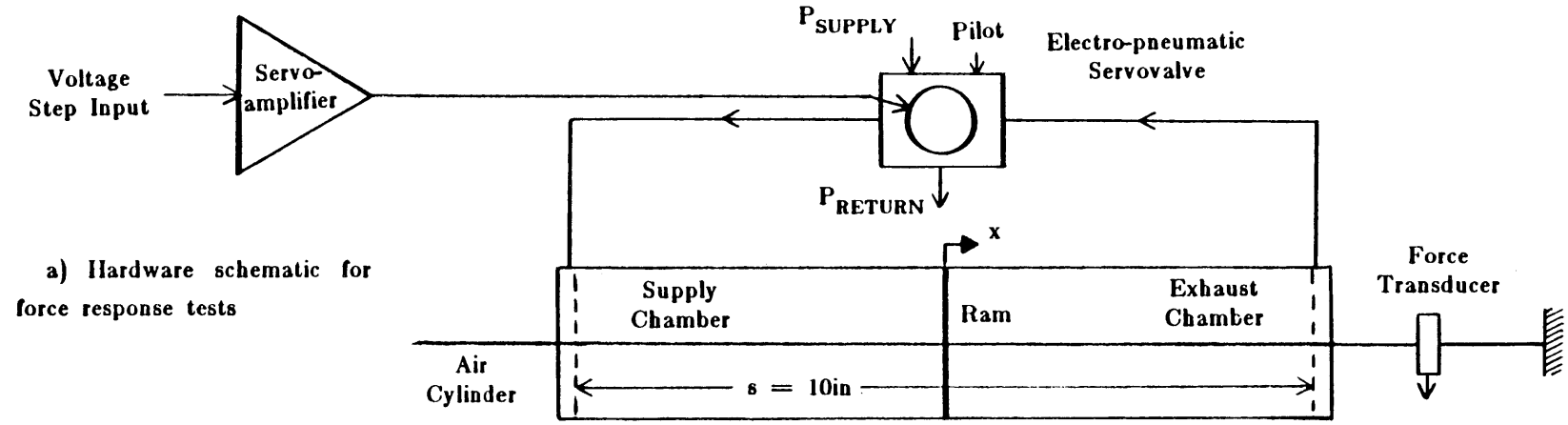

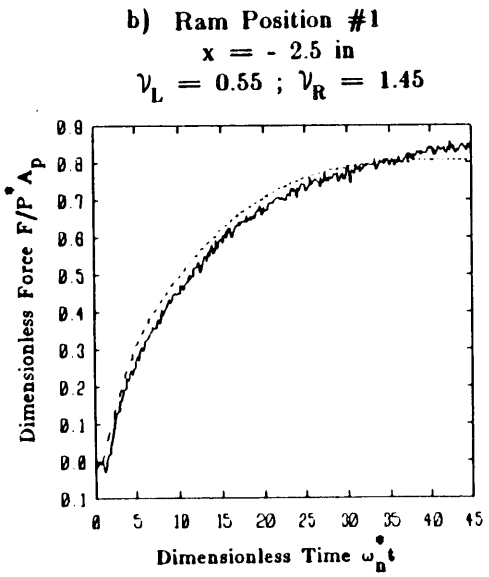

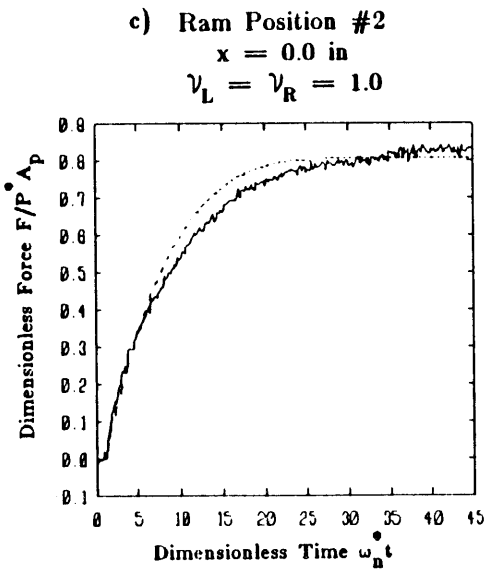

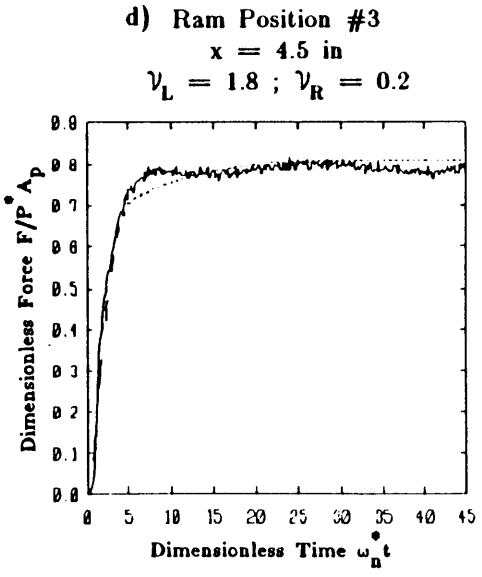

Figure 3-12: Force response with the actuator immobilized.

3.3.5.3 Open-loop Velocity Response

The results of the previous section provide some confidence in the relations and parameter values used to describe the air dynamics of the actuator. Simulating the velocity response requires the full fifth order model and demands the appropriate choice of several more critical parameter values. The most important of these being the mechanical and hydraulic friction parameters.

Figure 3-13 compares three hardware and model responses for various damper valve settings and a fourth in which the passive hydraulic sub-system has been physically removed. Note that the time required for deceleration after the step is turned off increases as hydraulic damping is increased. This is counterintuitive, as one would expect motion to cease more quickly when power is shut off in highly damped system. Before the actuator can come to rest though, more time is required to equalize the chamber pressures, since a greater damping force results in a larger pressure drop across the pneumatic piston for a given step magnitude.

It is assumed that the removal of the hydraulic damper will decrease the static and sliding friction forces since one less set of piston and rod seals is present to impede motion. This assumption is reflected in the choice of coulomb friction parameters for the two cases (see Table 3-IV).

It may appear that the friction parameters are simply being *juggled* in order to fit the experimental response. Please note however, that the set of friction parameters chosen for each configuration (one set for cases in which the hydraulic damper is included and another set for cases in which it is not) are unchanged throughout *all* the simulations presented. Even were this not the case, much is to be learned from a model in which only one parameter (e.g. damping) need be adjusted to characterize the response of a system.

No Hydraulic Damping

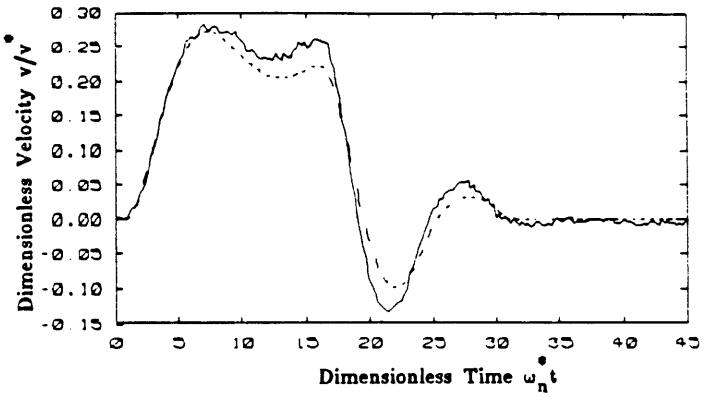

$a_d = 1.0$

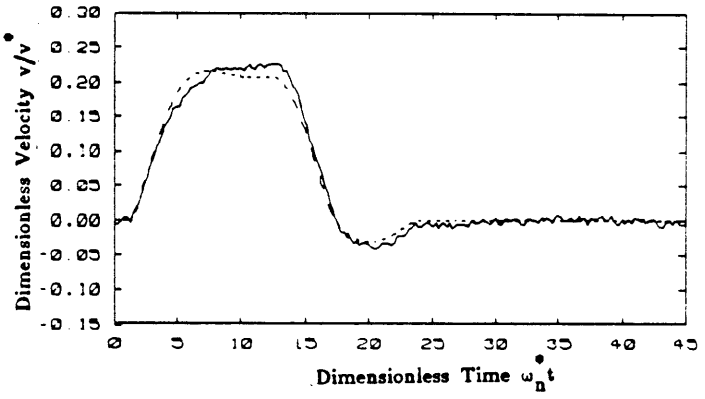

$a_d = 0.63$

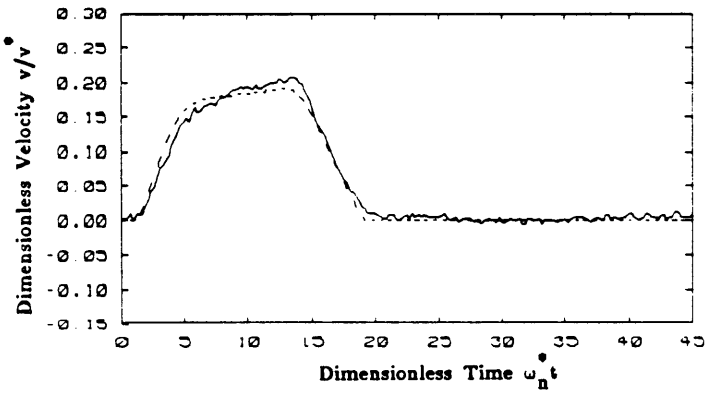

$a_d = 0.31$

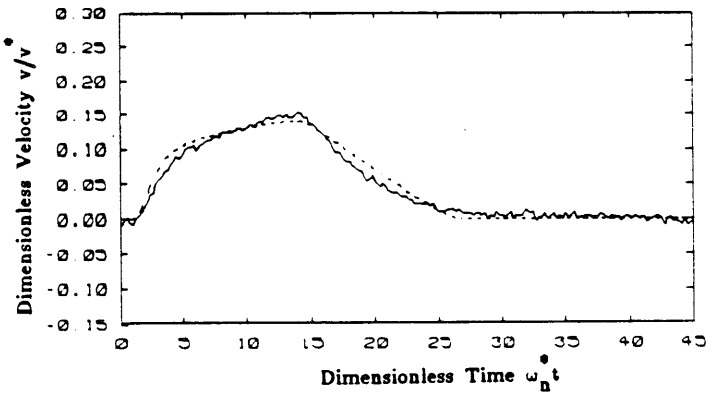

Figure 3-13: Open-loop velocity response.

3.3.5.4 Closed-Loop Position Response

Having arrived at acceptable parameter values in the previous section, the addition of linear feedback to the model is straightforward, requiring only that the feedback law be expressed in the appropriate dimensionless form. The details of this task are presented in Appendix B for position control as well as the other types of feedback considered later. Briefly, the control law in this case is given simply as

$$i_s = k_x(s_{x_{set}} - s_x) , \tag{3.32}$$

where

$$k_x = \frac{K_a K_x x^*}{I^*} ,$$

K_a being the servoamp gain in ma/volt and K_x the position gain in volts/ft.

Figure 3-14 compares the model and hardware responses for $k_x = 1.3$ (or $K_a K_x = 28$ ma/ft) and $k_x = 1.7$ (or $K_a K_x = 37$ ma/ft) for two cases with identical conditions save that the passive hydraulic damper has been removed in one case.[9]

A shortcoming of the model brought to light in these simulations lies in the model's steady state behavior. After the real actuator comes to rest *near* the command position, the effects of static friction and servovalve leakage past the spool near the null position combine to keep the ram at rest even though the position error produces a non-zero current input to the servovalve. The model instead exhibits a limit cycle behavior in which the position error allows flow into the cylinder raising the supply chamber pressure and decreasing the exhaust chamber pressure until the stiction threshold is reached. The simulated position response then *jumps* to the other side of the command position to a point where the chamber pressures have equalized enough such that stiction has stopped motion. An error signal of opposite

---

[9]Parameter values are given in Table 3-IV.

$k_x = 1.3$

$(K_a K_x = 28$ ma/ft)

No Hydraulic Damping

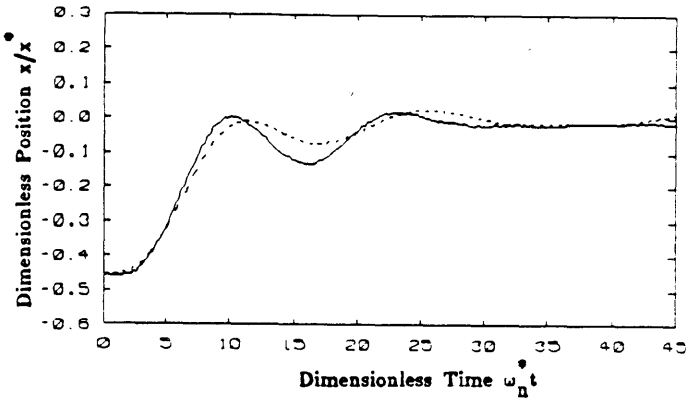

$k_x = 1.3$

$(K_a K_x = 28$ ma/ft)

$a_d = 1.0$

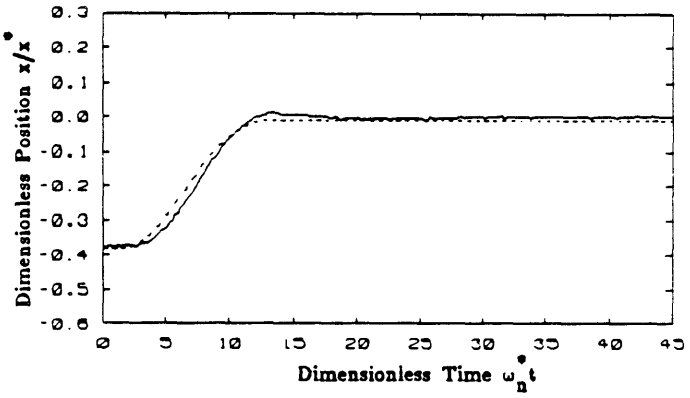

$k_x = 1.7$

$(K_a K_x = 37$ ma/ft)

No Hydraulic Damping

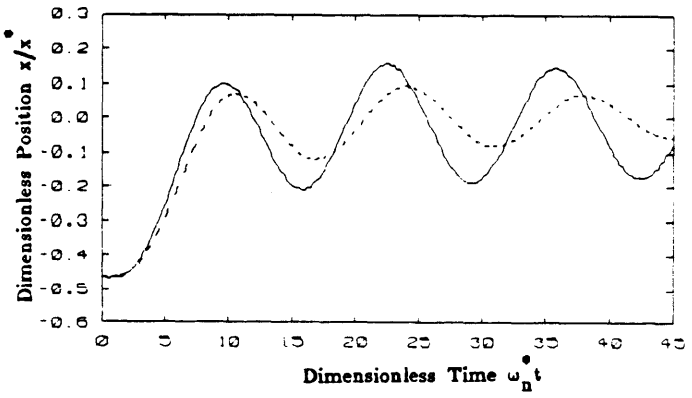

$k_x = 1.7$

$(K_a K_x = 37$ ma/ft)

$a_d = 1.0$

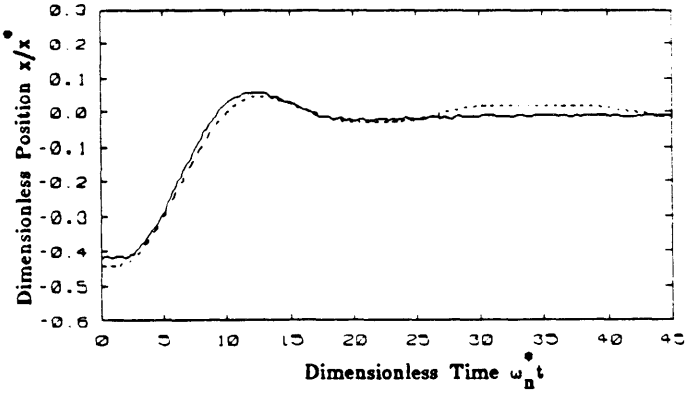

Figure 3-14: Closed-loop position response.

polarity is then present causing the simulated phenomenon to repeat indefinitely.

The form of the model might be improved both by including a description of air leakage past the servovalve spool and by developing a more sophisticated model of static friction. The benifits of such an approach are unclear and left as an area for further work.

Allowing for supply pressure, ram velocity, and gain measurement errors, errors in servovalve nulling, and the approximate nature of the model, the agreement between the simulations and the actual response is satisfactory, providing a useful tool for further analysis and future design of the actuator.

Chapter 4
Linear Analysis of the Hybrid Actuator

4.1 Linear Modeling Strategy

The non-linear analysis of Chapter 3 shows good agreement between the model and hardware responses and can be used to investigate parameter changes and test controller designs. However, the model is difficult to apply to the actual selection of controller types and feedback gain values. Though non-linear control design techniques do exist, the simplicity offered by the wide body of linear control theory available ([23], [20], [8], etc.) makes an applicable linear analysis a practical objective.

In this chapter a linearized model is first developed via a first-order Taylor series expansion of the non-linear state equations, reducing the model to a form similar to a linear model found in Chapter 16 of reference [7]. Evaluating the resulting partial derivatives associated with the pneumatic and hydraulic valve flow expressions is non-trivial since the linearized parameters tend to vary appreciably with the choice of operating point. In fact, because of the passive nature of the hydraulic damper, this technique of estimating parameter values breaks down completely when a stationary operating point is used, the corresponding partial derivative being identically zero.[10] This is not a problem if a velocity servomechanism is to be designed, since a non-stationary operating point is implied (defined by the desired steady state load velocity). Recall however, that the objective is to design an impedance controller, implying that the operating point must be stationary (i.e. having zero steady state

---

[10]Paynter [24] makes the distinction between static and stationary operating points in which a static operating point implies that none of the states change with time but all of the flow variables are non-zero, while a stationary operating point is one in which the flow variables are indeed zero.

load velocity and zero hydraulic damper flow).

To avoid the problem of static versus stationary operating points, the Taylor series expansion is used only to determine the form of the linear model. Instead of attempting to evaluate the partial derivatives, parameter values are chosen based on the experimental frequency response.

4.2 Linearization Via a First-order Taylor Series Expansion

Before expanding the non-linear equations of Chapter 3 into a Taylor series approximation two more simplifying assumptions are made:

1. Air compliance is given a constant mean value rather than being modulated by the change in air chamber volume with ram motion.
2. Coulomb friction is neglected.

The first assumption simplifies the series expansion and as will be seen (following more assumptions) allows the two air chamber pressures to be combined into a single state refered to as the pneumatic load pressure, P_{pl}, and defined as

$$P_{pl} = P_L - P_R .$$

Note also that, in the absence of position feedback, knowledge of the ram position is no longer required to simulate the velocity response. Hence, the resulting linearized model is only third order.

The loss of information implied by the second assumption is part of the price paid in obtaining the linearized model. Methods do exist for describing such non-linear effects in a linear analysis (such as describing functions [23] and statistical linearization [6]), however it is hoped (and later shown) that a model in which mechanical friction is assumed only linearly dependent on velocity is adaquate for controller design.

The most difficult part of this approach arises in the series expansion of the pneumatic

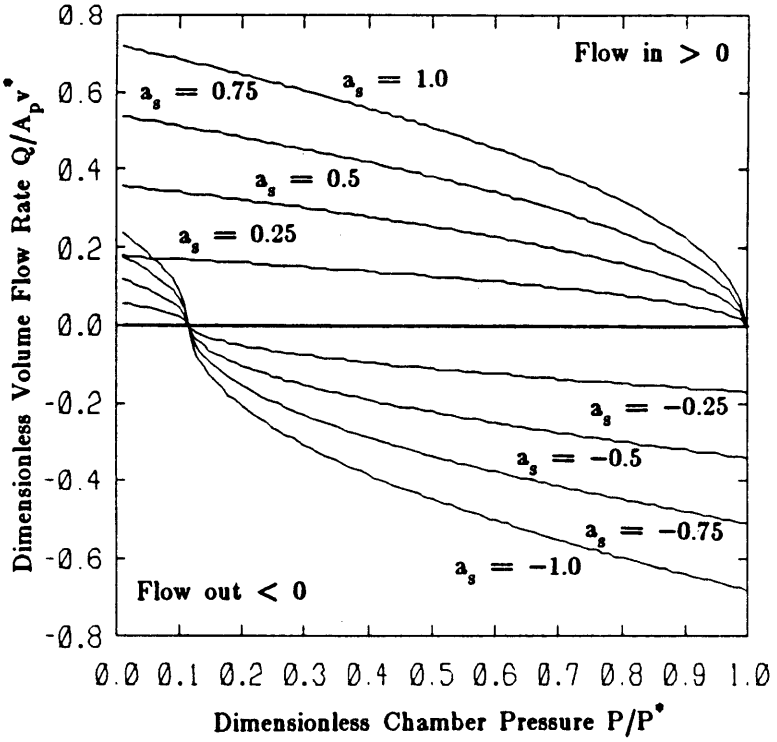

Figure 4-1: Ideal dimensionless pressure/volume flow characteristics.

orifice flow relations shown in Figure 4-1 in dimensionless form. Not only are the volume flow equations of Section 3.3.4 highly non-linear, they are also quite discontinuous, aggrevating the search for a linear, continuous description. This problem is hardly a new one, and there are several possible ways to proceed [21], [2]. The method used here is based on a somewhat qualitative argument found in reference [7] and proceeds as follows.

The volume flows through the servo-orifices (whether from supply or to exhaust) are assumed to be functions of the orifice area (which is a function of the servovalve spool position) and the pressure within the respective cylinder chamber only. Hence, the series expansions for the volume flows take the form

$$\frac{\partial Q_L}{\partial X}\Delta X = k_{P_L}\Delta P_L + k_{z_L}\Delta z \ , \tag{4.1}$$

and

$$\frac{\partial Q_R}{\partial X}\Delta X = k_{P_R}\Delta P_R + k_{z_R}\Delta z \ , \tag{4.2}$$

where $\Delta \mathbf{X}$ is the incremental state vector and

$$k_{z_L} = \frac{\partial Q_L}{\partial z}, \qquad k_{P_L} = \frac{\partial Q_L}{\partial P_L},$$
$$k_{z_R} = \frac{\partial Q_R}{\partial z}, \qquad k_{P_R} = \frac{\partial Q_R}{\partial P_R}.$$

Putting aside for the moment the task of selecting values for the constant coefficients, a good place to start is to choose their signs such that the linearized expressions at least predict the polarity of flow and flow changes correctly. With the theoretical pressure/flow characteristics of Figure 4-1 in mind, consider the possible flow conditions summarized below.

SPOOL POSITION	LEFT AIR CHAMBER	RIGHT AIR CHAMBER
$z > 0$	$Q_L > 0$ Flow into left chamber	$Q_R < 0$ Flow out of right chamber
	increase z: increase $+Q_L$	increase z: increase $-Q_R$
	increase P_L: decrease $+Q_L$	increase P_R: increase $-Q_R$
$z < 0$	$Q_L < 0$ Flow out of left chamber	$Q_R > 0$ Flow into right chamber
	increase z: increase $-Q_L$	increase z: increase $+Q_R$
	increase P_L: increase $-Q_L$	increase P_R: decrease $+Q_R$

Defining the coefficients C_{z_L}, C_{z_L}, C_{P_L}, and C_{z_R} as positive constants, the signs of the partial derivatives satisfying the conditions listed above are such that

$$k_{z_L} = C_{z_L}, \qquad k_{P_L} = -C_{P_L},$$
$$k_{z_R} = -C_{z_R}, \qquad k_{P_R} = -C_{P_R}.$$

Since the servovalve is symmetric it is reasonable to assume

3) $C_{z_L} = C_{z_R} = C_z$.

If in the initial state the externally applied load is small, it can be assumed that the initial chamber pressures are equal, or

4) $P_{L_{initial}} = P_{R_{initial}}$.

It is further assumed that[11]

5) $C_{P_L} = C_{P_R} = C_P$.

With assumptions 1, 3, 4, and 5 it is possible to combine the two chamber pressure states into a single state equation describing air flow in the actuator.

Based on the five assumptions of this section and the assumptions of the previous sections the resulting linearized model reduces to three relatively simple state equations. For the ram velocity:

$$(m + M_L) \frac{d}{dt} v = A_p P_{pl} - (b + b_L + b_h) v + F_{ext} , \tag{4.3}$$

and the pneumatic load pressure:

$$C_{air} \frac{d}{dt} P_{pl} = C_z z - A_p v - [C_p/2 + R_{al}] P_{pl} , \tag{4.4}$$

and the servovalve spool position:

$$T \frac{d}{dt} z = -z + K_s I , \tag{4.5}$$

where

$$C_{air} = \frac{V^*}{2kP_{av}} .$$

---

[11] In reference [7] it is argued that assumption 5 is reasonable provided the variation of the chamber pressures from their initial equilibrium values is not more than a few percent.

A bond graph corresponding to the linear model appears in Figure 4-2, while the model in dimensionless form can be found in Appendix A.

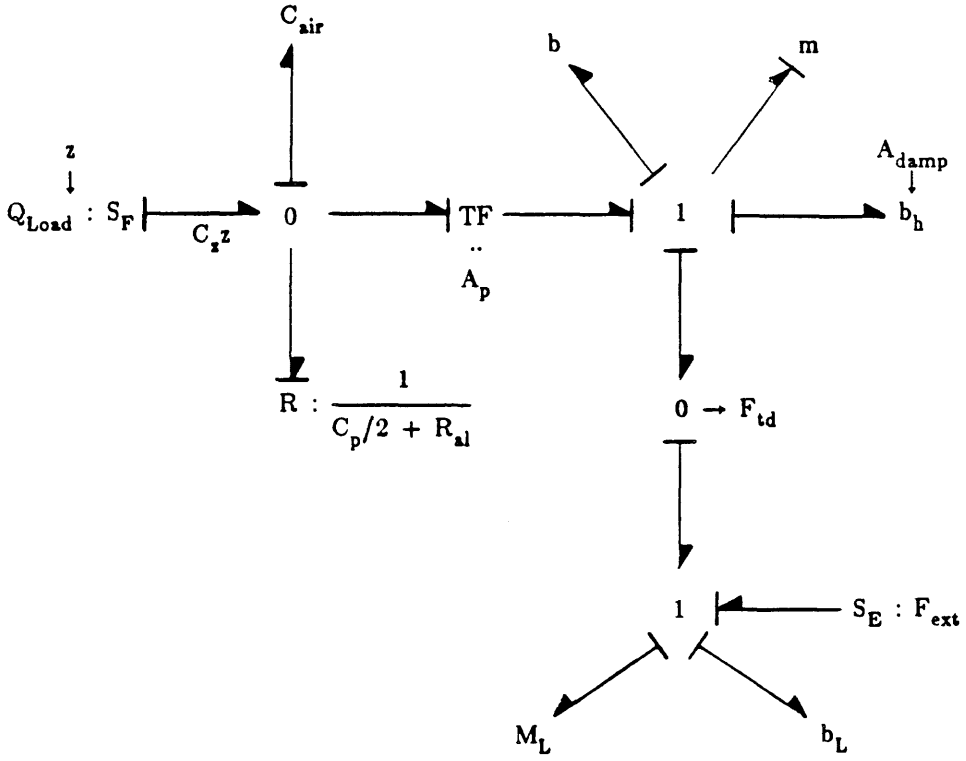

Figure 4-2: Bond graph corresponding to the linear model.

4.3 Experimental Frequency Response

Upon examination of the linear equations of the previous section it is seen that many of the parameters are already known from the non-linear analysis. Only the pneumatic flow and hydraulic damping coefficients (C_z, C_P, and b_h) need be determined.

Two transfer functions relating the load velocity to the input servo-current—one corresponding to the complete third order model and the other corresponding to a second order model neglecting the electro-pneumatic servovalve dynamics—are given below.

For the complete linear model

$$v(s) = \frac{\left[\frac{G_o}{TC_{air}M_T}\right]I(s) + \frac{1}{M_T}\left[\left(s + \frac{1}{T}\right)\left(s + \frac{C_1}{C_{air}}\right)\right]F_{ext}(s)}{s^3 + \left[\frac{1}{T} + \frac{C_1}{C_{air}} + \frac{B_o}{M_T}\right]s^2 + \left[\frac{1}{T}\left(\frac{C_1}{C_{air}} + \frac{B_o}{M_T}\right) + \frac{C_1B_o + A_p^2}{C_{air}M_T}\right]s + \left[\frac{C_1B_o + A_p^2}{TC_{air}M_T}\right]} \quad (4.6)$$

or, neglecting spool dynamics

$$v(s) = \frac{\left[\frac{G_o}{C_{air}M_T}\right]I(s) + \frac{1}{M_T}\left(s + \frac{C_1}{C_{air}}\right)F_{ext}(s)}{s^2 + \left[\frac{C_1}{C_{air}} + \frac{B_o}{M_T}\right]s + \left[\frac{C_1B_o + A_p^2}{C_{air}M_T}\right]} \quad (4.7)$$

where the following coefficients have been defined:

$$G_o = C_z K_s A_p ,$$

$$C_1 = C_P/2 + R_{al} ,$$

$$M_T = m + M_L ,$$

and

$$B_o = b + b_h + b_L .$$

Figures 4-3, 4-4, and 4-5 show the experimental frequency response for different inertial loading, different supply pressures, and different hydraulic damping conditions, respectively. Because the system is so inherently non-linear the response is amplitude dependent as well as difficult to evaluate at low frequencies as the ram tends to get hung up by static friction when changing direction of motion, introducing transients into the response.

For a third order system one would expect the phase shift at high frequencies to approach −270 deg. Before this can happen though, the limited bandwidth of the second

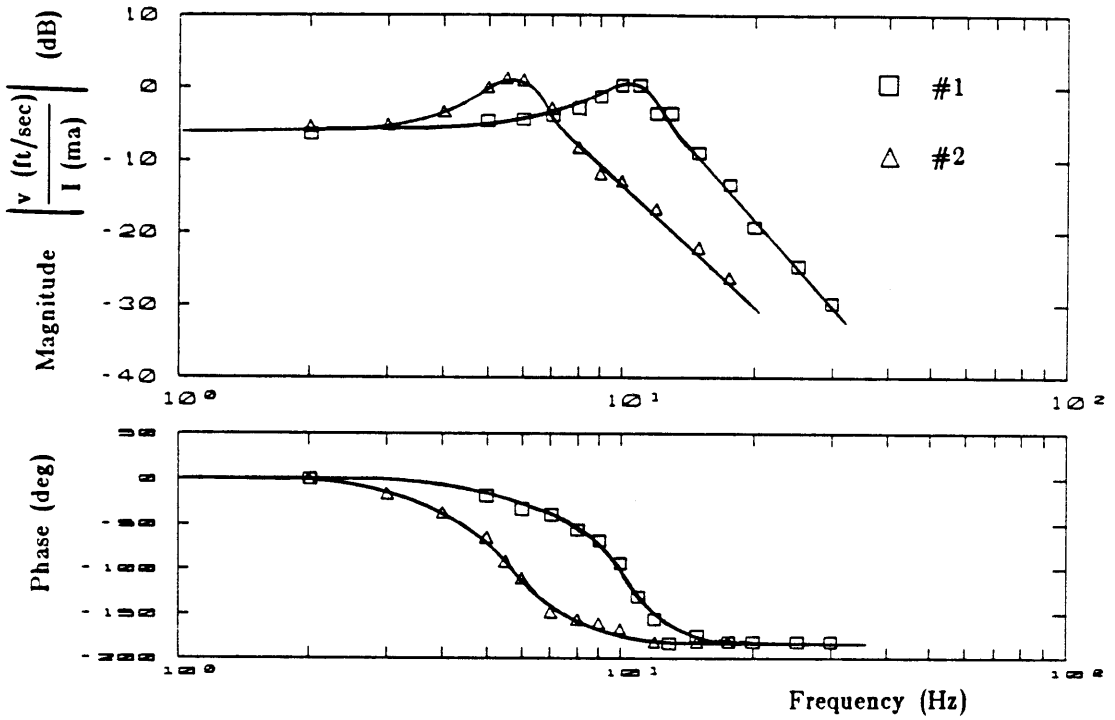

m_1 = 0.11 slugs m_2 = 0.37 slugs P_{SUPPLY} = 110 psig

Figure 4-3: Experimental frequency response – Variable mass/no hydraulic damping.

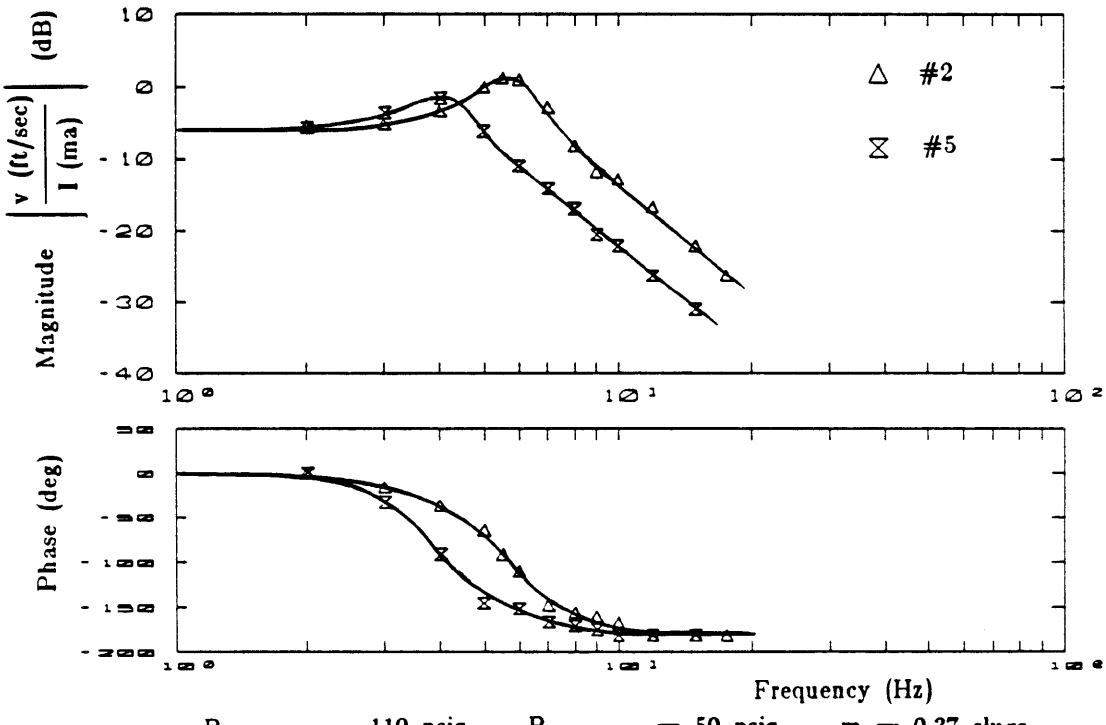

$P_{SUPPLY2}$ = 110 psig $P_{SUPPLY5}$ = 50 psig m = 0.37 slugs

Figure 4-4: Experimental frequency response – Variable pressure/no hydraulic damping.

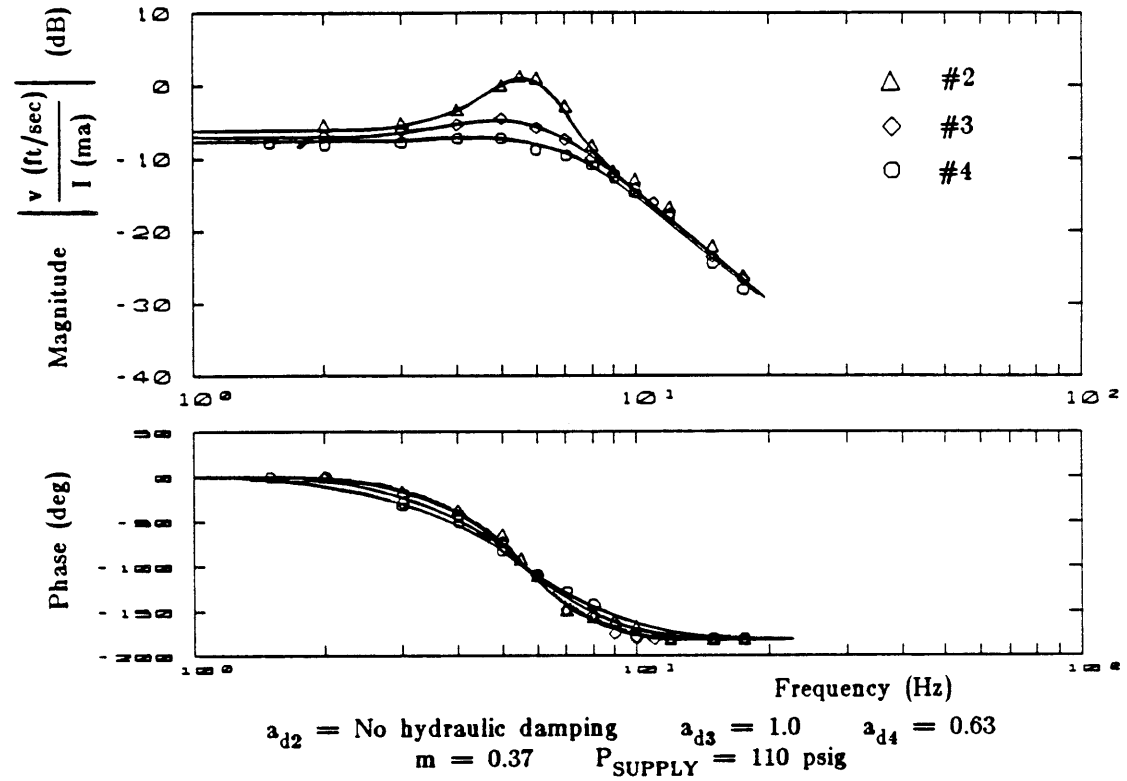

Figure 4-5: Experimental frequency response – Variable hydraulic damping.

order inertial load/air compliance dynamics (approximately 8 hz for $M_L = 0$ and $P_s = 110$ psig) allows static friction in the actuator to halt motion completely above approximately 20 hz. This implies that as inertial loading on the actuator increases (decreasing the bandwith–Figure 4-3), or as the air stiffness decreases because of lower supply pressure (also decreasing the bandwith–Figure 4-4) the first order spool dynamics become less important. This is not to say that servovalve dynamics should be forgotten entirely, for if the inertial load/air compliance bandwidth could be increased enough, say in the case of minimal loading or increased air stiffness due to higher supply pressure or smaller cylinder chamber volumes, then the first order lag corresponding to spool dynamics would effect both the frequency and transient responses.

Based on the reasoning of the preceding paragraph the theoretical transfer function neglecting spool dynamics, equation (4.7), is used for the majority of the analysis. Figure

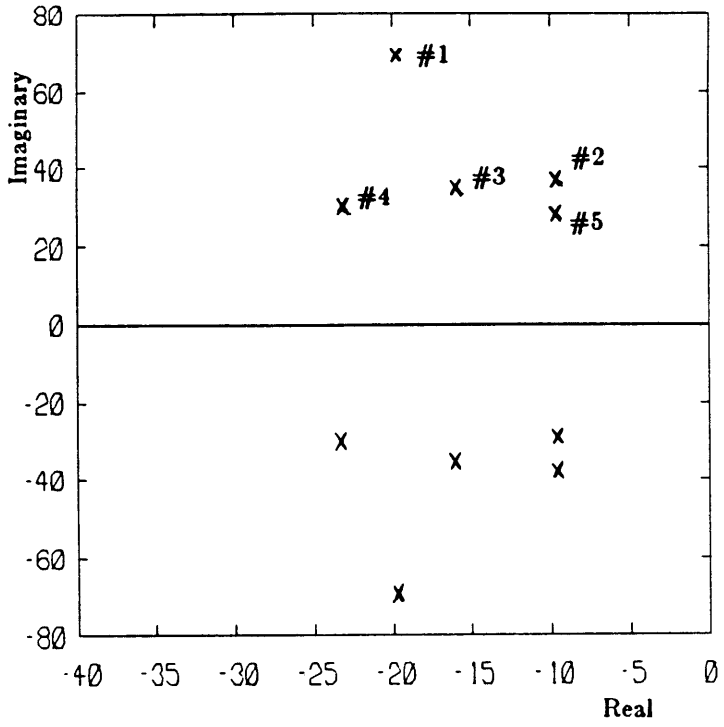

Figure 4-6: Placement of open-loop poles corresponding to experimental frequency responses.

4-6 shows the placement of open-loop poles in the complex plane corresponding to a second order fit of the five frequency responses performed. In order to derive parameter values for the linear model the second order transfer function is used to fit the experimental frequency response. Parameters used for the linear analysis are summarized in Table 4-I.

The reader will note that C_1 is given a value of zero. Recall that C_1 represents the combined effect of air leakage past the pneumatic ram and the loss of servovalve flow due to increased load pressure. Shearer [7] reasons that these effects are small provided that leakage is minimized by proper seal design and a critical lap (or closed-center) servovalve is used. Basically, this amounts to assuming that mechanical friction and the passive hydraulics provide the majority of damping in the system. The marvelous simplicity offered by setting C_1 equal to zero also serves to motivate the approximation.

Table 4-I: Parameters Used in Linear Analysis

Pneumatic Piston Area	$A_p = 1.1\ in^2 = 7.5x10^{-3}\ ft^2$
Payload Mass	$M_L = 10.3\ lb_m = 0.32\ slugs$
Total Mass	$M_T = 11.9\ lb_m = 0.37\ slugs$
Payload Damping	$b_L = 0.0\ \frac{lb_f\text{-sec}}{ft}$
Air Compliance	$C_{air} = 0.027\ \frac{in^5}{lb_f} = 1.1x10^{-7}\ \frac{ft^5}{lb_f}$
Servovalve Time Constant	$T = 8.0x10^{-3}\ sec$
No Hydraulic Damping	$G_o = 6.6x10^{-5}\ \frac{ft^4\text{-sec}}{ma}$
	$B_o = 7.0\ \frac{lb_f\text{-sec}}{ft}$
	$C_1 = 0.0\ \frac{ft^5}{lb_f\text{-sec}}$
Hydraulic Damping $a_d = 1.0$	$G_o = 5.3x10^{-5}\ \frac{ft^4\text{-sec}}{ma}$
	$B_o = 11.8\ \frac{lb_f\text{-sec}}{ft}$
	$C_1 = 0.0\ \frac{ft^5}{lb_f\text{-sec}}$
Hydraulic Damping $a_d = 0.63$	$G_o = 4.9x10^{-5}\ \frac{ft^4\text{-sec}}{ma}$
	$B_o = 16.7\ \frac{lb_f\text{-sec}}{ft}$
	$C_1 = 0.0\ \frac{ft^5}{lb_f\text{-sec}}$

4.4 Linear Model Augmented With Feedback

After adding position, velocity, and force feedback to the linear model, the second order transfer function of the previous section becomes third order (because the position state must be included). While the control law (in terms of model variables) for position and velocity feedback is trivial, the addition of force feedback is not simple and it is helpful to consider the bond graph of the linear model (Figure 4-2). Since the assignment of integral causality to either the actuator mass (m) or the workpiece mass (M_L) is arbitrary, the force transducer output has two possible expressions: either a sum forces acting on the actuator side of the interaction port,

$$F_{td} = A_p P_{pl} - (b + b_h)\, v - m\frac{d}{dt}v \,, \tag{4.8}$$

or the sum of forces on the environment side,

$$F_{td} = M_L\frac{d}{dt}v + b_L v - F_{ext} \,. \tag{4.9}$$

The choice is arbitrary since both expressions yield the same results, which are given in Figure 4-7.

4.4.1 Results of Position and Velocity Feedback

With position feedback only (K_v and $K_F = 0$) the root locus of Figure 4-8a shows the dominant closed-loop poles moving rapidly into the right half of the complex plane as the position gain, $K_a K_x$, increases. Figures 4-8a, b, c, and d show the experimental closed-loop response (with the hydraulic damper removed) for a step in the reference position corresponding to four points along the root locus. The model's prediction of the stability limit for this simple case is quite good.

Velocity feedback is marginally successful in stabilizing unstable step responses caused by large position gains. For the position gain used in the response of Figure 4-8d ($k_x = 1.7$)

Complete fourth order linear model:

$$v(s) = \frac{\left[\frac{G_o}{TC_{air}M_T}\right] I(s) + \frac{1}{M_T}\left[s^2 + \frac{1}{T} + \frac{C_1}{C_{air}} s + \frac{C_1 + G_oK_F}{TC_{air}}\right] F_{ext}(s)}{s^4 + \left[\frac{1}{T} + \frac{C_1}{C_{air}} + \frac{B_o}{M_T}\right] s^3 + \left[\frac{1}{T}\left(\frac{C_1}{C_{air}} + \frac{B_o}{M_T}\right) + \frac{C_1B_o + A_p^2}{C_{air}M_T} + \frac{G_oK_FM_L}{TC_{air}M_T}\right] s^2 + \left[\frac{C_1B_o + A_p^2 + G_o(K_v + K_Fb_L)}{TC_{air}M_T}\right] s + \left[\frac{G_oK_x}{TC_{air}M_T}\right]}$$

and neglecting servovalve spool dynamics:

$$v(s) = \frac{\left[\frac{G_o}{C_{air}M_T}\right] I(s) + \frac{1}{M_T}\left(s + \frac{C_1 + G_oK_F}{C_{air}}\right) F_{ext}(s)}{s^3 + \left[\frac{C_1}{C_{air}} + \frac{B_o}{M_T} + \frac{G_oK_FM_L}{C_{air}M_T}\right] s^2 + \left[\frac{C_1B_o + A_p^2 + G_o(K_v + K_Fb_L)}{C_{air}M_T}\right] s + \left[\frac{G_oK_x}{C_{air}M_T}\right]}$$

Figure 4-7: Transfer functions for position, velocity, and force feedback.

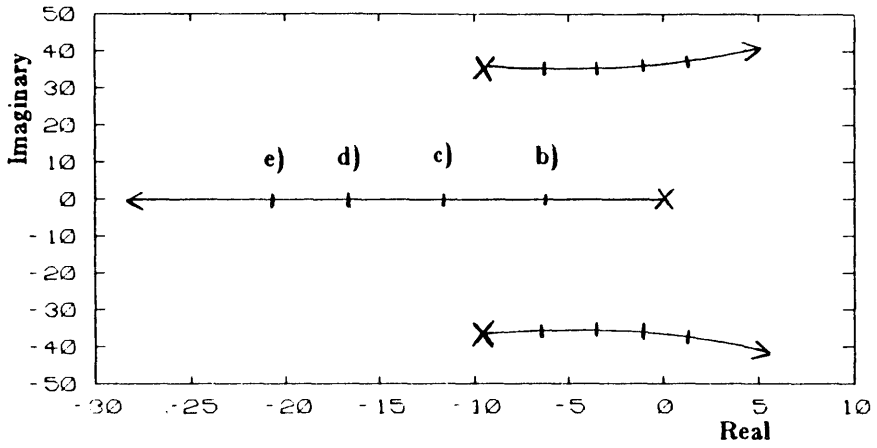

a) Root Locus - Position Feedback/No Hydraulic Damping

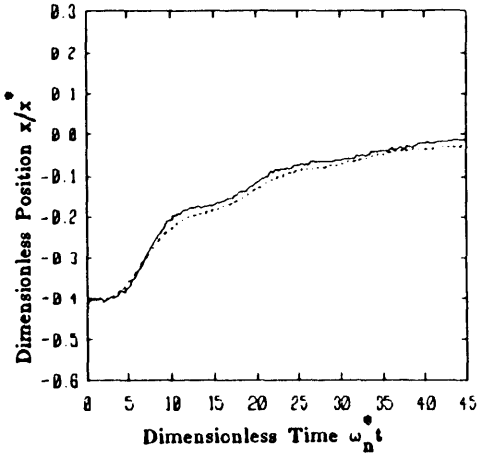

b) $k_x = 0.5$ ($K_a K_x = 10$ ma/ft)

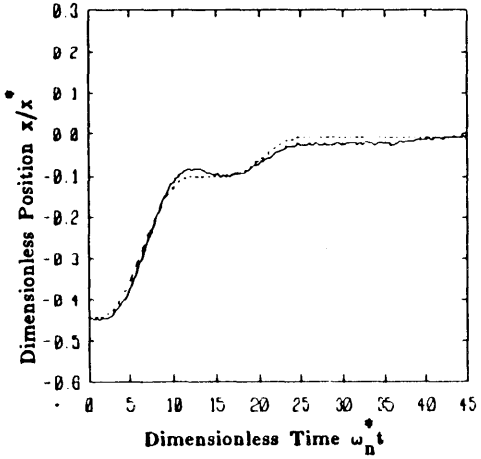

c) $k_x = 0.9$ ($K_a K_x = 19$ ma/ft)

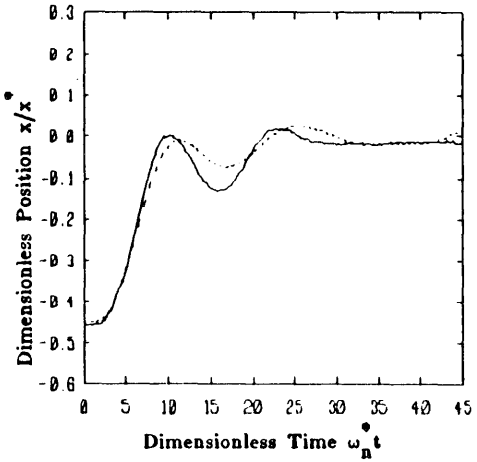

d) $k_x = 1.3$ ($K_a K_x = 28$ ma/ft)

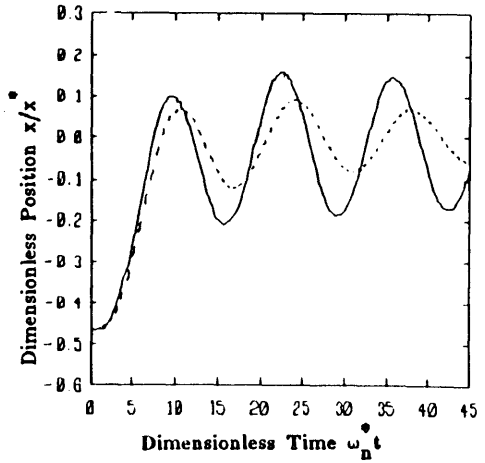

e) $k_x = 1.7$ ($K_a K_x = 37$ ma/ft)

Figure 4-8: Position feedback root locus and experimental responses.

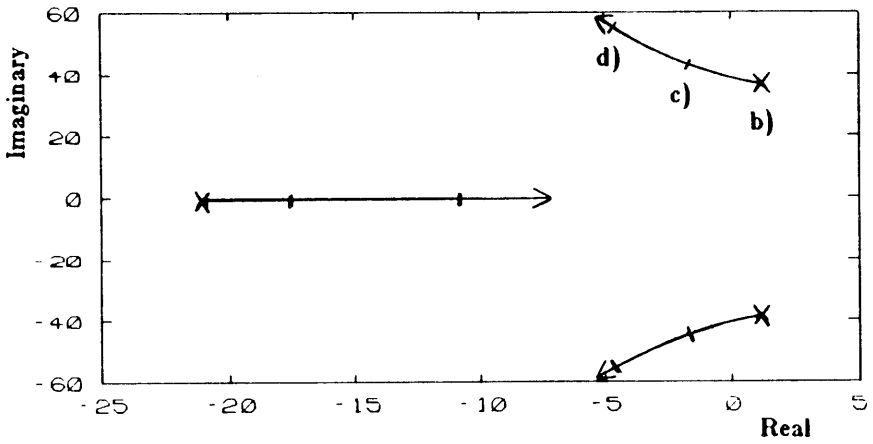

a) Root Locus - Velocity Feedback/No Hydraulic Damping
$k_x = 1.7$ ($K_a K_x = 37$ ma/ft)

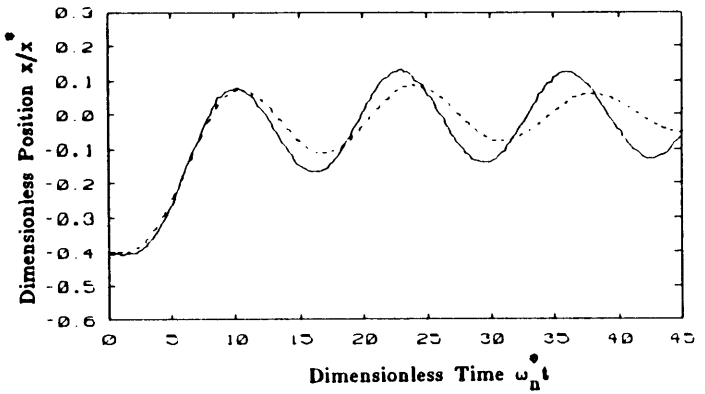

b) $k_v = 0.0$ ($k_a K_v = 0.0$ ma-sec/ft) $K_x = 1.7$

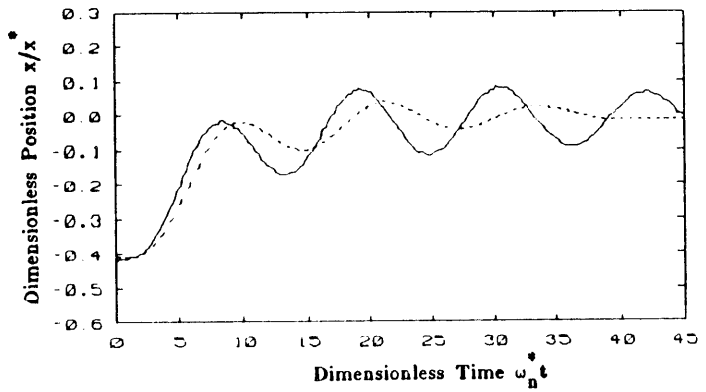

c) $k_v = 0.73$ (k_aK-v) = 0.75 ma-sec/ft) $K_x = 1.7$

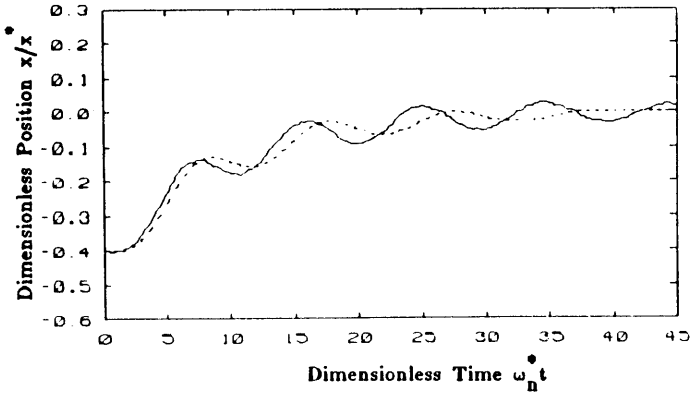

d) $k_v = 2.1$ ($k_a K_v = 2.2$ ma-sec/ft) $K_x = 1.7$

Figure 4-9: Velocity feedback root locus and experimental responses with constant position feedback gain ($k_x = 1.7$).

velocity feedback moves the unstable poles back into the right half of the complex plane (Figure 4-9a), but step responses with increasing velocity gain have slower rise times (since the pole on the real axis moves toward the origin) and, as the hardware data show (Figures 4-9b, c, and d), their setting times are still poor.

A much more effective way of improving the position response is to introduce the hydraulic damper back into the system, as shown in Figure 4-10a comparing the effect of damping on the position feedback root loci. The step response of the actuator for various points on the loci corresponding to the actuator with hydraulics appear in Figures 4-10b, c, d, and e.

It must be emphasized that the goal of this thesis is not to develop a position servo. This section merely demonstrates the ability of the linear model to provide qualitative and some quantitative insight into the results of various control schemes. In the following chapter the linear model is used in the design of an *impedance controller* for the actuator.

4.4.2 Results of Force Feedback

Consider the locus of closed-loop poles (Figure 4-11) as the force gain increases from zero with no position or velocity feedback (K_x and $K_v = 0$) and no friction in the environment ($b_L = 0$). In the limit as $K_F \rightarrow \infty$ one pole approaches $-\infty$ on the real axis, while another approaches the origin where the third pole has remained immobile (because $K_x = 0$). The resulting behavior is simply Newton's law for an external load acting on the workpiece mass, or

$$x(s) = \frac{F_{ext}(s)}{M_L s^2} \tag{4.10}$$

From the point of view of the workpiece, looking through the interaction port, the actuator with infinite force feedback has effectively dissappeared.

This, of course, is an ideal situation which, in practice, cannot be achieved. The

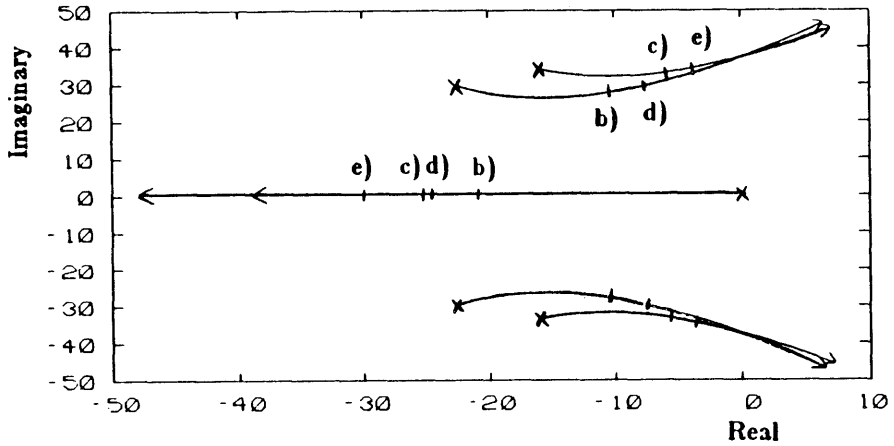

a) Root Locus - Position Feedback/Hydraulic Damping

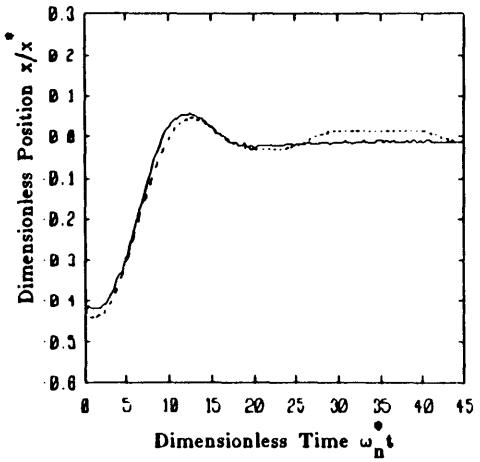

b) $a_d = 1.0$, $k_x = 1.7$

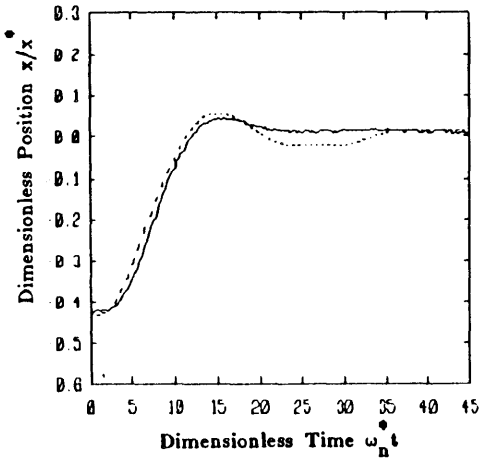

c) $a_d = 0.63$, $k_x = 1.7$

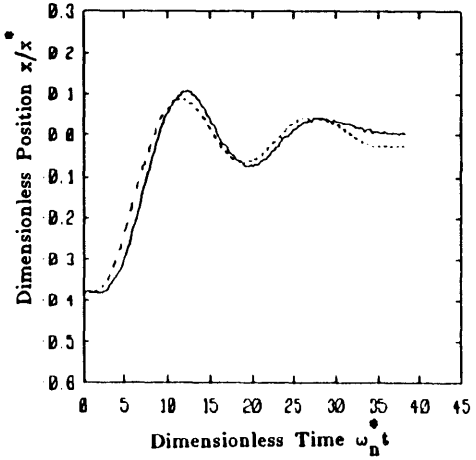

d) $a_d = 1.0$, $k_x = 2.2$

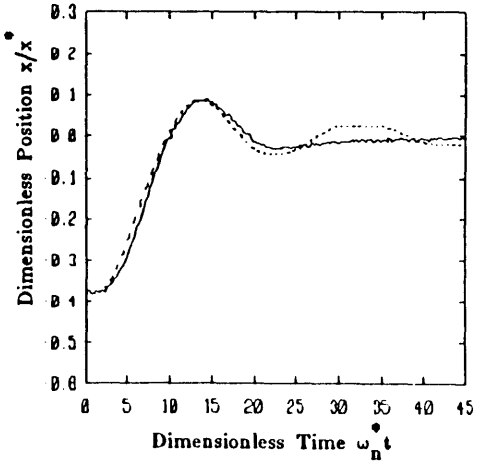

e) $a_d = 0.63$, $k_x = 2.2$

Figure 4-10: Position feedback root loci and experimental responses with variable hydraulic damping.

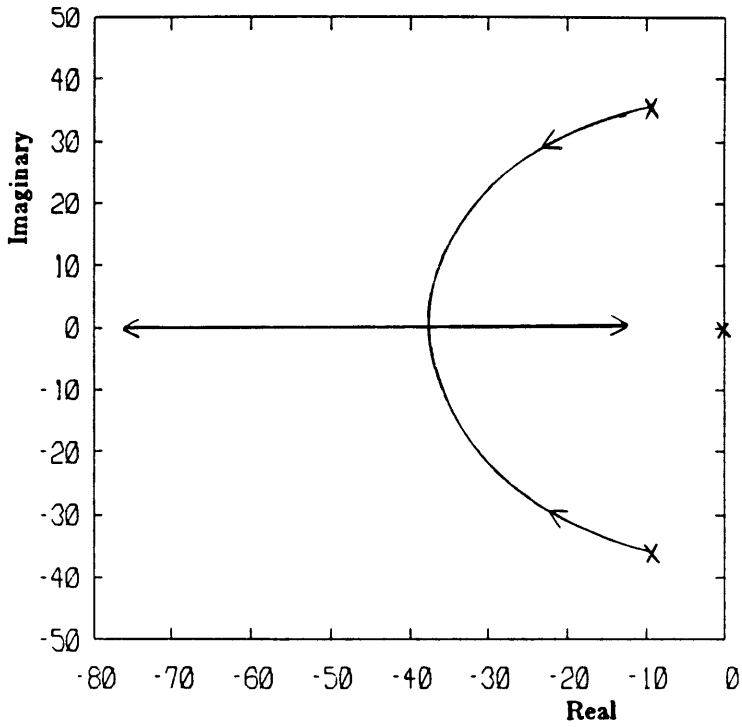

Figure 4-11: Force feedback root locus. No servovalve dynamics/no hydraulic damping.

experimental hardware exhibits unstable behavior at high force gains characterized by a high frequency oscillation that is not predicted by the linear model, nor by the more complex non-linear model. This same type of instability was obsevered in a force controlled knee prothesis simulator [10] and is most likely due to unmodeled higher order dynamics and transport delay in the air supply lines.

These unstable oscillations may be alleviated by lowering the supply pressure delivered to the electro-pneumatic servovalve, allowing a higher force gain. At the lowest supply pressure tested (approximately 10 psig) and the highest stable gain the actuator is amazingly back-drivable. In fact, with a workpiece load of 10 lb_m the inertia of the payload alone is enough to sustain motion after an externally applied force (a push of the hand) is removed. This is a pleasing result as it shows the advantage of having the ability to change the open-loop behavior of the device to improve closed-loop performance.

The results of this chapter demonstrate the applicability of a linear model which is based on the experimental frequency response. Although the model is inadaquate for predicting the actual time response of the actuator (recall this task is reserved for the non-linear model), it is a powerful tool when applied to the methods of linear control theory (modern or classical).

Chapter 5
Control of Impedance in the Hybrid Actuator

5.1 Impedance Control Strategy

Once it has been decided to control impedance a logical question to ask is *How is impedance controlled?* Section 5.2 of this chapter investigates the possibilities suggested by changing the inherent behavior of the mechine. Sections 5.3 and 5.4 concern the control of impedance using artificial means (i.e. electronic feedback), Section 5.3 limiting itself to position feedback only with Section 5.4 presenting the design of a relatively simple impedance controller that was implemented on the experimental hardware using analog circuits. The remaining sections discuss the success and shortcomings of the controller and possible causes of undesirable behavior.

5.2 Inherent Actuator Impedance

One method of controlling impedance is to adjust the natural properties of the device. The beauty of this approach is that the open-loop system, untroubled by phase lags which spell disaster when feedback is used, will never go unstable. The next two sections consider the theoretical and experimental stiffness and damping relations for the pneumatic and hydraulic portions of the system, respectively.

5.2.1 Air Stiffness

Consider a double acting air cylinder with the ports sealed and an external load applied. Treating the expansion and compression of air in the closed cylinder chambers as a polytropic

process of an ideal gas, pressure and volume are related by

$$PV^n = P_i V_i^n \tag{5.1}$$

where n is the polytropic exponent (equal to k—the ratio of specific heats—for an isentropic process and 1.0 for an isothermal process). For the displacement from equilibrium, x, and the external force, F, defined positive as shown, the resulting non-linear static stiffness characteristic becomes

$$F = A_p P_i \left[\left(\frac{V_{Li}}{V_{Li} - A_p x} \right)^n - \left(\frac{V_{Ri}}{V_{Ri} + A_p x} \right)^n \right] , \tag{5.2}$$

where P_i, V_{Li}, and V_{Ri} are the initial equilibrium pressure and volumes.

For small displacements from equilibrium a linear approximation for the average air compliance is given by equation (3.16). A double acting cylinder is basically two air springs in parallel; hence, if V_{Li} and V_{Ri} are the initial volumes of the cylinder chambers in equilibrium, then the net linear stiffness expression takes the form

$$F = n P_i A_p^2 \left[\frac{1}{V_{Li}} + \frac{1}{V_{Ri}} \right] . \tag{5.3}$$

In dimensionless form (for $V_{L_i} = V_{R_i} = V^*$ and $P_i = P^*$) the two expressions above reduce to

$$f = \frac{F}{A_p P^*} = \left(\frac{1}{1 - s_x} \right)^n - \left(\frac{1}{1 + s_x} \right)^n \tag{5.4}$$

for the non-linear case, and

$$f = \frac{F}{A_p P^*} = 2 n s_x \tag{5.5}$$

for the linear case. (Recall that the dimensionless variables (i.e. s_x, etc.) and the reference variables (*'s) are defined in Tables 3-I and 3-II in Chapter 3.)

The dimensionless characteristics are compared in Figure 5-1 for n=1 and n=1.4, the extremes of the polytropic exponent. The linear approximation is good for small excursions from equilibrium, but it must be kept in mind that both set of curves are theoretical.

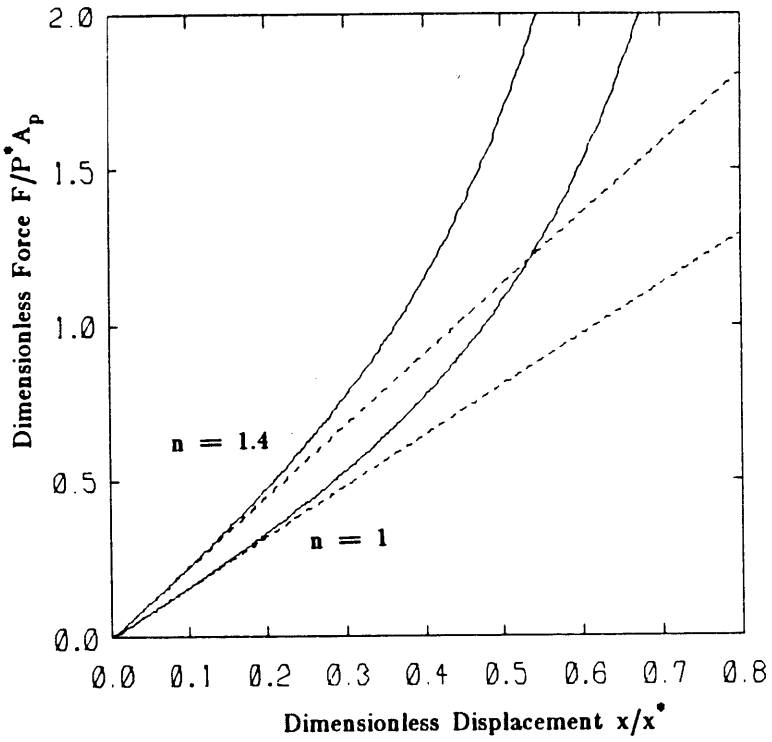

Figure 5-1: Dimensionless linear and non-linear stiffness curves.

Leakage past the spool in the servovalve and leakage in the cylinder seals make generation of accurate experimental static stiffness curves for the open-loop actuator difficult, as the restoring force acting on the piston displaced from equilibrium tends to decay with time. Hence, only approximate measurements of the air column's inherent stiffness were made by comparing the amplitudes of an oscillating disturbance force and the resulting displacement, providing an estimate of the range of natural stiffnesses achievable by varying the cylinder chamber volumes and the initial equilibrium pressure.

Figure 5-2 shows the variation of the air column stiffness with initial chamber pressure for the ram initially in equilibrium in the mid-position compared to the ideal linear relation. Equation (5.3) implies that the actuator in this position will have its lowest stiffness for a given initial pressure. Figure 5-3 shows the approximate stiffness variation for other equilibrium positions.

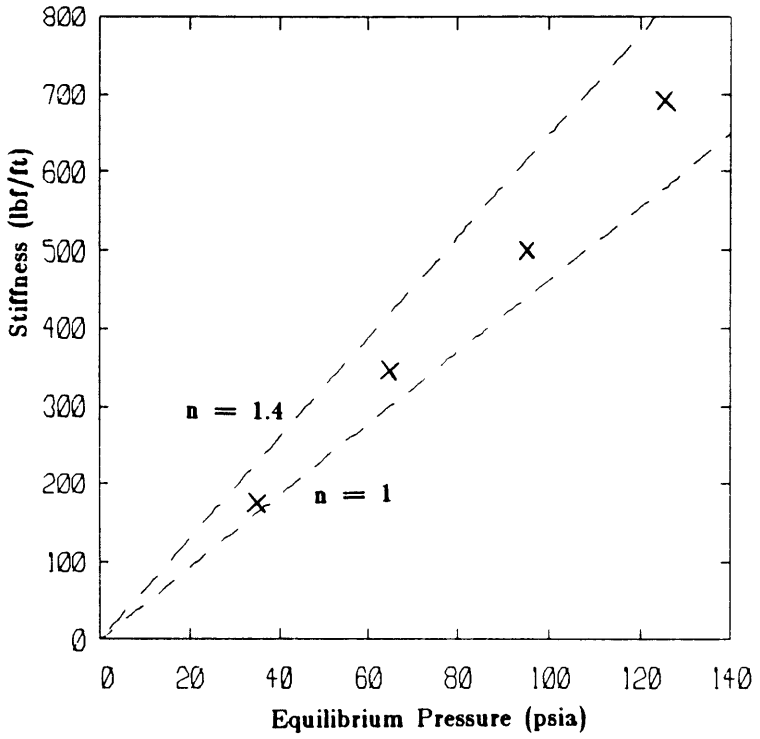

Figure 5-2: Variation of stiffness with air pressure.

At this point, thinking of the net stiffness in terms of two air springs is helpful. Though one of the springs becomes less stiff as the ram moves from center due to increased chamber volume, the stiffer, smaller volume spring dominates the total stiffness since the springs are in parallel. Hence as Figure 5-3 indicates, the stiffness becomes very high as the equilibrium position approaches the limits of piston travel.

The dimensionless linear stiffness expression (equation (5.5)) provides some insight as to the effects of geometric parameters on the inherent stiffness of the actuator. (Recall that the reference parameter x^* (defined by V^*/A_p) is characteristic of the length of the air cylinder.) Assuming that the polytropic exponent n is unchanged (or does not vary appreciably) with cylinder geometry, equation (5.5) implies that, for a given supply pressure, the air stiffness is maximized by increasing the piston area, A_p, while decreasing the characteristic length, x^*, as much as possible. Hence a pnuematic actuator with the potential for high stiffness will have a

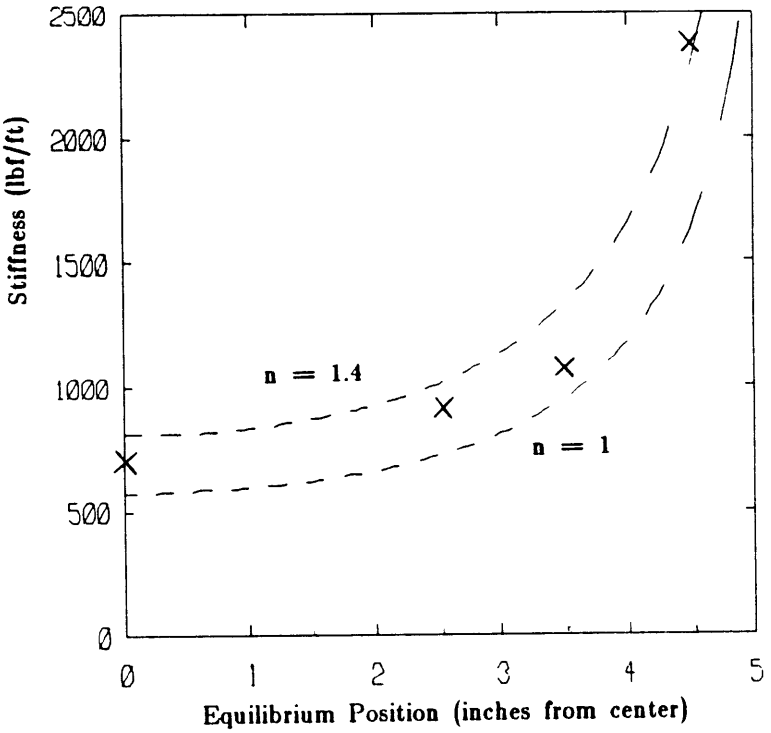

Figure 5-3: Variation of stiffness with equilibrium position.

large diameter cylinder and a short stroke.

5.2.2 Passive Hydraulic Damping

Using the Euler equation for incompressible orifice flow and assuming negligible leakage, the theoretical force/velocity characteristics for the hydraulic damper are given by

$$F_d = \frac{\rho_{oil} A_h^3}{2(C_{do}A_d)^2} |v| \, v \, . \tag{5.6}$$

The expression linearized about a steady state operating point takes the form

$$F_d = \frac{\rho_{oil} A_h^3 v_{ss}}{(C_{do}A_d)^2} \, v \, . \tag{5.7}$$

In dimensionless form the two expressions reduce to

$$f_d = \frac{F_d}{A_h P_{hl}^*} = \frac{1}{(C_{do}A_d)^2} |v_x| \, v_x \tag{5.8}$$

for the non-linear case, and

$$f_d = \frac{F_d}{A_h P^*_{hl}} = \frac{2}{(C_{do}A_d)^2} v_x \tag{5.9}$$

for the linear case.

As in the case of the air column stiffness, the experimental steady state characteristics for the passive hydraulic damper are also difficult to determine accurately. The range of damping provided by the passive hydraulics was estimated in the following manner. The experimental hardware was rearranged into a configuraton in which the pneumatic portion of the system acts as a force generator. The force input to the damper is then the output force measured by the load cell. With minimal inertial loading and a sinusoidal input to the electro-pneumatic servovalve the amplitudes of the force and velocity outputs were measured for several damper conditions.

Damping ranged from a minimum of approximately 7 lb_f-sec/ft with the damper valve full open to a maximum limited only by leakage in the fully closed valve and the oil cylinder seals. Further work should investigate the possibilities of lowering the minimum damping through special design of the hydraulic circuit. The experimental hardware in this project was limited by commercially available oil cylinders which are designed to operate at much higher pressure drops. Possible ways of solving such problems as well as other practical considerations for design of the oil circuit are discussed in Chapter 6.

5.3 Control of Stiffness With Position Feedback

Because the open-loop acuator is basically a flow source, simple position feedback does not make the system exhibit spring-like behavior. When the ram is displaced from its reference positon by an external force, the resulting error signal causes the pneumatic servovalve to supply a net *load flow* to the cylinder.[12] The load pressure and hence the net

[12]The terms load flow and load pressure result from combining the air chamber pressure states into a single equation. The load pressure is simply the pressure drop across the piston while the load flow is the net volume flow into the cylinder due to flows at the supply and exhaust ports.

force output increase with time as the supply chamber fills and the exhaust chamber empties.

The transfer function of equation (4.7) gives the steady state load sensitivity as

$$G_o K_x x(s) = C_1 F_{ext}(s) \tag{5.10}$$

where G_o and C_1 are defined in Section 4.3. As argued before, although a reliable value of C_1 is difficult to determine, in a well designed system, employing a closed-center servovalve, C_1 is small. Hence, in steady state the stiffness of the actuator with this control scheme should be quite high.

Experiments on the experimental hardware confirm the considerations mentioned above. Consider the two extremes of possible causal conditions in which the environment inposes either a constant external force independent of displacement or a constant displacement independent of force.

In the first case, for a constant external load, the steady state error need only be large enough to overcome internal leakage, providing a net load flow which, integrated with time, produces the load pressure necessary to balance the external force. In the latter case displacement of the ram from its reference position to a constant position independent of force is met with a time increasing restoring force that, allowing for leakage, stabilizes near the maximum force output of the actuator. The major effect of the position gain and the magnitude of the displacement from the reference position is in the rate at which the actuator force increases, as both act to increase the current input to the servovalve and hence the load flow.

One serious drawback of this type of control is stability. The basic problem is analogous to *integrator wind-up* often encountered in integral control systems. The servovalve, being a flow source, combined with an air cylinder chamber, a big capacitor, act as an integator in response to position errors.

When conducting the latter of the two experiments mentioned above, returning the ram

to its equilibrium position required extreme caution, lest the displaced ram, with a 120 lb_f restoring force behind it, be allowed to create havoc on the experimental hardware. The former case though, did demonstrate a vary stiff actuator (in pneumatic terms), provided external loads are kept below the maximum force output.

5.4 Impedance Controller Design

In order to make the actuator look as much like an ideal effort (force) souce as possible the impedance controller contains an inner force servo loop in which the actuator output force (measured by the load cell at the interaction port) is compared to a reference force with the resulting error signal amplified and input to the servovalve. If the actuator is not exerting the desired force on the environment the controller tells the servovalve to increase (or decrease as necessary) the load flow thereby altering the load pressure such that the required force is seen at the interaction port.

If the reference force is identically zero, then the controller tries to make the actuator apprear to the environment as though it were completely backdrivable. (This is identical to pure force feedback considered in Section 4.4.2.) In practice, the limit of backdrivability is dependent on the maximum force gain that can be used without instabilities arrising in the system.

Control of stiffness and damping is achieved by adding two outer feedback loops—one position and the other velocity. The complete impedance controller is shown in the block diagram of Figure 5-4 in conjuction with the linear model of Chapter 4. The position signal is compared to a reference signal generating an error proportional to the displacement from equilibrium. The same is done with the velocity to generate a signal proportional to the

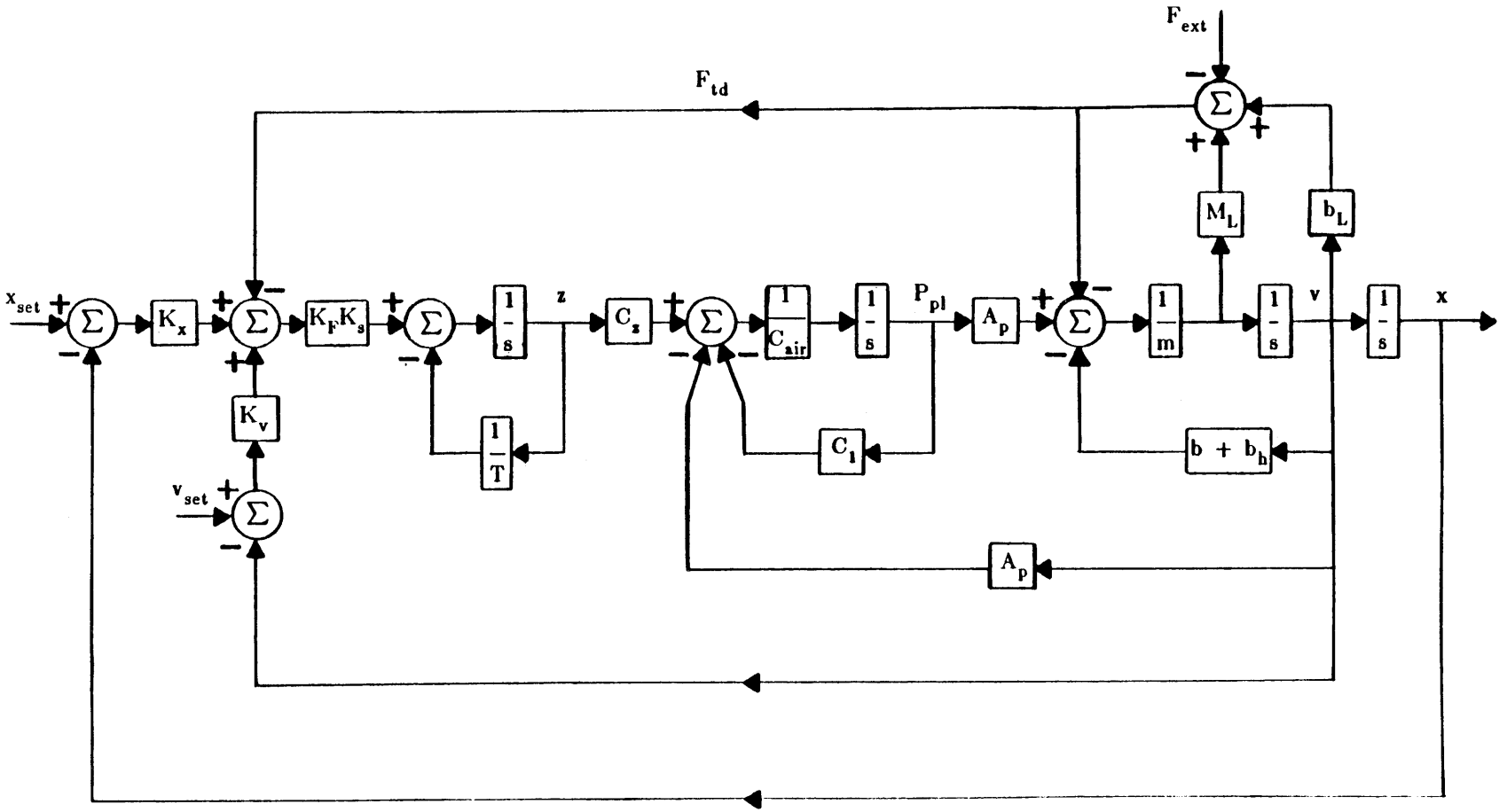

Figure 5-4: Block diagram of impedance controller with linear model.

error in desired velocity.[13] Each error signal is then multiplied by a respective gain (K_x and K_v) and the sum of the two signals becomes the reference signal for the inner force servo loop.

Provided the force gain can be made large enough without unstable behavoir resulting, the gains K_x and K_v give direct control over the closed-loop stiffness and damping seen by the environment at the interaction port. To see this consider the control law for this scheme and the resulting closed-loop transfer function. The control law is given by

$$I = -K_a K_F[\, K_x(x - x_{set}) + K_v(v - v_{set}) - F_{td}\,] , \tag{5.11}$$

where K_a is the servoamp gain and F_{td} is the force measured by the load cell at the interaction port. The closed-loop transfer function (neglecting servovalve spool dynamics) then takes the form

$$v(s) = \tag{5.12}$$

$$\frac{\left[\frac{G_o}{C_{air}M_T}\right] I(s) + \frac{1}{M_T}\left(s + \frac{C_1 + G_o K_F}{C_{air}}\right) F_{ext}(s)}{s^3 + \left[\frac{C_1}{C_{air}} + \frac{B_o}{M_T} + \frac{G_o K_F M_L}{C_{air}M_T}\right] s^2 + \left[\frac{C_1 B_o + A_p^2 + G_o K_F(K_v + b_L)}{C_{air}M_T}\right] s + \left[\frac{G_o K_F K_x}{C_{air}M_T}\right]}$$

In the limit as $K_F \to \infty$, the closed-loop transfer function reduces to

$$F_{ext}(s) = [\, M_L s^2 + (b_L + K_v)s + K_x \,]\, x(s) , \tag{5.13}$$

where the reader will recall M_L and b_L are the mass and damping assumed present on the

---

[13]The reference velocity in all cases was zero though there is no fundamental reason why this must be the case.

environment side of the interaction port. The result of equation (5.13) is exactly the type of actuator behavior sought in an impedance control scheme [15], [3]. Though it is not possible to achieve infinite force feedback gain, the control scheme performed quite well for a wide range of impedances.

5.5 Performance of the Impedance Controller

Implementation of the impedance controller described in Section 5.4 provides better control of stiffness and damping than can be achieved through natural means alone. Table 5-I compares results of open versus closed-loop control of impedance. Section 5.5.1 discusses the static performance of the impedance controlled actuator and ways of maintaining stability in the face of external disturbances. In Section 5.5.2 results of dynamic tests are considered, including initial condition response, tracking response, and the ability to *catch* a mass with non-zero initial velocity.

5.5.1 Range of Reachable Stiffness

With the impedance controller described in Section 5.4 it was possible to vary the dynamic and static behavior of the actuator from that of near a completely backdrivable mechanism to that of a spring with stiffness more than three times the natural stiffness of the centered open-loop air cylinder. Unlike the uncontrolled system, the stiffness of the impedance controlled actuator does not vary with ram position, though it is less stable at the extremes of its travel.

At the compliant end of the impedance spectrum backdrivability is limited by natural damping in the system and the maximum force gain realizable without exciting the high frequency (but well behaved) oscillations described in Section 4.4.2. Lowering the supply pressure delivered to the servovalve results in improved compliant performance both by

Table 5-I: Stiffness and Damping Ranges of the Natural and Controlled Actuator

	STIFFNESS $\frac{lb_f}{ft}$		DAMPING $\frac{lb_f\text{-sec}}{ft}$	
	Min	Max	Min	Max
	@0 psig x=0	@120 psig x=4.5 in	ports open	
Open-loop w/out hydraulics	70	2400	2	–
			full open	full closed
Open-loop w/ hydraulics	–	–	7	$3x10^4$
	within stability limits		within stability limits	
Closed-loop w/out hydraulics	<< 1	2000	<< 1	200

decreasing the inherent stiffness of the air column in the cylinder chambers and by allowing a higher stable force gain.

At the stiff end of the spectrum unstable behavior is characterized by low frequency, high amplitude oscillations physically abusive to the experimental hardware and anything else in the immediate vicinity of the test bench. This type of instability is similar to that observed using only position feedback, suggesting that such behavior is due to the dominant closed loop poles slipping into the right half of the complex plane.

With no velocity feedback (and $b_L = 0$) and a desired stiffness of 300 lb_f/ft Figure 5-5 shows the impedance controller root locus sans spool dynamics for increasing force gain for three different desired stiffnesses. In the limit as $K_f \rightarrow \infty$, the dominant poles are purely imaginary. Considering the highly approximate nature of the linear model, it is not hard to

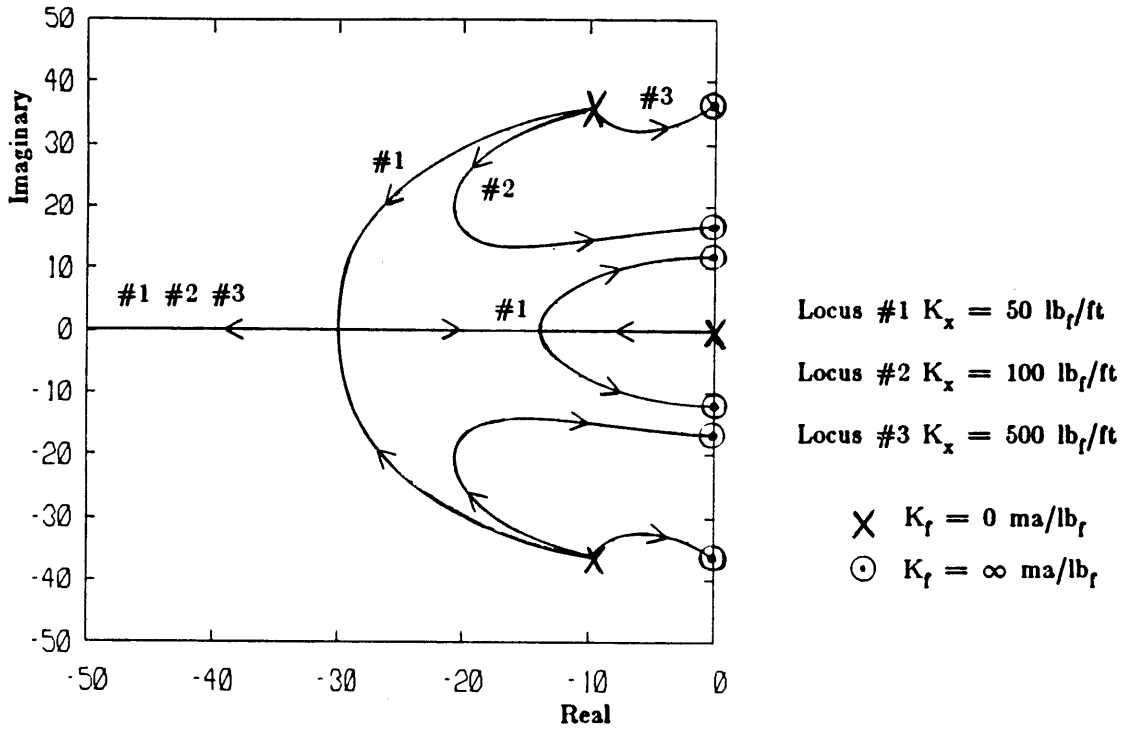

Figure 5-5: Root locus for impedance control with increasing force gain. (No servovalve dynamics/K_v = 0.0 lb_f-sec/ft)

believe that under some conditions these poles may indeed have positive real parts. Figure 5-5 indicates that controlling only the static stiffness of the closed-loop system is not enough. The proper dissipative behavior must also be included to ensure dynamic stability.

There are three possible ways of controlling damping in the actuator using the control scheme implemented. The most obvious way is to use the velocity feedback loop contained in the impedance controller. This technique is successful in changing damping characteristics well within the system's stability limits but is marginally effective for stabilizing the actuator at high stiffnesses. At low stiffnesses large velocity feedback gains excite high frequency instability, requiring a lower force gain to maintain stability.

Another way to control damping is to simply reduce the force gain. As Figure 5-5 shows this moves the dominant poles away from the imaginary axis adding damping to the system. A lower force gain results in a more sluggish response containing higher order dynamics which

cannot be described in terms of a simple second order system. However, this technique proved more successful than velocity feedback allowing a maximum, marginally-stable steady state stiffness of more than 2000 lb_f/ft to be achieved.

The third possibility, which wasn't implemented on the experimental hardware, involves placing the passive hydraulic damper on the environment side of the force transducer, giving control of damping independent of the pneumatic actuator and its impedance controller. Theoretically, such a configuration should allow very high pneumatic stiffness with improved stability, especially as the damper flow area is reduced. However, backdrivability at the other impedance extreme will correspondingly suffer unless careful attention is given to damper design.

5.5.2 Dynamic Response of the Impedance Controlled Actuator

As a demonstration of the versatility of an impedance controlled actuator this section presents the dynamic response of the closed-loop system for various operating conditions and different controlled impedances (all well within the system's stability limits).

The set of plots in Figure 5-6, in which the actuator is rigidly coupled to a 10 lb mass free to move in one horizontal dimension, show how the initial condition response is altered by changing the commanded stiffness and damping via the variable gains K_x and K_v, respectively. The impedance controller makes the high order, non-linear system look very nearly like a simple second order spring-mass-damper with tunable stiffness and damping.

In a second set of experiments a compliant element was placed between payload and ground in the form of a *bungee cord*, providing simulated stiffness in the environment. Rather than look at the initial condition response, the system's ability to follow a commanded trajectory under these conditions is tested. The *commanded trajectory* amounts to manually varying the contoller's reference position.

K_x = 82 lb_f/ft

K_v = 0 lb_f-sec/ft

P_{SUPPLY} = 30 psig

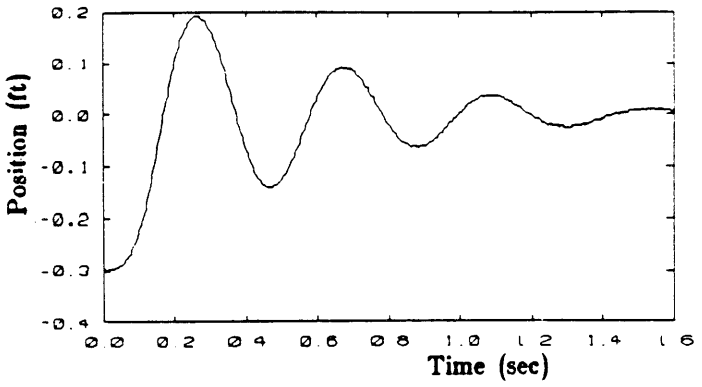

K_x = 82 lb_f/ft

K_v = 7.8 lb_f-sec/ft

P_{SUPPLY} = 30 psig

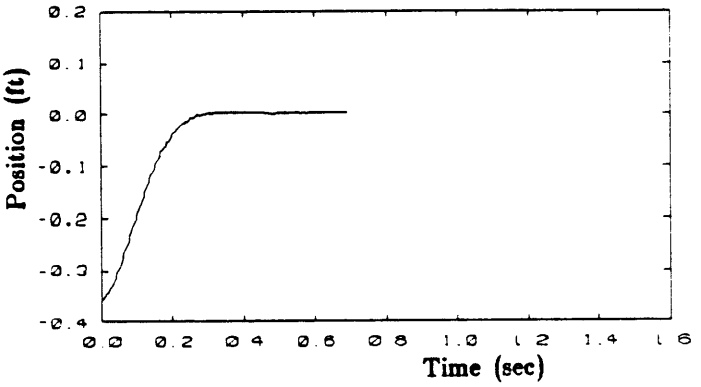

K_x = 305 lb_f/ft

K_v = 0 lb_f-sec/ft

P_{SUPPLY} = 60 psig

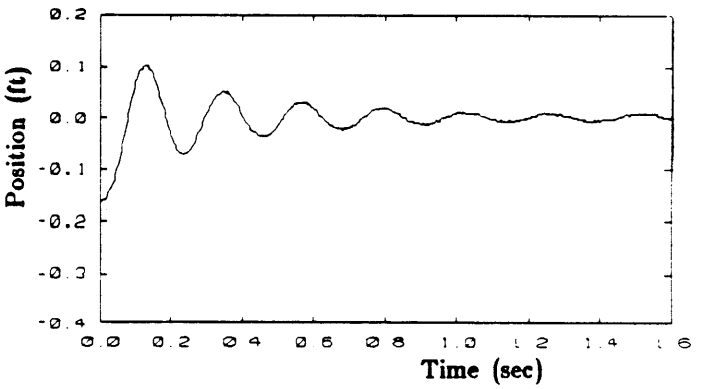

K_x = 305 lb_f/ft

K_v = 13.5 lb_f-sec/ft

P_{SUPPLY} = 60 psig

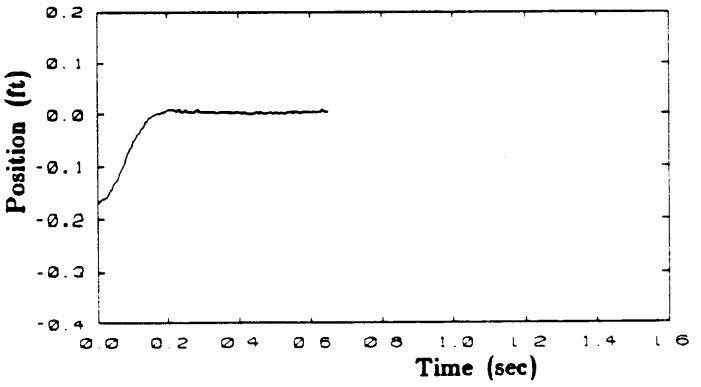

Figure 5-6: Initial condition response of the impedance controlled actuator.

Without knowing specifically the dynamic characterstics of the environment (bungee cord stiffness, external damping, and payload), the stiffness of the actuator can be chosen to either minimize the position error (high stiffness) or minimize the interaction force (low stiffness) or anywhere in between depending on the desired performance. Damping is chosen to maintain dynamic stability.

Consider the case of minimizing the position error by tuning the actuator stiffness as high as stability will allow (2050 lb_f/ft). For quasi-static changes in the reference position this situation is somewhat trivial, as the product of the position error and the actuator stiffness is merely the difference bettween the bungee cord restoring force were the position error zero (i.e. $x = x_0$) and the actual interaction force.

At the other extreme consider minimization of the interaction force. In principle, the actuator could be adjusted to have zero stiffness, in which case, regardless of the controller's reference position, it would seek the bungee cord's equilibrium position, where the interaction force is zero. Hence, tunable impedance allows the same actuator to function both as a position or a force controller—depending upon which extreme of its stiffness range is desired—through changes of control parameters only, rather than major changes in controller structure.

Operation of the impedance controlled actuator as a force or position controller are only two special cases of possible application. While most manipulators are designed to exploit these two types of workless—or nearly workless—interactions (i.e. either $\Delta x = 0$, or $F = 0$, hence $W = F*\Delta x = 0$), there are many practical situations which require significant energy exchange between manipulator and environment (e.g. drilling, sanding, and other power tool applications, as well as assembly of close fitting parts).

Consider the relatively simple-sounding task of *catching* a mass initially decoupled from the rest of the system, given a constant initial velocity directed at the stationary actuator.

Here the actuator plays the role of an active *allowalator*. That is: the actuator with tuned stiffness and damping *allows* the mass, upon impact, to displace it from its equilibrium position, absorbing the kinetic energy to bring the mass to rest at maximum displacement, before returning it to the environment less the energy dissipated by controlled damping.

Such a situation is anything but a workless interaction and would require a very sophisticated control algorithm were either position or force control implemented (e.g. position control would require accurate, real time knowledge of the mass' position and velocity, and unless able to track the mass precisely, large and unpredictable interaction forces would result).

Since the interaction between the free mass (0.53 slugs) and the system occurs in a relatively short time, mass catching provides an opportunity to compare the control of stiffness in the pneumatic actuator via natural means (e.g. variable air pressure) and control using feedback, as leakage in the passive air cylinder has insufficient time to be a significant effect.

Figure 5-7 shows the uncontrolled actuator's position and force responses after impact. Since the air cylinder is not a pure spring, a spike in force occurs as the rod, piston, and force transducer mass is accelerated. For the rest of the process the environment and actuator masses are rigidly coupled until after motion is reversed and the cylinder reaches its equilibrium position, at which time the masses decouple and the interaction force drops to zero.

The response of the impedance controlled actuator, tuned to roughly the same stiffness as the passive case is shown for different force gains in Figure 5-8. In both cases there is no velocity feedback, damping being controlled by the force gain. As part of the impedance controller, force feedback acts to reduce the magnitude of the initial force spike slightly, but since the transducer-controller-servovalve combination is not infinitely fast, and because there

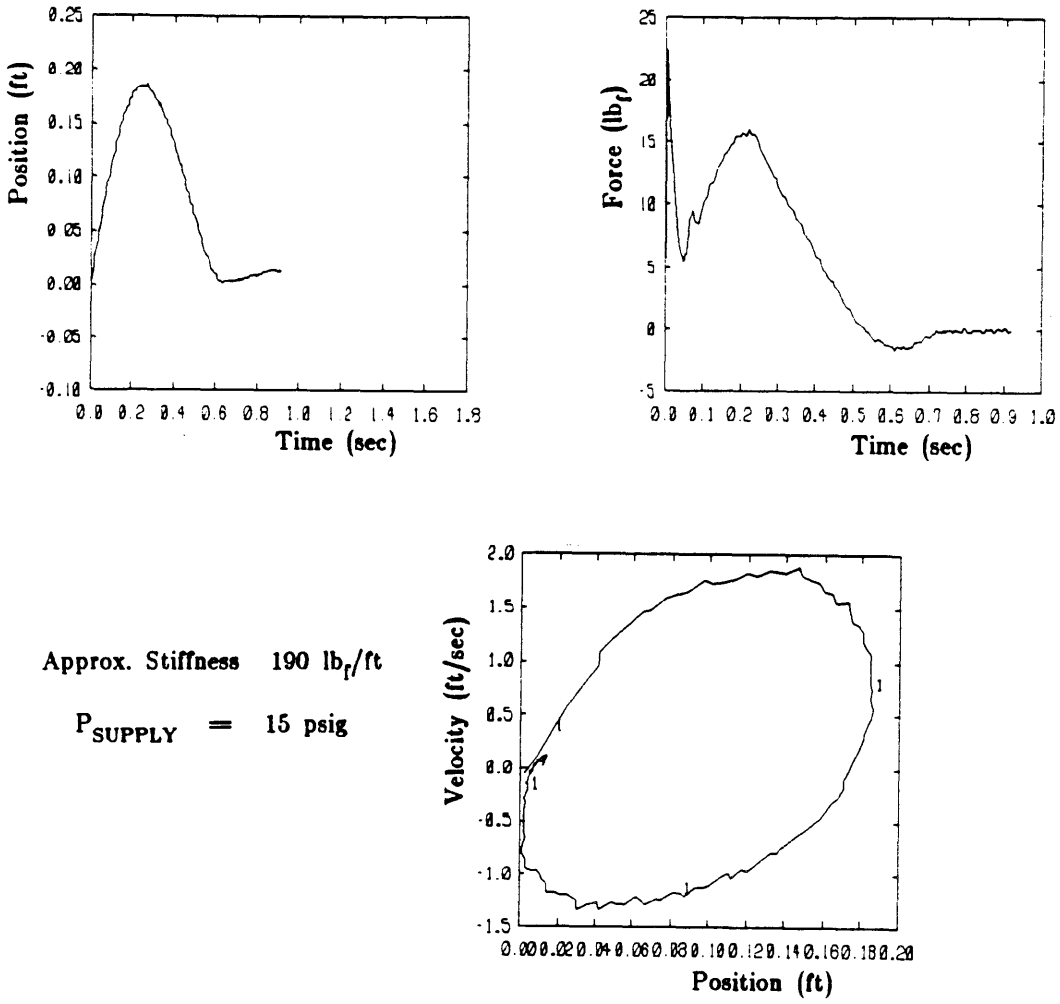

Figure 5-7: Open-loop actuator *catching* a mass.

is still a small amount of transducer mass on the environment side of the interaction port, the spike can never be avoided—though with careful design it might be substantially reduced.

Attempting to reduce the level of the force spike by increasing the force gain is of little help (as Figure 5-8 shows) and actually degrades performance, as the combination of the spike in force and large gain cause the actuator to *jump* out of the way of the approaching mass only to be impacted again, generating another spike, after the large error signal subsides.

K_x = 180 lb_f/ft

K_v = 0 lb_f-sec/ft

K_f = 2.0

P_{SUPPLY} = 20 psig

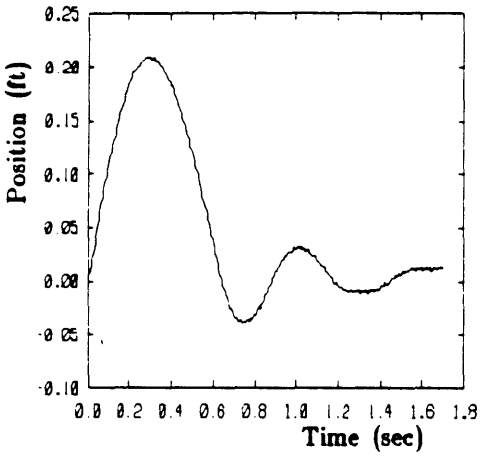

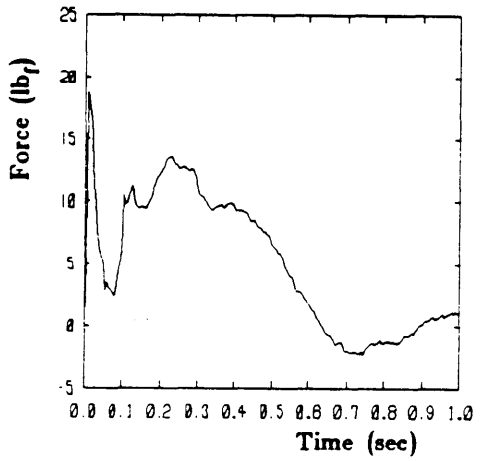

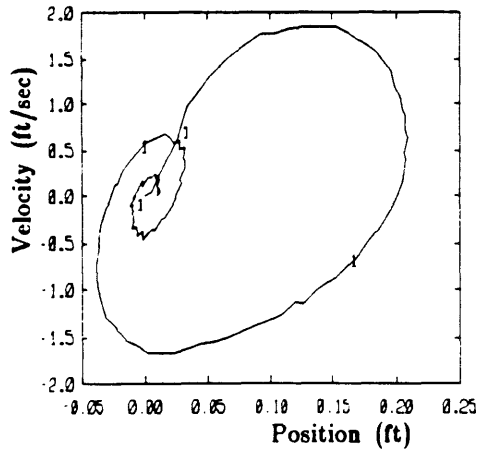

K_x = 180 lb_f/ft

K_v = 0 lb_f-sec/ft

K_f = 3.6

P_{SUPPLY} = 20 psig

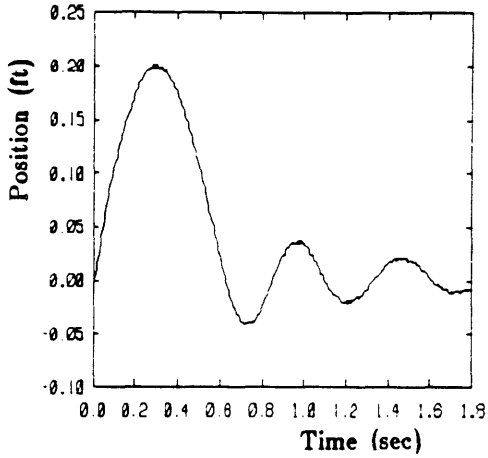

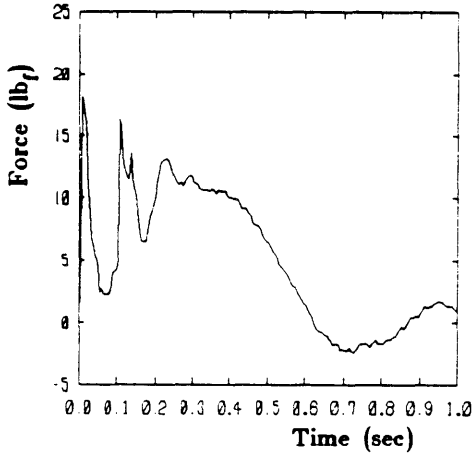

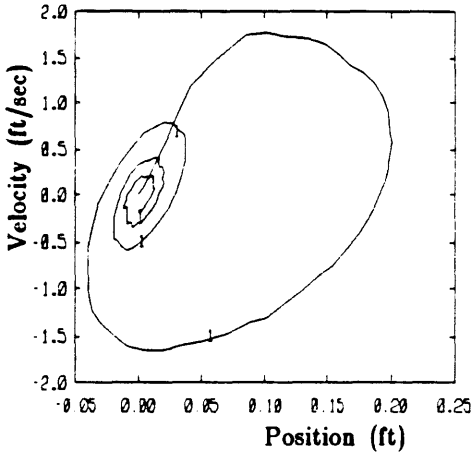

Figure 5-8: Impedance controlled actuator *catching* a mass.

Passive control of stiffness through natural machine behavior is advantageous in that under such conditions the actuator will never go unstable. On the other hand, the impedance controlled actuator, though requiring steps to insure stability, provides greater control of stiffness a damping over a wide range, while compensating for non-ideal effects such as coulomb friction and air leakage.

Chapter 6
Design Recommendations

6.1 Design Strategy

This project is primarily a design study. It is an attempt to identify the issues of importance in controlling mechanical impedance. Further, the actuators considered are limited to active pneumatic and passive hydraulic components. Something which becomes immediately apparent is that thinking of these components in terms of cylinders, pistons, and valves only limits creativity. It is more helpful to consider what need each part of the actuator fulfills and then determine those which can be performed by components already available and those which require modification of existing components or special design.

The results of the previous chapter imply that a combination of feedback and control of inherent machine behavior may provide the best opportunity to tune the actuator impedance seen at the interaction port. This chapter is segmented into the discussion of the major forward path elements (e.g. servovalve, air cylinder, damper) and the feedback path elements (e.g. sensors, controller).

6.2 Forward Path Elements

This section discusses the actuator's forward path elements which, in general terms, consist of: a controlled energy gate to meter the power flow from an unlimited source to the rest of the system; a power transducer to convert the source energy into mechanical force and translation; and a passive, but actively controlled, dissipator enhancing control of the mechanical energy transmitted to the environment.

6.2.1 Controlled Energy Gate (Electro-pneumatic Servovalve)

Most pneumatic actuators in use at present are so called *one-shot* cylinders contolled by *ON/OFF* electrically or pneumatically actuated valves. The actuator considered in this thesis is unusual in the realm of pneumatic application in that the part of the system which meters the flow of energy from the main power source (a compressed air reservoir) to the main power transducer (an air cylinder) is proportionally controlled. That is: the electro-pneumatic servovalve modulates the effective flow area between cylinder and source proportional to a low level electrical input rather than simply opening and closing an orifice. Without this type of performance *none* of the feedback control techniques described herein and implemented on the experimental hardware would have been possible.

Though the best electro-pneumatic servovalve available has a bandwidth of approximately 20 hz, it is still fast enough to control most pneumatic systems whose bandwidths typically do not exceed 10 hz. Improving pneumatic servovalve technology should not be a goal of further work in this area, as the design and construction of servovalves is a highly refined art, and constantly being improved upon by experienced people (Atchley Controls, Inc., Moog, Inc.). Rather, at this stage of development it makes more sense to gain an understanding of the limitations of the valve and refrain from building controllers which call on the servovalve to operate under conditions for which it was not designed.

The impedance controller with high force feedback gain places an extreme burden on the servovalve to rapidly adjust the load flow to control the force output of the air cylinder. In the limit of an infinitely fast valve the root locus for pure force control, Figure 4-11, predicts no stability problems whatsoever. However, when only a first order lag corresponding to spool dynamics is included in the linear model, two of the less dominant closed-loop poles move away from the real axis (Figure 6-1), suggesting the possibility of high frequency oscillations and interaction with higher order unmodelled dynamics in the closed-loop response.

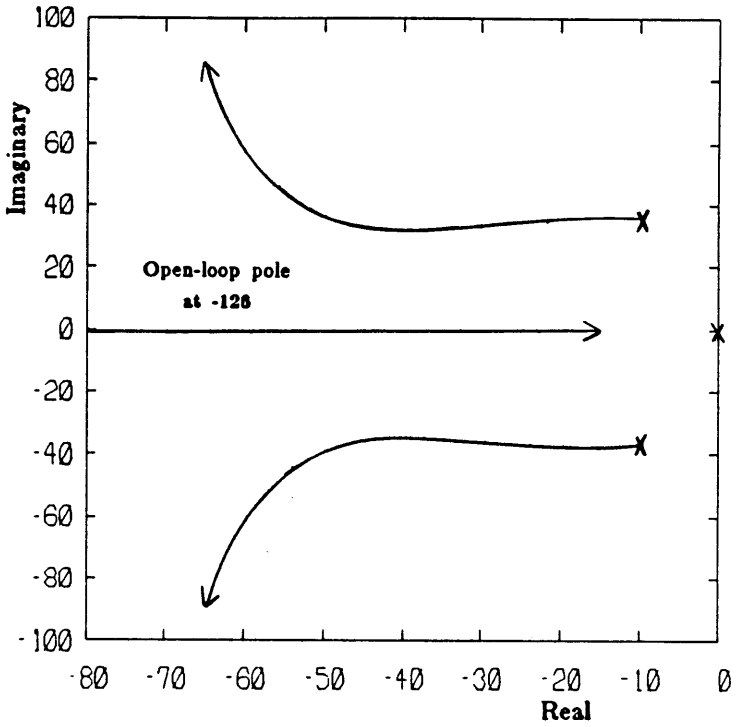

Figure 6-1: Root locus for force control with servovalve dynamics included.

In addition to having non-negligible dynamics the servovalve cannot supply infinite flow to the actuator regardless of how fast the spool can respond to commands. That is to say: the servovalve flow saturates at a value dependent on port width and maximum spool displacement (approximately 16 SCFM for the valve used). Hence, even in the case of an infinitely fast valve, flow saturation attenuates large error signals, making increased force gain virtually ineffective past a certain point.

Other considerations for servovalve choice include the first-stage pilot flow supply and the materials used for constuction. As mentioned before the valve used required oil-free air, complicating coulomb fricton problems in the pneumatic cylinder. If absolutely necessary Atchley Controls, Inc. will construct valves capable of operating with moist or lubricated air using dry-lubed, or in severe cases, hard coated stainless steels (with a corresponding increase in cost).

In the standard two-stage, four-port servovalve the pilot flow to the first-stage jet-pipe preamplifier is taken directly from the supply pressure port, which is adaquate for most applications. This application, however, relies on variable supply pressure in order to change the natural behavior of the actuator, hence the standard valve is inadequate as the dynamic response of the spool is substantially degraded as the pilot pressure drops. Modification of the valve to include a fifth port accomodating the pilot flow independent of the supply pressure seen by the servo-orifices cannot be overlooked.

An area for further work on the servovalve portion of the actuator, suggested by the behavior of the system with position feedback only, is the possible use of an underlapped valve spool to make the actuator look more like an effort source. As yet it is not clear whether the results of such an approach will justify the loss of efficiency due to continuous leakage from supply to exhaust inherent in open-center valves.

While pressure control servovalves are available, their dynamics are considerably more complex than flow control valves which have proved, under certain conditions, to present control problems of their own. Basically a pressure control servovalve is a flow control valve with a physical (i.e. non-electronic) pressure feedback loop to regulate the pressure difference between the two output ports proportional to an input (usually a current in the coils of a torque motor).

6.2.2 Power Transducer (Air Cylinder)

While the main power transducer used in the hardware assembled in this project was a rectilinear double-acting pneumatic piston, there is no fundmental reason why linear actuators must be used nor is it necessary to limit the design to only one transducer. Whatever the final choice may be, two considerations crucial to achieving the widest range of stable mechanical impedances are the maximization of inherent stiffness and minimization of coulomb friction in the power transducer.

6.2.2.1 Maximize Inherent Stiffness

Results of tests on the experimental hardware show that control of closed-loop actuator becomes extremely difficult (because of the tendency for instabilities to arise) at the high end of the stiffness range. Because of leakage in the cylinder seals and servovalve spool, the open-loop actuator will not behave as a spring and seek its original equilibrium position after being displaced by external forces. The controlled actuator servos air between cylinder chambers and supply to regulate the restoring force, compensating for leakage, making the actuator appear more like an ideal spring.

This thesis offers little explanation as to the fundamental restrictions limiting the maximum stable stiffness of the actuator; however, since the combination of high force gain and adjustable air pressure has proved successful at the low end of the controlled stiffness range, it makes sense that the range of stable stiffnesses can be widened by maximizing the actuator's inherent stiffness. That is to say: while maximizing the open-loop stiffness will improve closed-loop behavior for high stiffness, it should not impair closed-loop performance at the other extreme of backdrivability. In fact, decreasing the air chamber volumes to increase the inherent stiffness of the system's power transducer should actually improve compliant performance since the pressure response of the air cylinder under such conditions is much faster (because less air need pass through the cylinder ports to effect a pressure change).

One problem associated with the short fat pneumatic actuators required for high air column stiffness is the limited travel of such air cylinders (often refered to as *pancake* cylinders for obvious reasons). In order to provide adaquate range of motion some type of transmission mechanism is necessary leaving much room for creative design.

One approach to the travel problem is suggested by the linear actuators found on the IBM RS/1 Robot [26]. Briefly, this mechanism is composed of several small hydrualic pistons,

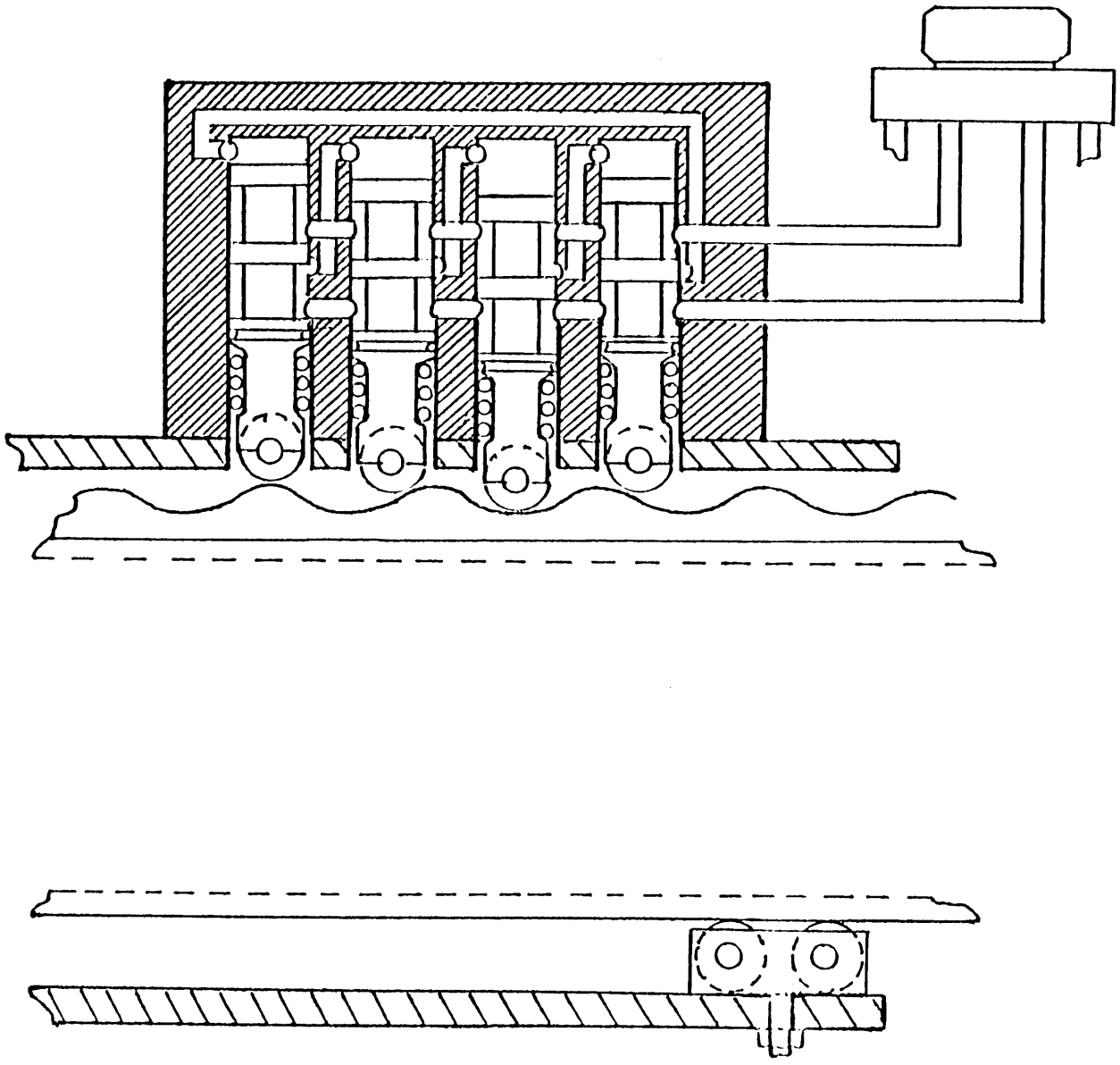

Figure 6-2: Linear actuator design in the IBM RS/1 Robot.

precisely controlled by a series of timing valves, acting on a continuous parabolic surface (see Figure 6-2). In this way unlimited linear travel is achieved while keeping the oil volume seen by each piston small, maintaining stiffness in the hydraulic cylinders.

Sizing of the ram area will also depend on the maximum force output desired of a given supply pressure as well as the nature of the transmission mechanism used (if one is used at all). Keep in mind that a reduction mechanism to increase travel will decrease stiffness at the interaction port by a factor of the reduction ratio squared. It is for this reason that the drive trains in the RS/1 contain more than one hydraulic cylinder.

6.2.2.2 Minimize Coulomb Friction

The great nemesis of high precision servo-systems, coulomb friction, is no stranger to pneumatic systems. Coulomb friction in the air cylinder places a tremendous burden on the electro-pneumatic servovalve when a force loop is closed around the actuator, severely limiting the maximum stable force gain that can be achieved in practice. For the hardware used in this project stiction in the air cylinder seals is particularly complicated by the electro-pneumatic servovalve's need for oil-free air. Though this property of the valve is a plus for operation in *clean-room* environments, in terms of positional accuracy and force control, it is disastrous. Careful attention to the design of piston and rod seals in such systems is imperative—the use of O-rings to be avoided at all costs, as they introduce *backlash* as well as excessive static friction into the system.

6.2.3 Controlled Dissipator (Semi-active Damper)

Once the decision has been made to control damping hydraulically, the problem breaks down into two specific tasks to be performed: transduction of mechanical power (F*v) into hydraulic power (P*Q), and controlled dissipation of that hydraulic power (into heat). Solution of these problems need not be limited to thinking only in terms of conventional hydraulic

equipment. This section considers first the role of hydraulic damping in various types of control—impedance and otherwise. In later sections the problems of component selection are addressed before specific design recomendations are made.

6.2.3.1 Hydraulic Damping Role in Various Control Schemes

Though it is not yet clear exactly what role a semi-active damper might play in the actuator with the inner force servo-loop as part of the impedance control scheme, the completely passive, but statically adjustable, hydraulic damper used in this project showed promise as a way of improving the closed-loop behavior of simpler control schemes. With only position feedback hydraulic damping is much more successful in stabilizing the transient response than velocity feedback and with dynamic control of the damper valve many sophisticated control techniques are possible (e.g. see reference [5]). As part of the impedance control scheme of Section 5.4, located on the actuator side of the force transducer, however, the hydraulic damper actually degrades performance when force feedback is used.

It is intuitively obvious that increased damping would impair performance on the compliant end of the impedance spectrum since the controller must work harder to make a highly damped system backdrivable. It is not obvious that this would also be the case at the stiff end of the spectrum. Increasing hydraulic damping does not attenuate the high frequency oscillations observed at high force gains and does not curtail wild unstable lower frequency oscillations resulting when the controlled stiffness is too high. Instead, hydraulic damping only places an increased load on the air cylinder requiring a higher pneumatic load pressure in order to exert the same force at the interaction port. A high load pressure implies that more time is required to switch the polarity of force output and direction of motion since more air must enter and leave the cylinder chambers.

In order for hydraulic damping to have a beneficial effect on performance, the closed oil cylinder cicuit must lie on the environment side of the force transducer. In this way damping

is controlled independent of the force loop closed around the pneumatic part of the system. Note that such a configuration requires careful design of the hydraulic components since the minimum impedance limit is then heavily dependent on the mechanical friction and oil flow properties of the circuit. These same considerations are just as important when the damper is used in other control schemes such as that of a position servo.

6.2.3.2 Selection of Hydraulic Components

Practical design of the hydraulic circuit is complicated by commercially available oil cylinders and valves, most of which are designed to operate at pressure drops of 1000 psi or more. Modification of cylinders for minimum damping (such as widening of ports and minimization of seal friction), though non-trivial, does not pose one-half the problems that arise in selecting the appropriate valve.

In this project—which is a feasibility study rather than a specific design—valve selection was made easy by using a crude hand-operated proportional valve. In the final actuator however, a semi-active dissipator (i.e. dynamic control of the flow area) is desired. Hence, the damper valve must be remotely actuated by a control input, and the faster its response the better. Also, because the damper is purely dissipative, supplying no power to the system, an unusually large maximum orifice area is necessary to accomodate high flows at the low pressure drops inherent in the passive hydraulic circuit.

Anyone familiar with the state of practice in the electro-hydraulic servovalve industry will appreciate the difficulty in finding a commercially available valve with a maximum orifice area large enough to provide minimal damping in a passive circuit when full open.

Most manufacturers rate their servovalves in terms of the volume flow of oil in gallons per minute (gpm) for a 1000 psi pressure drop. Using the Euler equation for incompressible orifice flow and the linearized damping relation derived in Section 5.2.2, it is straightforward and helpful to construct a valve selection chart giving the approximate linearized damping

coefficient (neglecting mechanical friction, fluid friction and leakage) in terms of the rated flow at 1000 psi for a particular valve.

The Euler equation is of the form

$$Q = C\sqrt{\Delta P} \tag{6.1}$$

where

$$C = C_{do}A_d\sqrt{\frac{2}{\rho_{oil}}}.$$

Given a valve's rated flow, Q_{rated}, in gpm at 1000 psi, the coefficient C with a factor to adjust for the correct units is given by

$$C = 5.9X10^{-6}\ Q_{rated}\ \frac{ft^4}{lb_f^{1/2}\text{-sec}}$$

In terms of C the linearized damping coefficient corresponding to equation (5.7) is

$$b_h = \frac{2A_h^3 v_{ss}}{C^2}, \tag{6.2}$$

where v_{ss} is a steady state velcity of the oil cylinder ram. Combining results yields

$$b_h = 5.8X10^{10}\ \frac{2A_h^3 v_{ss}}{Q_{rated}}\ \frac{lb_f\text{-sec}}{ft}, \tag{6.3}$$

where A_h is in ft^2, v_{ss} in ft/sec, and Q_{rated} in gpm at 1000 psi.

The linearized hydraulic damping coefficient, b_h, is plotted in Figure 6-3 versus Q_{rated} for various values of v_{ss} in the range of commercially available valves for $A_h = 0.0014\ ft^2$ ($0.21\ in^2$). To compute b_h for a different oil cylinder bore multiply the b_h value read from the chart by

$$\left[\frac{(A_h)_{new}}{(A_h)_{old}}\right]^3$$

or for a different steady state velocity multiply by

$$\frac{(v_{ss})_{new}}{(v_{ss})_{old}}.$$

For flows rated at other pressure drops either construct a new chart or multiply b_h by

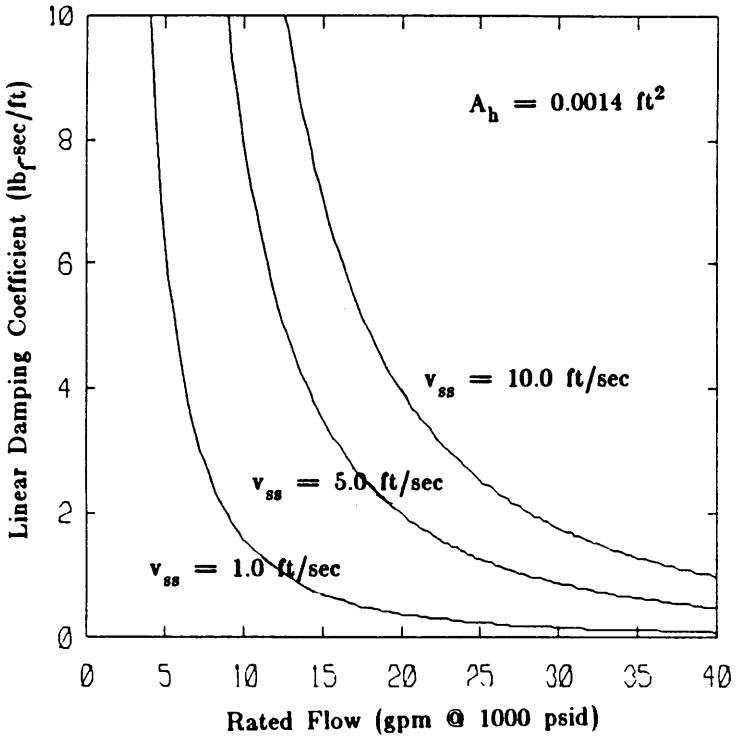

Figure 6-3: Damper valve selection chart.

$$\frac{\Delta P_{new}}{\Delta P_{old}}$$

The problem with selecting valves in this way is that a very high value of Q_{rated} is necessary for minimum damping. Such high flow servovalves, built to withstand large pressure and flow forces and having several stages (as many as three) requiring high pressure pilot flows, tend to be expensive (in the neighborhood of $3000.00) and are rediculously over-designed for application in a passive circuit in which pressures rarely exceed a few hundred psi.

There appears to be some hope, however. Proportion valves for low pressure operation are becoming more common as the interest in controlled dissipators and semi-active dampers grows [18], [5]. Recently several manufacturers have begun to offer proportionally controlled hydraulic valves intended for operation at lower pressure drops. Olsen Controls, Inc., Towler Hydraulics, Inc., and Robert Bosch Corp. are but a few.

Olsen carries a line of proportional valves employing stepper motors and spool position feedback for precise control of flow area. Towler manufactures inexpensive cartrige valves using a first-stage solenoid and low pressure pilot (approx. 200 psi) to throttle flow in the second stage. Bosch makes high precision proportional valves rated at only 8 bar (120 psi) using servo-controlled push pull solenoids to adjust spool position.

6.2.3.3 Leakage in the Closed Circuit

Because the passive hydraulic damper is a closed circuit provisions must be made to account for fluid loss through external leakage. Also, the problems of cavitation in the low pressure oil chamber and air leaking in through the rod seals must be addressed. Including a pressurized accumulator in the circuit solves each of these problems, however it is necessary to *isolate* the accumulator from the damper load pressure by introducing check valves into the closed circuit.

Way back in 1966 Feldstein [12] investigated the feasibility of a controlled hydraulic damper in a pneumatic powered position servo-system. Figure 6-4 shows a schematic of his oil circuit. The oil cylinder is symmetic (double rodded), otherwise the fluid level in the accumulator will oscillate as the ram cycles back and forth. Pressurization of the circuit by the accumulator is essential as it is much better to have oil leak out rather than have air leak in. (Pressurization also helps prevent cavitation.)

This circuit requires two symmetrical orifices, through they were part of the same sliding plate valve. The circuit might be redesigned into the configuration of Figure 6-5, requiring only one orifice, but two more check valves are required.

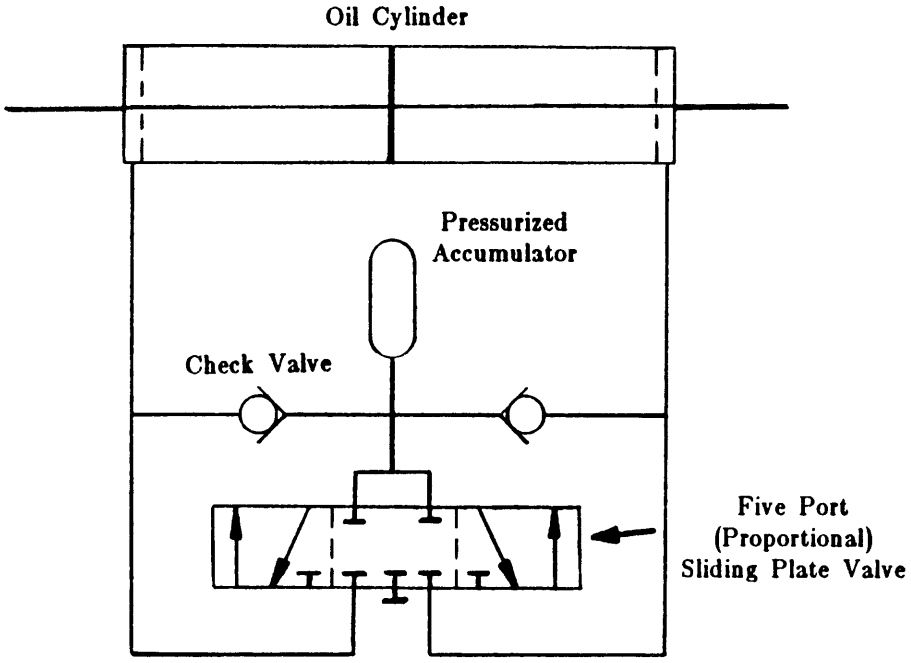

Figure 6-4: Passive hydraulic circuit from reference [12].

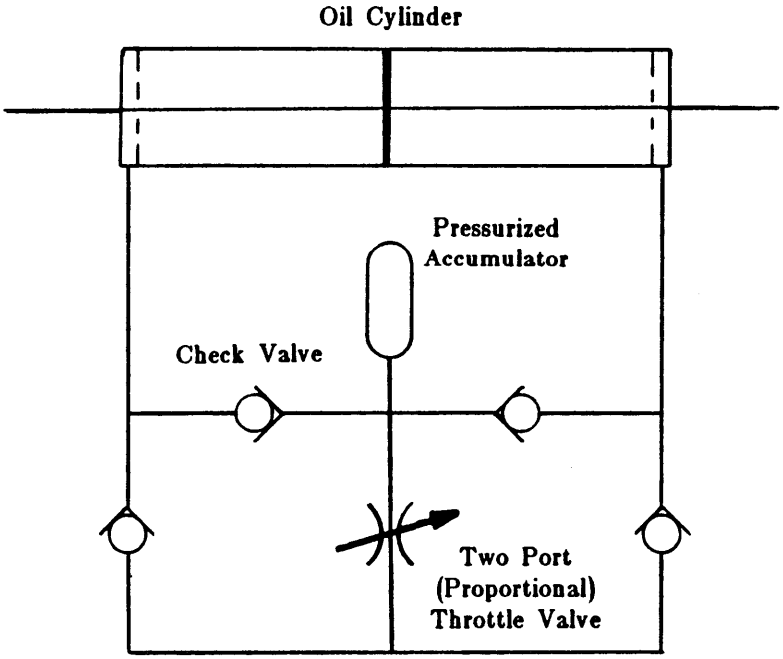

Figure 6-5: Passive hydraulic circuit requiring only one orifice.

6.3 Feedback Path Elements

This section discusses the actuator's feedback path elements which, in general terms, consist of sensors to provide real time measurements of key system variables and a real time controller to process these measurements in conjunction with input commands form a higher level supervisory controller.

6.3.1 Sensors

While the sensitivity and noise properties of sensors are not the only factors limiting the performance of sophisticated control systems, as many control engineers seem to think—this thesis argues that attention to the forward path is just as important—their choice and design cannot be taken lightly.

Unless special provisions are made to measure velocity directly (e.g. with a tachometer or LVT[14]), the position transducer must be such that differentiation of the output to obtain a velocity signal does not excessively amplify noise in the position signal. In this project use of a conductive plastic linear potentiometer and an analog differentiator with a low pass filter to attenuate high frequency noise provided adaquate position and velocity information for both feedback and time response measurement.

By far, the most crucial sensor making up the impedance controller implemented is the force transducer located at the actuator/environment interaction port. This sensor, while having a very small maximum deflection (0.005 in. at a maximum of 500 lb_f for the load cell used), must be sensitive to low force levels (less than 1 lb_f) for the controller to perform well at the compliant end of the impedance spectrum. Low noise is essential in order to avoid undesirable effects due to noise amplification in the force loop at high gains, as the physics

---

[14]Linear velocity transducer.

of the actuator alone pose enough control problems.

In future applications of impedance control in pneumatic systems it may prove helpful to instrument the air cylinder with dynamic pressure transducers (one for each chamber) as *transient pressure feedback* (the negative derivative of pressure) has been shown to be an effective method of increasing closed-loop stability in pneumatic servo-systems [7], [2], not to mention the possibilities suggested by modern control and full state feedback.

6.3.2 Controllers

This section concerns itself with the possibilities and limitations of controller designs. A brief discussion of classical control is followed by consideration of the more promising techniques suggested by modern control theory.

6.3.2.1 Classical Control

It was suggested that instabilities arising in the impedance controlled actuator might be alleviated by introducing a lead-lag filter into the inner force feedback loop. The unstable behavior at high force gain is in part due to the additional phase lag of the electro-pneumatic servovalve as well as other factors including amplified force measurement noise. The low pass filter provides attenuation of high frequency noise while adding the feedfoward path reduces phase lag in order to maintain stability.

Donath [10] attempted to improve stability of a hydraulic knee prothesis simulator containing a similar force control loop in this way and was unsuccessful, finding that stability remained marginal.

6.3.2.2 Modern Control

Though the prospective of improving performance of the impedance controlled actuator using classical control techniques appears marginal at best, there exists a strong possibility

that the system can be stabilized over a wider range of impedances using full state feedback and the more sophisticated methods of modern control theory.

Full state feedback was not implemented on the experimental hardware because of insufficient instrumentation to determine state variables in real time. (It was decided that more inportant objectives of the project would suffer were the design and construction of an observer to estimate unmeasurable states undertaken.)

The full linear model of Section 3.3.4 contains four states: the ram position and velocity, the pneumatic load pressure and the servovalve spool position, of which only the position and velocity of the ram were measured. For the parameter values determined from the experimental frequency response the system is both controllable and observable with only the electro-pneumatic servovlave control input and the position measurement.

Those familiar with modern linear control thoery will realize that both controllability and observability imply, theoretically at least, that the closed-loop poles (using full state feedback and an observer) can be placed arbitrarily in the complex plane. Of course in reality, effects such as unmodeled dynamics and actuator saturation will restrict pole placement. However, this is still a substantial improvement over the limitations of classical control.

Adding a second control input in the form of dynamic modulation of the damper flow area, though complicating the computation of controller parameters, will further enhance the system's controllability.

6.4 Summary of Design Recommendations

This section presents a brief summary of the more important issues in the design of the hybrid actuator. It is divided into two catagories: forward path elements and feedback path elements.

6.4.1 Forward Path

1. Maximize the inherent stiffness of the main power transducer, by minimizing the air volume, and maximizing the piston area (or vane area in a rotary actuator), assuming that variable pressure in the air chambers will insure that compliant behavior is also possible.

2. Minimize coulomb friction throughout the entire actuator, especially through careful selection of seals in the pneumatic power transducer.

3. Through special design, minimize the inherent damping in the passive hydraulic circuit when flow area is at its maximum, taking care to insure that sensitivity at high damping (i.e. small flow area) is not impaired.

4. Add a second control input in the form of dynamic modulation of the hydraulic damper flow area.

5. When controlling impedance artificially, place the hydraulic damper outside of the force feedback loop to give control of damping independent of force control in the pneumatic actuator.

6. Investigate the possibilities of using open-center and pressure control electro-pneumatic servovalves in order to make the natural actuator look more like an effort source.

6.4.2 Feedback Path

1. Use a high performance force sensor with resolution down to less than 1 lb_f, but having a small maximum deflection (less than 0.01 in).

2. Instrument the pneumatic actuator with dynamic pressure transducers—one for each chamber—so that pressure and transient pressure feedback are realizable control options.

3. Apply the methods of modern control theory to the two input system to increase the range of stable impedance controlled behavior.

6.5 Concluding Remarks

This project has shown the feasibility of an impedance controller employing force feedback in a pneumatic actuator. The performance of the controller is enhanced by the ability to alter the natural properties of the device.

Control of open-loop impedance was marginally successful, limited by the minimum damping in the passive hydraulic circuit, and by the maximum inherent stiffness of the fixed volume of an air chamber and a maximum supply pressure of only 120 psig.

A combination of special design of the forward path elements and modern control techniques to maintain closed-loop stability should result in a versatile impedance controlled actuator capable of a variety of tasks including those requiring non-negligible work interactions.

Appendix A
Dimensionless Models

A.1 Dimensionless Non-Linear Model

STATE EQUATIONS

RAM POSITION

$$\frac{x^*}{v^*}\,\omega_n^*\,\frac{d}{d\tau}\,s_x = s_v \tag{A.1}$$

RAM VELOCITY

$$r_m\,\frac{1}{2\zeta^*}\,\frac{d}{d\tau}\,s_v = p_L - p_R - r_b\delta_b s_v - \delta_h p_{hl} + f_{ext} + f_{coul} \tag{A.2}$$

LEFT AIR CHAMBER PRESSURE

$$\frac{\gamma_L}{kp_{av}}\,\frac{x^*}{v^*}\,\omega_n^*\,\frac{d}{d\tau}\,p_L = q_L - s_v - l_a(p_L - p_R) \tag{A.3}$$

RIGHT AIR CHAMBER PRESSURE

$$\frac{\gamma_R}{kp_{av}}\,\frac{x^*}{v^*}\,\omega_n^*\,\frac{d}{d\tau}\,p_R = q_R + s_v + l_a(p_L - p_R) \tag{A.4}$$

SPOOL POSITION

$$T\,\omega_n^*\,\frac{d}{d\tau}\,a_s = -a_s + i_s \tag{A.5}$$

AUXILIARY EQUATIONS

AIR CHAMBER VOLUMES

$$\gamma_L = 1 + s_x \tag{A.6}$$

$$\gamma_R = 1 - s_x \tag{A.7}$$

HYDRAULIC LOAD PRESSURE

$$p_{hl} = \frac{|s_v|\,s_v}{(C_{do}a_d)^2} \tag{A.8}$$

AIR CHAMBER VOLUME FLOW RATES

$$q_L = C_d|a_s| \quad \frac{1}{r_\rho} |p_{S_L} - p_L| \quad \text{sgn}(p_{S_L} - p_L) \tag{A.9}$$

$$q_R = C_d|a_s| \quad \frac{1}{r_\rho} |p_{S_R} - p_R| \quad \text{sgn}(p_{S_R} - p_R) \tag{A.10}$$

For: $a_s > 0 : p_{S_L} = 1 \quad ; p_{S_R} = p_{atm}$

$a_s = 0$: null position

$a_s < 0 : p_{S_L} = p_{atm} ; p_{S_R} = 1$

A.2 Dimensionless Linear Model

RAM POSITION

$$\frac{x^*}{v^*} \omega_n^* \quad \frac{d}{d\tau} s_x = s_v \tag{A.11}$$

RAM VELOCITY

$$r_m \frac{1}{2\zeta^*} \quad \frac{d}{d\tau} s_v = p_{pl} - [r_b \delta_b + b_h/b] s_v + f_{ext} \tag{A.12}$$

PNEUMATIC LOAD PRESSURE

$$\frac{1}{kp_{av}} \frac{x^*}{v^*} \omega_n^* \quad \frac{d}{d\tau} p_{pl} = c_z a_s - s_v - c_1 p_{pl} \tag{A.13}$$

SPOOL POSITION

$$T \omega_n^* \quad \frac{d}{d\tau} a_s = -a_s + i_s \tag{A.14}$$

Appendix B
Dimensionless Feedback Laws

B.1 Position, Velocity, and Force Feedback

For position, velocity, and force feedback the fully dimensioned control expression is of the form

$$I = -K_a V_a = -K_a[\, K_F F_{td} + K_v(v - v_o) + K_x(x - x_o)\,] \tag{B.1}$$

where, from equation (4.9),

$$F_{td} = M_L \frac{d}{dt} v + b_L v - F_{ext} .$$

For $x_o = 0$ and $v_o = 0$,

$$I = K_a K_F F_{ext} - K_a[\, K_F M_L \frac{d}{dt} v + (K_F b_L + K_v) v + K_x x\,] . \tag{B.2}$$

In dimensionless form this becomes

$$i_s = k_f f_{ext} - \{\, k_f \frac{(r_m - 1)}{2\zeta^*} \frac{d}{d\tau} s_v + [\, k_f(r_b - 1)\delta_b + k_v\,] s_v + k_x s_x \,\} , \tag{B.3}$$

where

$$k_x = \frac{K_a K_x x^*}{I^*}$$

$$k_v = \frac{K_a K_v v^*}{I^*}$$

$$k_f = \frac{K_a K_F A_p P^*}{I^*}$$

B.2 Impedance Controller

The fully dimensioned control expression for the impedance controller (for $x_o = 0$ and $v_o = 0$) is given by

$$I = K_a K_F\{ F_{ext} - [M_L \frac{d}{dt} v + (b_L + K_v + K_x] \} , \tag{B.4}$$

and in dimensionless form by

$$i_s = k_f\{ f_{ext} - (\frac{(r_m-1)}{2\zeta^*} \frac{d}{d\tau} s_v + [(r_b-1)\delta_b + k_v] s_v + k_x s_x) \} , \tag{B.5}$$

where k_x, k_v, and k_f are defined as before.

References

[1] Abul-Haj, C.J.
The Design of an Upper-arm Prosthesis Simulator With Variable Mechanical Impedance.
Master's thesis, Massachusetts Institute of Technology, 1981.

[2] Andersen, B.W.
The Analysis and Design of Pneumatic Systems.
John Wiley & Sons, New York, 1967.

[3] Andrews, J.R.
Impedance Control as a Framework for Implementing Obstacle Avoidance in a Manipulator.
Master's thesis, Massachusetts Institute of Technology, 1983.

[4] Atchley, R.D.
A More Reliable Electro-hydraulic Servovalve.
In *Robots VI Conference Proceedings.* Robots VI Conference, 1982.

[5] Bass, G.A.
Modeling and Control of a Hydro-Pneumatic Actuator.
Master's thesis, University of California, Davis, 1979.

[6] Beaman, J.J.
Statistical Linearization for the Analysis and Control of Stochastic Systems.
PhD thesis, Massachusetts Institute of Technology, 1979.

[7] Blackburn, J.F., Reethof, G., and Shearer, J.L.
Fluid Power Control.
The MIT Press, Cambridge, Mass, 1960.

[8] Bryson, A.E., and Ho, Y.
Applied Optimal Control.
Hemisphere Publishing Corp., New York, 1975.

[9] Cotter, S.L.
Non-linear Feedback Control of Manipulator Endpoint Imdedance.
Master's thesis, Massachusetts Institute of Technology, 1982.

[10] Donath, M.
Proportional EMG Control For Above Knee Protheses.
Master's thesis, Massachusetts Institute of Technology, 1974.

[11] Drake, S.H.
Using Compliance In Lieu of Sensory Feedback For Automatic Assembly.
PhD thesis, Massachsetts Institute of Technology, 1977.

[12] Feldstein, M.A.
A Pneumatically Powered Position Servomechanism Employing Passive Hydraulic Control.
Master's thesis, Massachusetts Institute of Technology, 1966.

[13] Hogan, N.
Mechanical Impedance Control in Assistive Devices and Manipulators.
In *Priceedings of the Joint Automatic Control Conference.* Joint Automatic Control, 1980.

[14] Hogan, N.
Programmable Impedance Control of Industrial Manipulators.
In *Proceedings of the Conference on CAD/CAM Technology in Mechanical Engineering.* Massachusetts Institute of Technology, 1982.

[15] Hogan, N., and Cotter, S.L.
Cartesian Impedance Control of a Non-linear Manipulator.
In *Proceeding of the ASME WAM Robotics Symposium.* 1982.

[16] Hogan, N.
Impedance Control as an Approach to Manipulation PART I: Control of Mechanical Interaction.
Massachusetts Institute of Technology. Submitted to the Journal of Dynamic Systems Measurement and Control, June 1983.

[17] Karnopp, D.
Bond Graph Models For Fluid Dynamic Systems.
ASME Journal of Dynamic Systems Measurement and Control 94(3):222-229, September, 1972.

[18] Karnopp, D., Crosby, M.J., Harwood, R.A.
Vibration Control Using Semi-Active Force Generators.
ASME Journal of Engineering for Industry 96(2):619-626, May, 1974.

[19] Karnopp, D., and Rosenberg, R.
System Dynamics: A Unified Approach.
John Wiley & Sons, New York, 1975.

[20] Kwakernaak, H., and Sivan, R.
Linear Optimal Control Systems.
Wiley Interscience, New York, 1972.

[21] McCloy, D., and Martin, H.R.
Control of Fluid Power: Analysis and Design.
John Wiley & Sons, New York, 1980.

[22] Nevins, J.L., and Whitney, D.E.
Computer Controlled Assembly.
Scientific American 238(2):62-74, Febuary, 1978.

[23] Ogata, K.
Modern Control Engineering.
Prentice-Hall, Inc., Englewood Cliffs, NJ, 1970.

[24] Paynter, H.M.
Analysis and Design of Engineering Systems.
The MIT Press, Cambridge, Mass, 1960.

[25] Rosenberg, R., and Karnopp, D.
Introduction to Physical System Dynamics.
McGraw Hill, New York, 1983.

[26] *Advanced Manufacturing Systems IBM RS/1 Maintenance Education Student Guide* 1981.

[27] Shapiro, A.H.
The Dynamics and Thermodynamics of Compressible Fluid Flow.
John Wiley & Sons, New York, 1953.